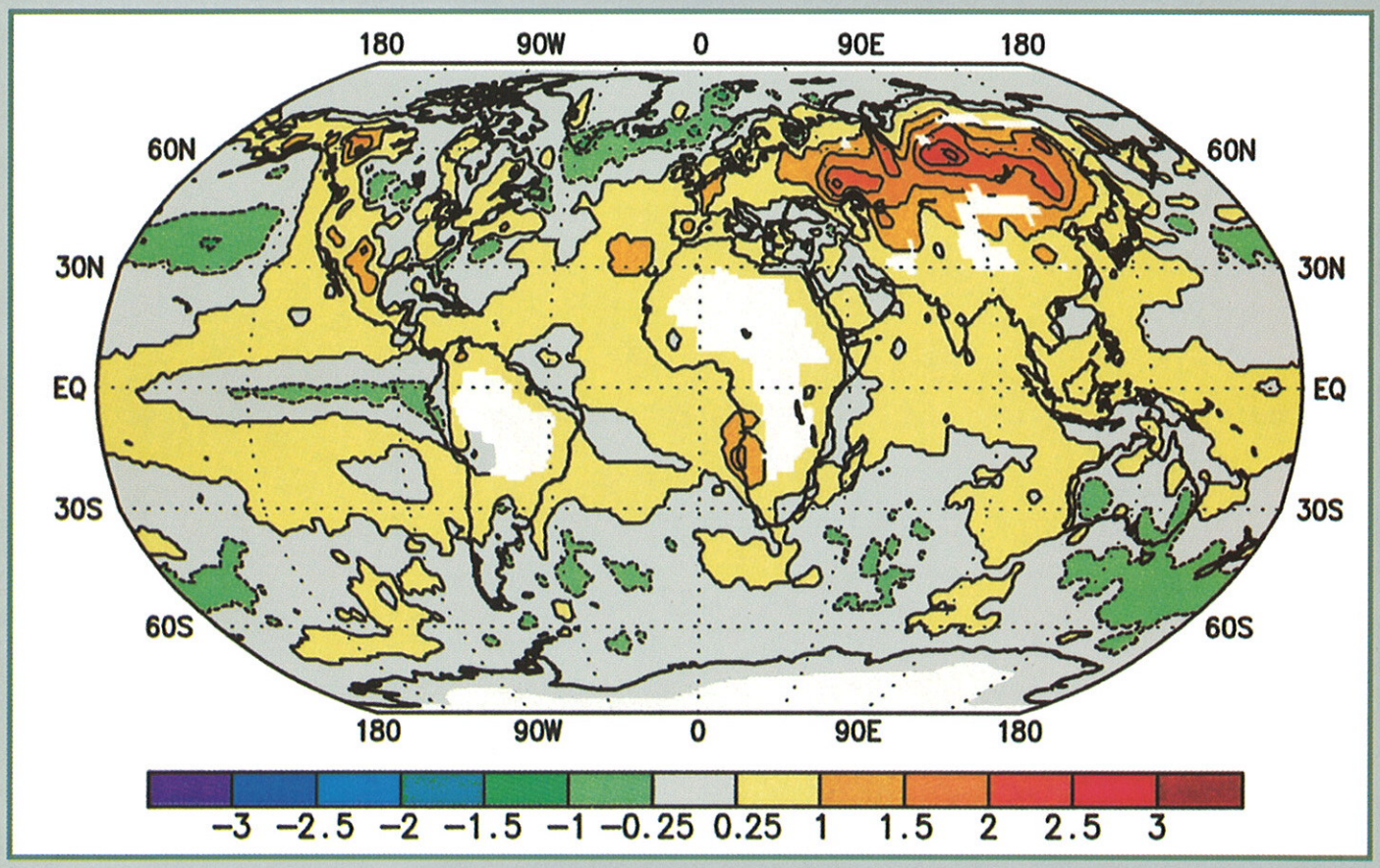
CLIMATE ASSESSMENT FOR 1995

Michael S. Halpert, Gerald D. Bell, Vernon E. Kousky, and Chester F. Ropelewski
Climate Prediction Center, NCEP/NWS/NOAA, Washington, D.C.



Reprinted from *Bulletin of the American Meteorological Society*, Vol. 77, No. 5, May 1996

Climate Assessment for 1995



Michael S. Halpert, Gerald D. Bell, Vernon E. Kousky and Chester F. Ropelewski
Climate Prediction Center, NCEP/NWS/NOAA, Washington, D.C.

ABSTRACT

The El Niño–Southern Oscillation (ENSO) phenomenon is a major contributor to the observed year-to-year variability in the Pacific Ocean and in the global atmospheric circulation. The short-term climate system witnessed the return to the mature phase of warm ENSO conditions (commonly referred to as the El Niño) during early 1995 for the third time in four years. This frequency of occurrence is unprecedented in the last 50 years and is comparable to that observed during the prolonged 1911–15 ENSO episode.

These warm ENSO conditions contributed to a large-scale disruption of the normal patterns of wind, rainfall, and temperature over much of the tropics and middle latitudes, particularly during the December 1994–February 1995 period. This period was followed by a dramatic decrease in sea surface temperatures in the tropical Pacific, resulting in a complete disappearance of all warm episode conditions during June–August and in the development of weak cold-episode conditions during September–November.

Changes in the tropical Pacific were accompanied by pronounced, large-scale changes in the atmospheric circulation patterns from those that had prevailed during much of the early 1990s. Particular examples of these changes include 1) a dramatic return to a very active hurricane season over the North Atlantic, following four consecutive years of significantly below-normal hurricane activity; 2) the return to above-normal rainfall throughout Indonesia, northern Australia, and southern Africa, following a prolonged period of below-normal rainfall and periodic drought; and 3) a northward shift of the jet stream and storm track position over the eastern half of the North Pacific during the latter part of the year, following several winter seasons (three in the last four) characterized by a significant strengthening, southward shift, and eastward extension of these features toward the southwestern United States.

Other regional climate anomalies during 1995 included extreme warmth throughout western and central Asia during January–May and colder than normal conditions in this region during November–December, severe flooding in the midwestern United States (April–May), abnormally wet conditions in California and the southwestern United States (December–February) combined with near-record warmth over eastern North America, deadly heat waves in the central United States (mid-July) and India (first three weeks of June), drought in the northeastern United States (August), a drier-than-normal rainy season in central Brazil (September–December), and an intensification of drier-than-normal conditions over southern Brazil, Uruguay, and northeastern Argentina at the end of the year.

The global annual mean surface temperature for land and marine areas during 1995 averaged 0.40°C above the 1961–90 mean. This value exceeds the previous warmest year in the record (1990) by 0.04°C. The Northern Hemisphere also recorded its warmest year on record during 1995, with a mean departure from normal of 0.55°C. The global annual mean surface temperature for land areas only during 1995 was the second warmest since 1951.

The year also witnessed near-record low ozone amounts in the Southern Hemisphere stratosphere, with minimum values only slightly higher than the record low values observed in 1993. The areal extent of very low ozone values during 1995 was as widespread over Antarctica as in the record low year of 1993.

Corresponding author address: Michael S. Halpert, Climate Prediction Center, NCEP/NOAA, W/NP52, NSC, Rm. 605, 5200 Auth Rd., Camp Springs, MD 20746

Table of Contents

1. Introduction S3

2. Climate and global change issues S3
   a. Surface temperatures S3
   b. Tropospheric/stratospheric temperatures S7
      1) Troposphere S7
      2) Lower stratosphere S9
   c. Trace gases S10
      1) Ozone S10
      2) Carbon Dioxide S12
      3) Methane S12
   d. Northern Hemisphere snow cover S13

3. The evolution of recent oceanic and atmospheric anomalies in the global tropics S15
   a. Large-scale conditions in the tropics: 1990–94 ..... S15
   b. The 1994–95 warm (ENSO) episode S16
   c. The 1995 Pacific cold episode S17

4. Regional climate highlights S19
   a. North America S19
      1) December 1994–January 1995: Wet in Western U. S., warm in East S19
      2) April–May 1995: Midwest U. S. floods S20
      3) The 1995 Atlantic hurricane season S24
      4) Mid-July 1995: Midwest U. S. heat wave S26
      5) August 1995: Northeast U. S. drought S26
      6) November-December 1995: Wet in Northwest U. S., cold in East: S28
   b. Eurasia S29
      1) January-May 1995: Asian warmth S29
      2) June–August 1995: European/Western Asian hot spell S30
      3) June–September 1995: Southeast Asian/Indian summer monsoon S31
   c. South America S33
   d. Australia S34
   e. Africa S36
      1) June–September 1995: Western Africa rainy season S36
      2) October 1994–April 1995: Southern Africa rainy season S37

5. Seasonal summaries S39

Appendix: Contributors S43

Acknowledgments S43

References S43

1. Introduction

There is considerable interest in interannual climate variations over the globe, as well as concern about the possibility of anthropogenic climate change. For the past five years, the Climate Prediction Center (CPC) has produced an annual Climate Assessment designed to provide a timely summary of both the short-term climate system and of longer-term climate variations. This article is the first of this series to appear in the *Bulletin of the American Meteorological Society*.

This Annual Assessment documents global-scale climate variations and trends, the evolution of recent oceanic and atmospheric anomalies in the global tropics, and selected regional climate variations. A discussion of global atmospheric temperatures, trace gases and the cryosphere is found in section 2. In section 3, the large-scale conditions in the tropics between 1990 and 1994 are described, followed by a discussion of the transition from warm episode to cold episode conditions in the Pacific during 1995. Section 4 documents regional climate highlights during the past year, including the Indian Monsoon, African rainfall, and notable short-term climate events in the extratropics. Finally, section 5 shows seasonal maps for temperature anomalies, precipitation percentiles and 500-hPa heights and anomalies. These maps are included to continue the set of maps which have appeared in the previous five Annual Climate Assessments.

There are a variety of data sources used in the compilation of this Assessment. The surface data are from preliminary reports obtained over the operational Global Telecommunications System (GTS). Owing to the nature of such reports, the data have not been subject to strict quality control and validation procedures. However, based on past experience we do not expect significant qualitative changes to these preliminary results as more data are accumulated. Other data sources include satellites, radiosonde and ship reports, and gridded analyses from the National Center for Environmental Prediction (NCEP) operational Global Data Assimilation System (GDAS) and from the NCAR/NCEP Climate Data Assimilation System (CDAS)/Reanalysis Project. Selected analyses were also obtained from international climate data centers.

A companion article, to be published in the *Journal of Climate,* will provide a more detailed diagnostic description of major oceanic and atmospheric anomalies observed during 1995. That annual article will replace the Seasonal Climate Summaries, which have appeared previously in the *Monthly Weather Review* and more recently in the *Journal of Climate*.

2. Climate and global change issues

a. Surface temperatures

Estimated global (*land area only*) mean temperature anomalies during 1995 [computed using meteorological station data received over the Global Telecommunications System (GTS) relative to the 1951–80 base period means] were the second largest in the historical record (0.42°C), ranking behind the warmest year of 1990 (0.52°C), and slightly ahead of 1991 (0.41°C) and 1994 (0.41°C) (Fig. 1). This marks a continuation of the warmer-than-normal global-land

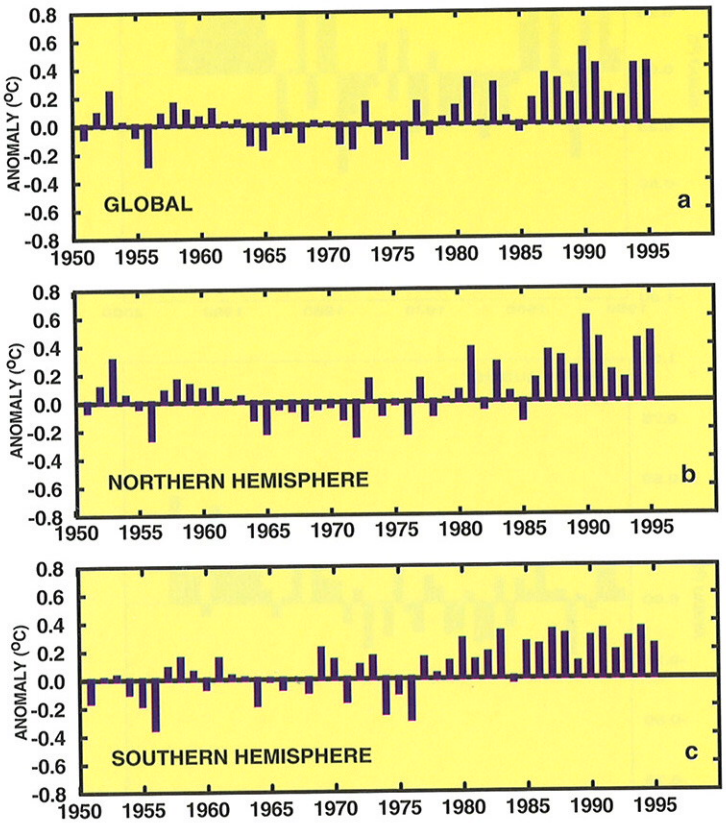


FIG. 1. Annual temperature anomalies (land only, °C): (a) global, (b) Northern Hemisphere, and (c) Southern Hemisphere. Anomalies are departures from the 1951–80 base period means. (Source: CPC)

temperatures that have been observed for the past 10 years. In addition, the four warmest years since 1951 have occurred during the decade of the 1990s. Much of the warmth during 1995 was concentrated in the Northern Hemisphere (Fig. 1b), as the mean annual Southern Hemisphere temperature was only the eleventh warmest since 1951 (Fig. 1c).

Record warmth over land occurred during the December 1994–February 1995 (DJF) and June–August 1995 (JJA) seasons (Figs. 2a, c). The 1994/95 DJF temperature was slightly more than +0.80°C above normal and was larger than any seasonal departure observed since 1951. The estimated global-land temperatures during the March–May (MAM) and September–November (SON) seasons were also above normal during 1995 (Figs. 2b, d), but not at the record extremes observed during the winter and summer. This observation contrasts with the past decade, in which much of the anomalous warmth occurred during the first half of the year. For example during the last 10 years, the global DJF and MAM land temperatures averaged more than 0.40°C above normal, while the JJA and SON temperatures averaged near 0.25°C and 0.15°C above normal, respectively.

The estimated global mean surface temperature for *land and marine* areas combined is derived from observations at land stations and from sea surface temperatures (SSTs) measured by ships and buoys. The global temperature for 1995 was 0.40°C above the 1961–90 average (Fig. 3). This anomaly exceeds the previous warmest year in the record (1990) by 0.04°C. The Northern Hemisphere also experienced record

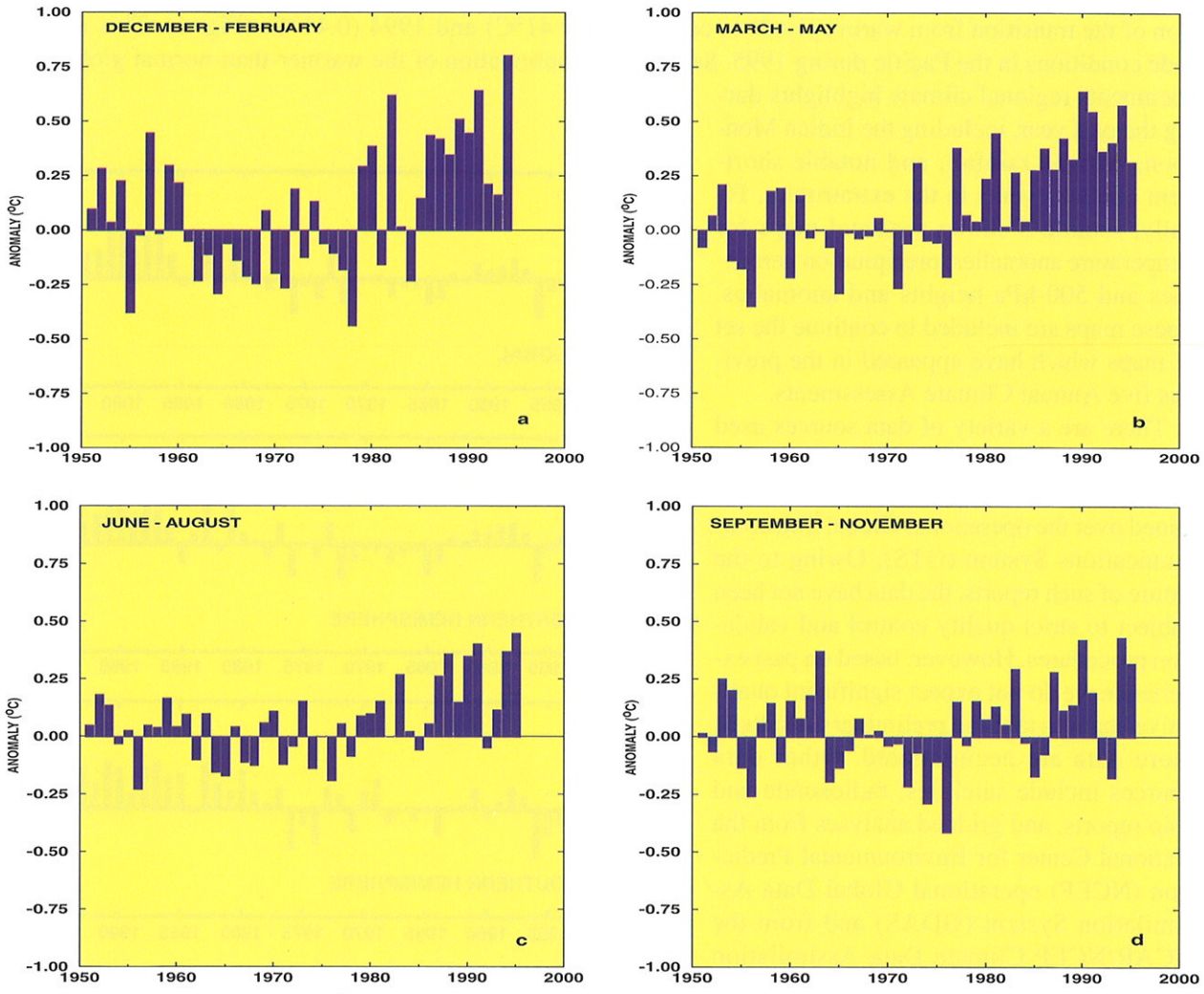


FIG. 2. Global temperature anomalies (land only, °C) for (a) December–February, (b) March–May, (c) June–August and, (d) September–November. Anomalies are departures from the 1951–80 base period means. (Source: CPC)

warmth during 1995 with temperatures averaging 0.55°C above normal, while Southern Hemisphere temperatures (0.23°C above normal) were not as warm as 1983 or 1987 and were about equal to 1990, 1991, and 1993.

A major contributor to the anomalous warmth during 1995 was well-above-normal temperatures over northern Eurasia (Fig. 4). Temperatures averaged more than 3.0°C above normal over Siberia during the year, with monthly anomalies during January and February exceeding +10.0°C across parts of this region (see Section 4b). A time series averaged over the countries which formerly comprised the Soviet Union (Fig. 5) shows 1995 to be the warmest year since 1891 for that region (+2.1°C above normal), far surpassing the previous record anomaly of +1.4°C set in 1990.

Elsewhere, annual mean surface land temperatures were also significantly above normal across Alaska, northwestern Canada, and Europe (which experienced a very warm summer, see Section 4b). Colder-than-normal annual mean land temperatures during the year

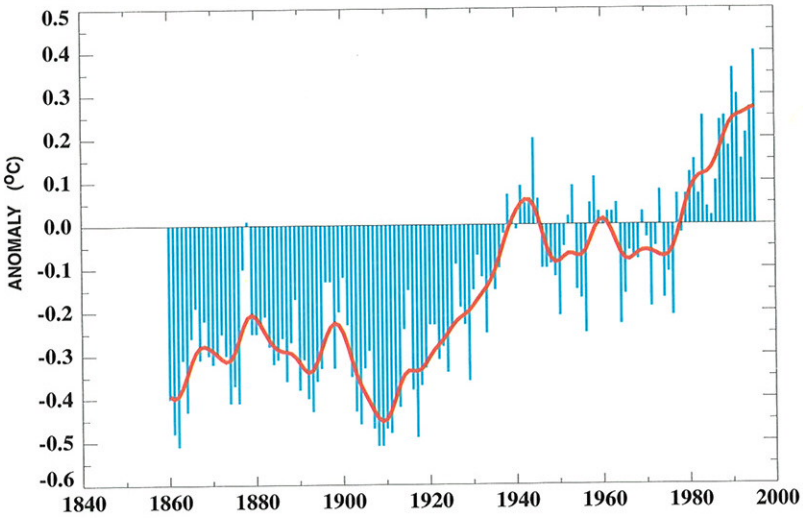


FIG. 3. Global annual averages of combined land-air and SST anomalies (°C). Anomalies are departures from the 1961–90 base period means. Yearly values are indicated by the bars. Smoothed values (red curve) were obtained using a 13-term Gaussian filter designed to suppress variations on time scales less than 10 years. (Source: Hadley Centre for Climate Prediction and Research, UK, and Climatic Research Unit, Univ. of East Anglia, UK)

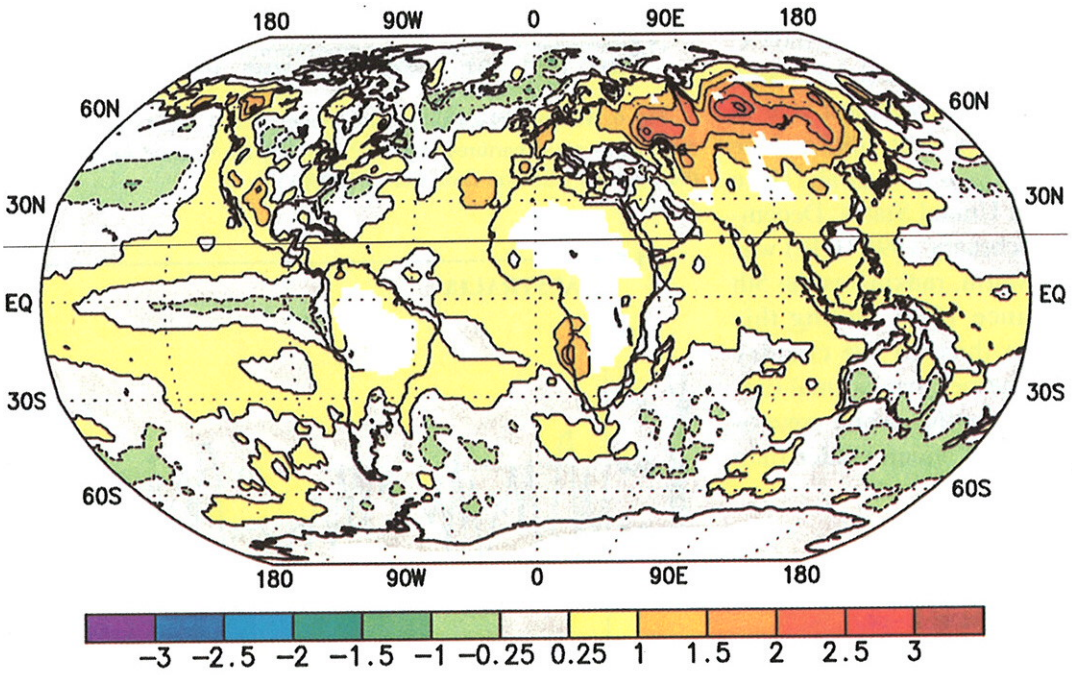


FIG. 4. Surface temperature anomalies (°C) for January–December 1995. Analysis is based on station data over land and on SST data over the oceans. Anomalies for station data are departures from the 1961–90 base period means, while SST anomalies are departures from the 1950–79 adjusted OI climatology (Reynolds and Smith 1995). White areas are regions with insufficient data for analysis. (Source: CPC)

were restricted to southern Australia and Greenland (Fig. 4).

The dissipation of warm episode (El Niño–Southern Oscillation) conditions in early 1995 and the development of weak cold-episode conditions by the end of the year (see Section 3) is evident in the pattern of below-normal SSTs in the eastern equatorial Pacific (Fig. 4). However, most of the remainder of the tropical and subtropical oceans recorded above-normal temperatures for the year as a whole, with anomalies greater than 1.0°C covering parts of the Atlantic Ocean (Fig. 4). In contrast, temperatures averaged cooler than normal during 1995 throughout the North Pacific and the northern North Atlantic. Large parts of the Southern Hemisphere oceans south of 40°S also averaged colder than normal during 1995, especially south of New Zealand.

Regional time series for the contiguous United States (Fig. 6) and Australia (Fig. 7) show that 1995 temperatures were also above normal in these countries (0.3°C and 0.08°C above normal, respectively). Overall, 1995 was the 20th warmest year in the United States since 1895 and the 23rd warmest year in Australia since 1910. In the United States, December 1994–February 1995 (DJF) was especially warm, ranking as the 5th warmest since 1895. During this season, one-third of the country was much warmer than normal (upper tenth percentile), while none of the country was much colder than normal.

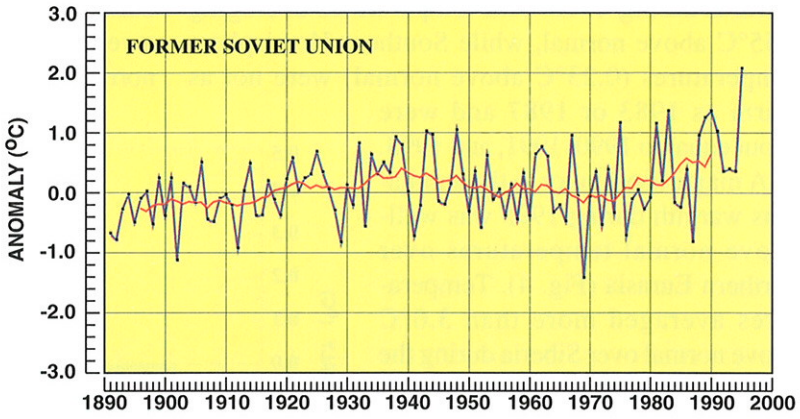


FIG. 5. Annual surface temperature anomalies (°C) for the former Soviet Union. The red curve is an 11-year running mean. Anomalies are departures from the 1951–80 base period means. (Source: Institute for Global Climate and Ecology, Russia)

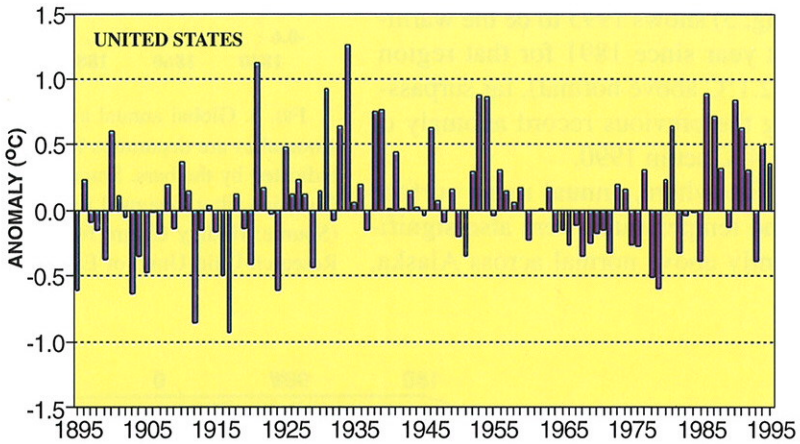


FIG. 6. Annual surface temperature anomalies (°C) for the contiguous United States. Anomalies are departures from the 1961–90 base period means. (Data provided by the National Climatic Data Center/NOAA)

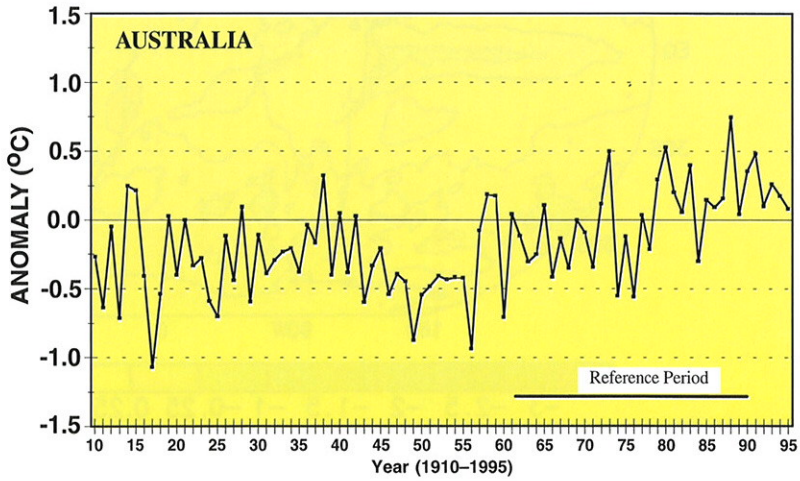


FIG. 7. Annual surface temperature anomalies (°C) for Australia. Anomalies are departures from the 1961–90 base period means. (Source: Australian Bureau of Meteorology)

b. Tropospheric/stratospheric temperatures

1) TROPOSPHERE

The global-mean tropospheric temperature is monitored by two independent observing systems: radiosondes and polar-orbiting satellites. The global radiosonde record began in 1958 and has the advantage of a relatively long time series of directly measured temperatures. The satellite record began in 1979 and has the advantages of 1) sampling the atmosphere with one type of instrument at any given time; and 2) global sampling, with most of the earth sampled twice-daily from each of two instruments flying concurrently on different satellites (Spencer et al. 1990).

The radiosonde observations for 1995 (Fig. 8a) indicate a mean tropospheric temperature anomaly of 0.25°C, computed with respect to the 1961–90 base period (red bars). This value is the highest annual, global mean anomaly observed since the eruption of Mt. Pinatubo in 1991, but is below the extremely warm 1987–1991 period. The 1995 radiosonde-estimated anomaly is also larger than any value recorded prior to 1979, the beginning of the satellite record.

The satellite-based temperature anomalies (Fig. 8b), obtained from measurements taken by the Microwave Sounding Unit (MSU) channel 2R flown aboard the polar-orbiting satellites (Spencer et al. 1990) and

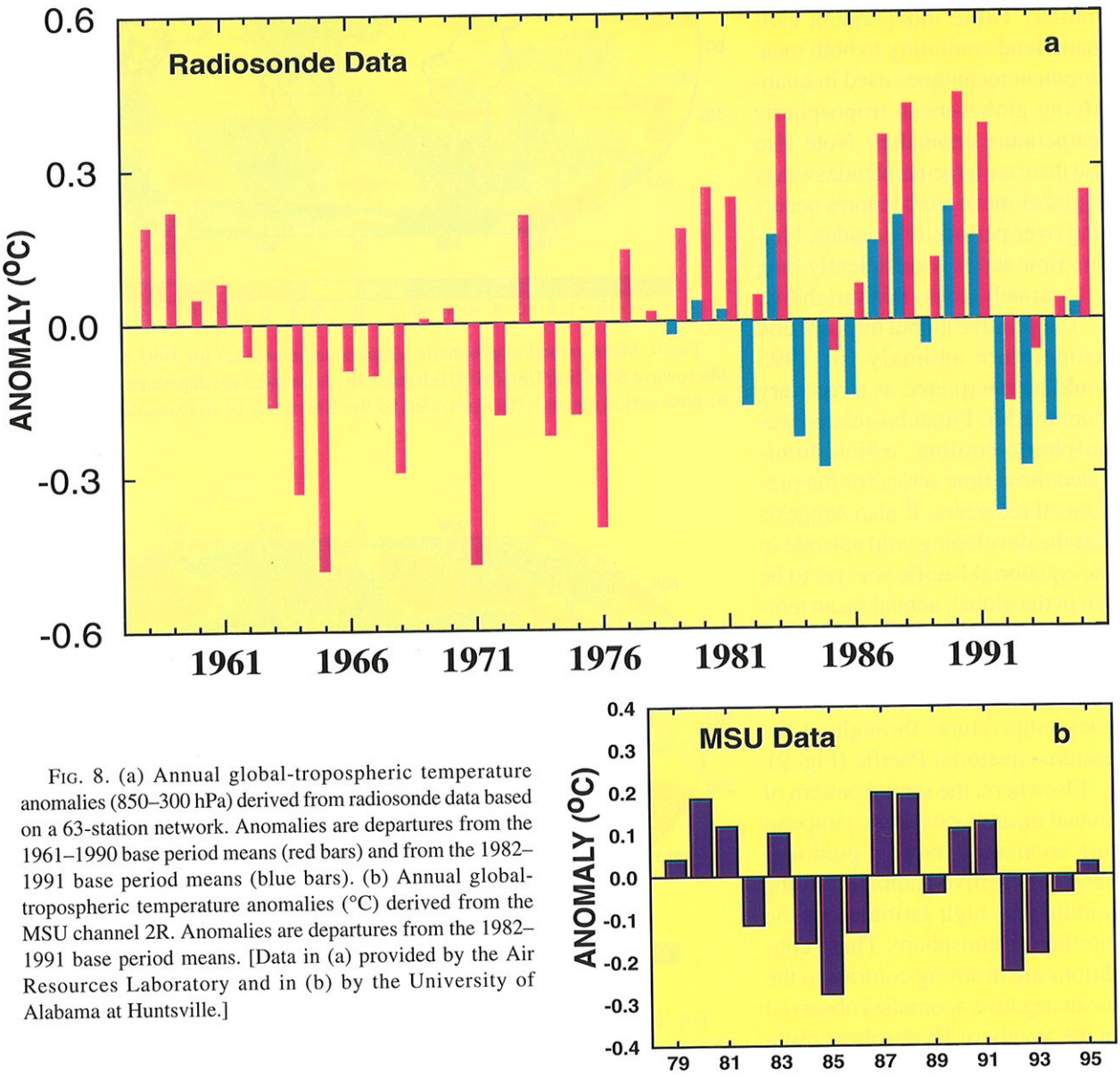


FIG. 8. (a) Annual global-tropospheric temperature anomalies (850–300 hPa) derived from radiosonde data based on a 63-station network. Anomalies are departures from the 1961–1990 base period means (red bars) and from the 1982–1991 base period means (blue bars). (b) Annual global-tropospheric temperature anomalies (°C) derived from the MSU channel 2R. Anomalies are departures from the 1982–1991 base period means. [Data in (a) provided by the Air Resources Laboratory and in (b) by the University of Alabama at Huntsville.]

calculated with respect to the 1982–91 period, show an annual global-mean anomaly of 0.03°C for 1995. This value is well below the magnitude of the positive anomalies experienced during the 1987–1991 period.

The radiosonde time series (red bars in Fig. 8a) appears to show substantially larger departures in tropospheric mean temperature than the MSU time series for the past two decades (Fig. 8b). However, these differences are largely attributed to the different base periods from which the anomalies are calculated. When the radiosonde and MSU anomalies are calculated from the same base period (1982–91), both time series (blue bars in Figs. 8a, b) become remarkably similar. These independent estimates lend credibility to both measurement techniques used in quantifying global-mean tropospheric temperature anomalies. Note also that there are large-amplitude swings in global-mean temperatures occurring over periods of decades. Neither time series is sufficiently long to accurately assess this variability.

The positive global tropospheric temperature anomaly for 1995 could be interpreted as a recovery from the Mt. Pinatubo-related tropospheric cooling, which dominated these time series for the previous three years. It also suggests that the developing cold episode in the equatorial Pacific was yet to be felt in the global, annual mean temperature. However, the influence of this cold episode is evident in the pattern of below-normal mean annual temperatures throughout the eastern equatorial Pacific (Fig. 9).

Elsewhere, the spatial pattern of annual mean tropospheric temperature anomalies shows a predominance of positive anomalies in the middle and high latitudes of the Northern Hemisphere. These conditions are in strong contrast to the mean negative anomalies observed in the Southern Hemisphere poleward of 30°S at most longitudes.

December 1995 featured a dramatic drop to below-normal global mean tropospheric temperatures (–0.23°C). This drop resulted from a pronounced shift to below-normal temperatures in the Northern Hemisphere extratropics (Fig. 10), and from a continued decrease in temperatures throughout the global tropics, presumably in association with a strengthening of cold episode conditions in the tropical Pacific.

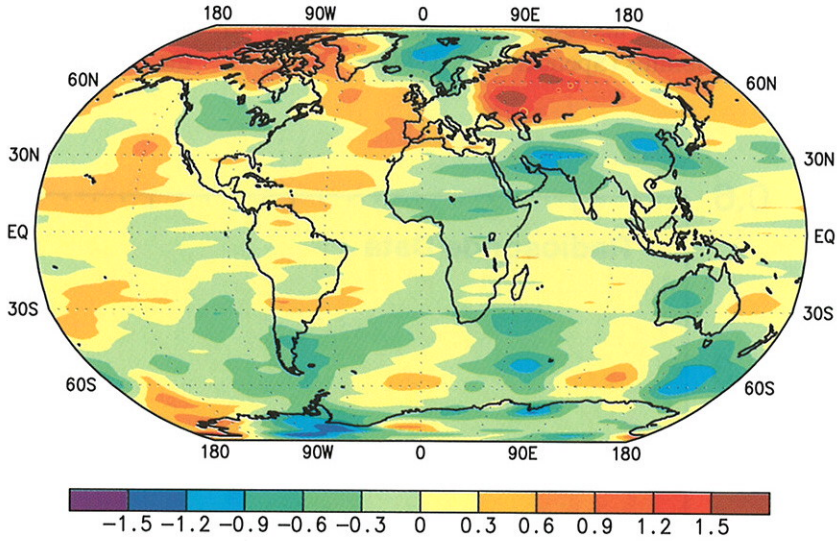


FIG. 9. Mean annual tropospheric temperature anomalies for 1995 derived from the Microwave Sounding Unit (MSU) channel 2R. Anomalies are departures from the 1982–91 base period means. (Data provided by the University of Alabama at Huntsville.)

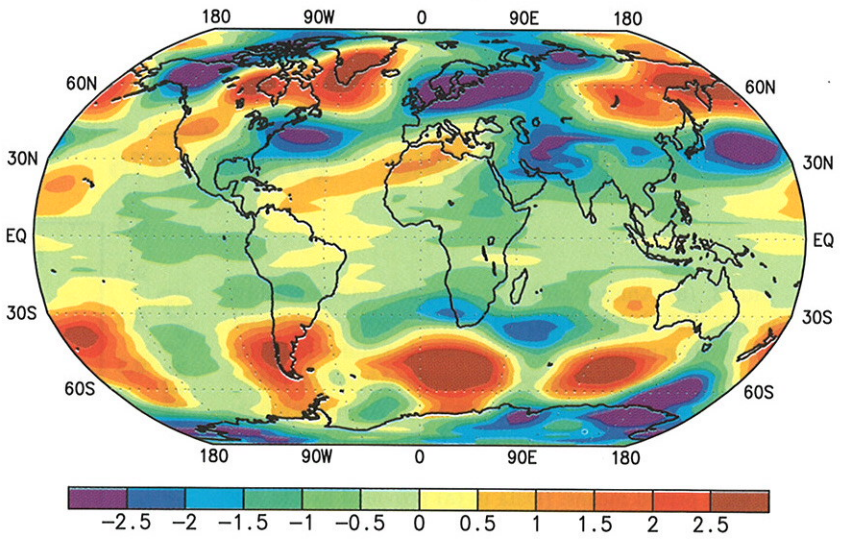


FIG. 10. December 1995 tropospheric temperature anomalies derived from the Microwave Sounding Unit (MSU) channel 2R. Anomalies are departures from the 1982–91 base period means. (Data provided by the University of Alabama at Huntsville.)

2) Lower stratospheric temperatures

Global lower-stratospheric temperatures are estimated from radiosonde observations (Fig. 11), satellite observations (Fig. 12), and analyses obtained from a global data assimilation system that utilize both sources of data (Fig. 13) (Kalnay et al. 1996). During 1995, all three analysis techniques showed a continuation of well below-normal temperatures in the lower stratosphere. The radiosonde estimate shows 1995 to be the coldest year in the 37-year record and the tenth out of the past eleven years with negative temperature anomalies (only 1992 had a positive anomaly). One difference in the relative behavior of the three time series is that the satellite derived anomalies show 1995 to be slightly warmer than 1994, whereas both the radiosonde-derived anomalies and the reanalyzed data obtained from the NCAR/NCEP Reanalysis Project (Fig. 13) show 1995 to be colder than 1994.

Both the satellite and Reanalysis time series also show pronounced warm periods during 1982/83 and 1991/92. These periods are also relatively warm in the radiosonde data (Fig. 11) and immediately follow the major volcanic eruptions of El Chichon (April 1983) and Mt. Pinatubo (June 1991), respectively. These eruptions contributed to markedly increased aerosol concentrations, resulting in elevated temperatures in the lower stratosphere. This is in contrast to the cooler-than-normal lower-stratospheric temperatures that would have been expected during the 1982/83 and 1991/92 ENSO episodes.

In the years following these eruptions stratospheric temperatures decreased to lower values than were observed prior to the volcanic eruptions (Figs. 11, 12, and 13). One possible explanation for this decrease is that the increased aerosol concentrations in the stratosphere contribute to a decrease in ozone, and subsequently to a cooling in that region. Ozone depletion would be expected to continue after a volcanic eruption until aerosol concentrations return to normal. Thereafter, a gradual increase in ozone and temperature would be expected.

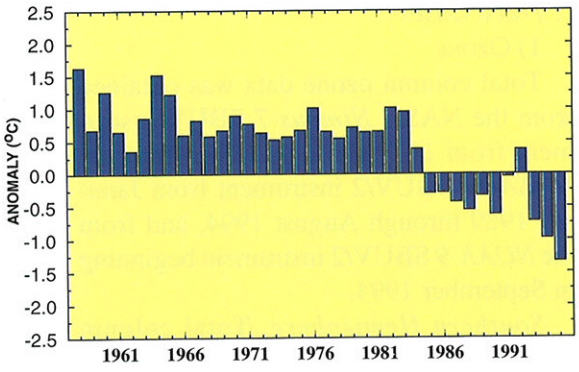


Fig. 11. Annual global-stratospheric temperature anomalies (100–50 hPa, in °C), derived from radiosonde data based on a 63-station network. Anomalies are departures from the 1982–91 base period means. (Data provided by the Air Resources Laboratory.)

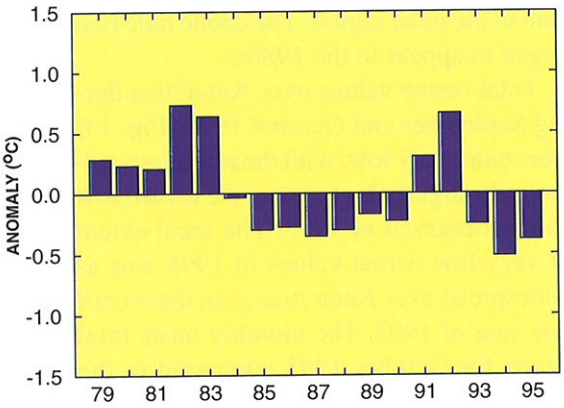


Fig. 12. Annual global-stratospheric temperature anomalies (°C) derived from the MSU channel 4. Anomalies are departures from the 1982–91 base period means. (Data provided by University of Alabama at Huntsville.)

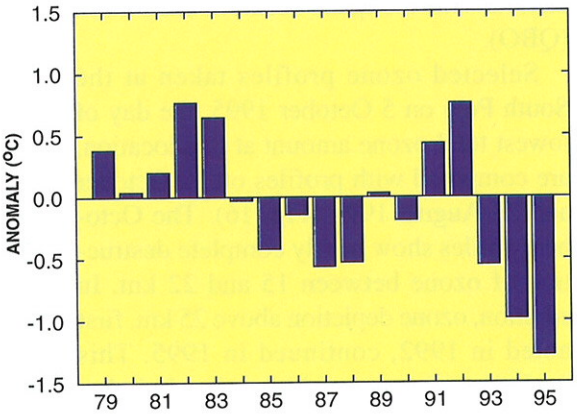


Fig. 13. Annual global 50-hPa temperature anomalies (°C) derived from the NCAR/NCEP reanalysis data set. Anomalies are departures from the 1982–91 base period means. (Source: CPC)

c. Trace Gases

1) Ozone

Total column ozone data was obtained from the NASA *Nimbus-7* SBUV instrument from 1979 through 1988, from the *NOAA-11* SBUV/2 instrument from January 1989 through August 1994, and from the *NOAA-9* SBUV/2 instrument beginning in September 1994.

Southern Hemisphere. Total column ozone concentrations exhibit a well-defined annual cycle in the Southern Hemisphere, with lowest values observed during September and October. It is during these two months that the well-known "ozone hole," denoted by total ozone concentrations less than 220 Dobson Units (DU), is most evident in the polar region. The ozone hole first began to appear in the 1980s.

Total ozone values over Antarctica during September and October 1995 (Fig. 14) were extremely low, with the minimum values only slightly higher than the record low values observed in 1993. The areal extent of very low ozone values in 1995 was as widespread over Antarctica as in the record low year of 1993. The monthly mean total ozone for October 1995 compared to the 1979–86 October mean values (Fig. 15) indicates decreases of 20% to 50% over a large portion of Antarctica. Conversely, small percent increases during October 1995 are evident over some areas of the tropics and midlatitudes, probably in association with the quasi-biennial oscillation (QBO).

Selected ozone profiles taken at the South Pole on 5 October 1995, the day of lowest total ozone amount at this location, are compared with profiles on 12 October and 23 August 1993 (Fig. 16). The October profiles show nearly complete destruction of ozone between 15 and 22 km. In addition, ozone depletion above 25 km, first noted in 1992, continued in 1995. This depletion of ozone at higher levels is believed to be related to increases in chlorine.

Temperatures in the lower stratosphere are closely coupled to ozone through dynamics and photochemistry. Extremely low stratospheric temperatures (less than -78°C)

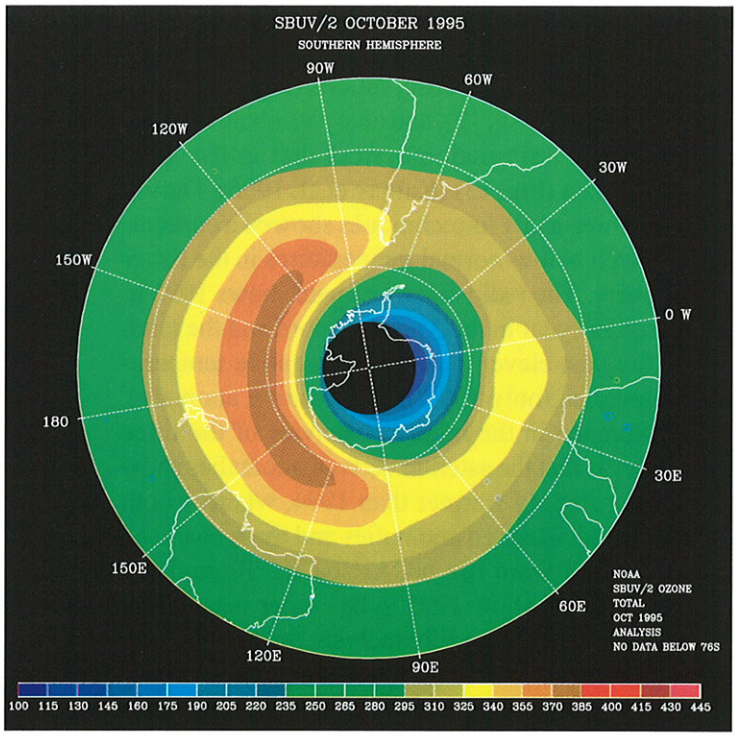


Fig. 14. Monthly mean total ozone for October 1995. Areas of total ozone less than 220 DU (ozone hole) are shown in blue. Regions of no data are shown in black. (Source: CPC)

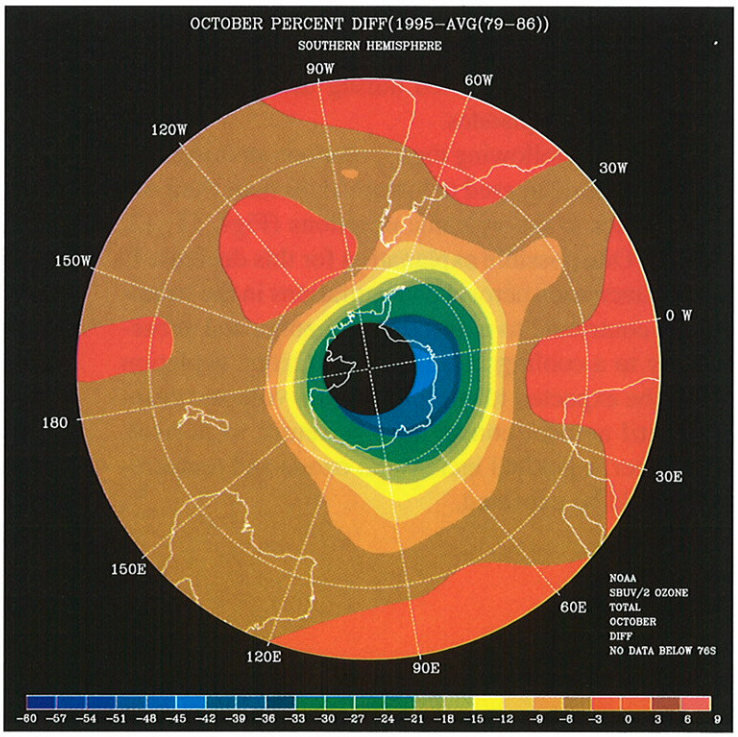


Fig. 15. Total ozone percent difference between October 1995 and the October 1979–86 base period means. Regions of no data are shown in black. (Source: CPC)

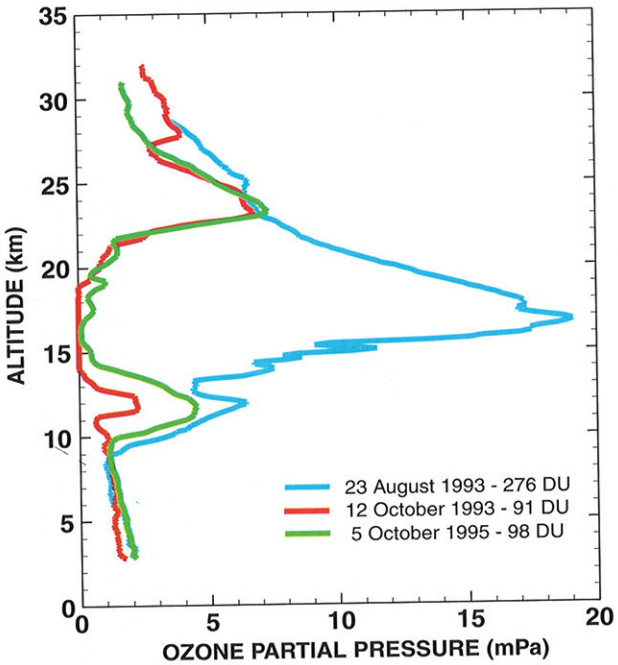


FIG. 16. Ozone profile (partial pressure, mPa) measured by balloon-borne ozonesonde at the South Pole on 5 October 1995 (green line), and comparison to profiles measured in 1993. (Source: CPC)

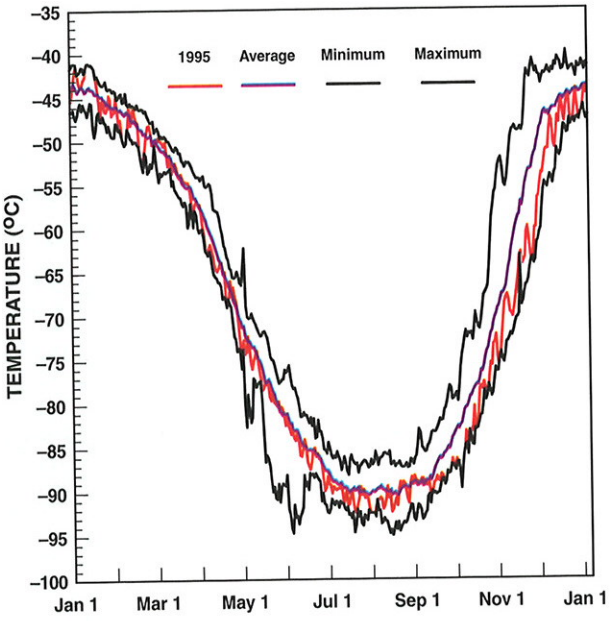


FIG. 17. Daily minimum temperatures at 50-hPa (19 km) in the region 65°S to 90°S for 1995 (red line). Mean daily values for the period 1978–94 are shown in blue. Daily extreme maxima and minima for any year are also shown (black lines). (Source: CPC)

over the Antarctic region are believed to lead to ozone depletion, in that they contribute to the presence of polar stratospheric clouds. These clouds enhance the production and lifetime of reactive chlorine, which leads to ozone depletion.

Daily minimum temperatures over the polar region (65°S–90°S) at 50 hPa (approximately 19 km) (Fig. 17) indicate that temperatures were substantially below normal during the Southern Hemisphere winter and spring seasons. These temperatures were sufficiently low to allow for polar stratospheric clouds and enhanced ozone depletion. Temperature anomalies for the 100–50 hPa layer, derived from radiosonde data (Fig. 18), also indicate record low temperatures during September–November 1995. These low values are consistent with an overall trend toward colder temperatures in the lower stratosphere observed since the late 1960s.

Northern Hemisphere. Total column ozone values in the Northern Hemisphere are generally lowest during the January-March period. In the middle and high latitudes, total column ozone values during January–March 1995 were 10%–20% lower than was typically observed during the late 1970s and early 1980s. In these regions, a decrease of 2%–4% per decade in total ozone is evident.

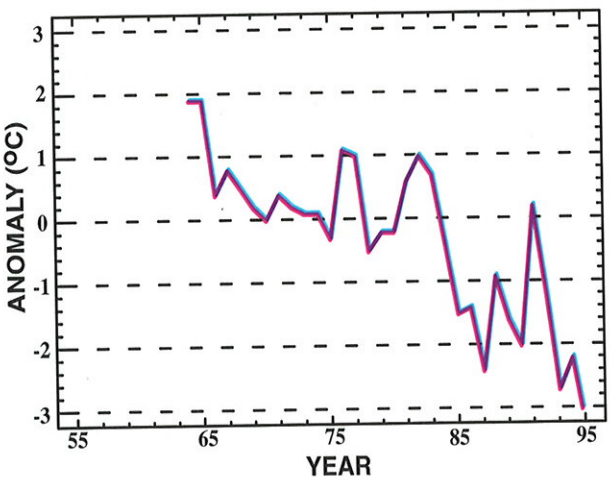


FIG. 18. Southern Hemisphere 100–50 hPa average temperatures anomalies (°C) for September–November. Anomalies are departures from the 1964–90 base period means. (Data provided by the Air Resources Laboratory.)

Monthly mean total ozone amounts for March 1995 (Fig. 19) indicate very low ozone totals over the polar region extending from north-central Siberia to northern Greenland. In these regions, the total ozone concentration is more than 40% below the values observed in 1979 (Fig. 20). However, it should be noted

that regional variations in total ozone in the Northern Hemisphere are highly variable from one year to the next, and tend to be strongly associated with the existing planetary-scale circulation features.

2) Carbon Dioxide

The atmospheric carbon dioxide (CO_2) measurements made at Mauna Loa Observatory, Hawaii, since 1958 provide strong evidence for human alteration of the environment (Fig. 21). The data through 1973 are from Keeling et al. (1982), while data since 1973 are from the NOAA program (Thoning et al. 1989).

Mauna Loa Observatory, located at an elevation of 3350 m on the flank of Mauna Loa volcano, is an ideal site for carbon dioxide measurements. There is no nearby vegetation and the prevailing nighttime downslope winds give a representative sampling of mid-tropospheric air from the central North Pacific Ocean. As such, the record is a reliable indicator of long-term carbon dioxide growth.

The average ozone concentration increase at Mauna Loa during the 1980s was about 1.4 ppm per year, but with significant year-to-year variability in this growth rate. In 1992–93, the growth rate decreased to near 0.5 ppm per year. However, it increased to more than 2 ppm per year during the last year. Contributing factors to these variations in growth rate include ENSO and the natural exchange of carbon dioxide by the oceans and/or the terrestrial biosphere with the atmosphere. The global temperature decrease resulting from the eruption of Mt. Pinatubo in mid-1991 may also have contributed to the slower growth rate during 1992–93.

3) Methane

Globally averaged methane mixing ratios are collected approximately weekly from various sites in the NOAA/CMDL cooperative air sampling network (Dlugokencky et al. 1994). Air sampling sites are distributed between 90°S and 82°N. The average increase in the glo-

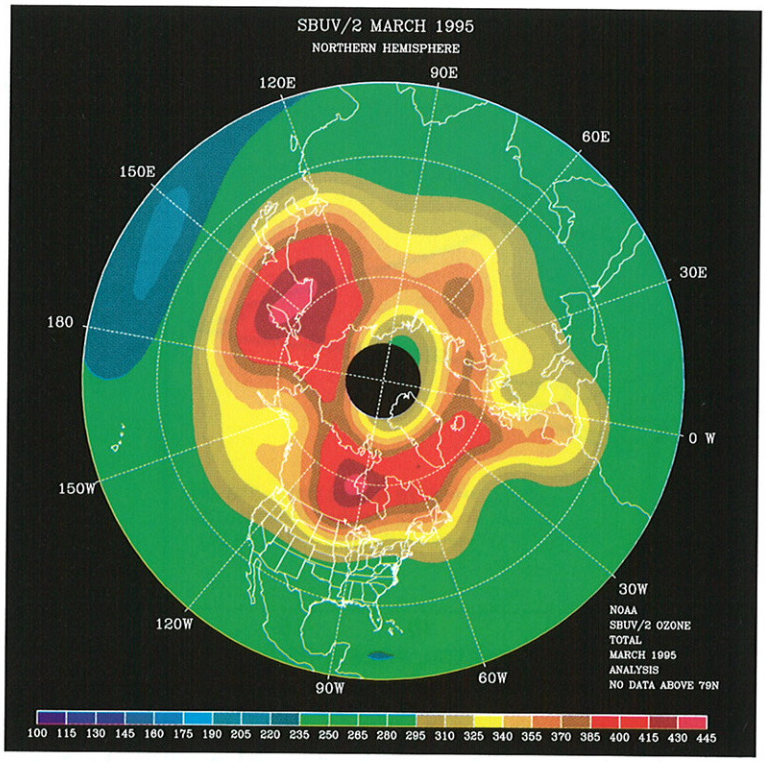


Fig. 19. Monthly mean total ozone for March 1995. Regions with no data are shown in black. (Source: CPC)

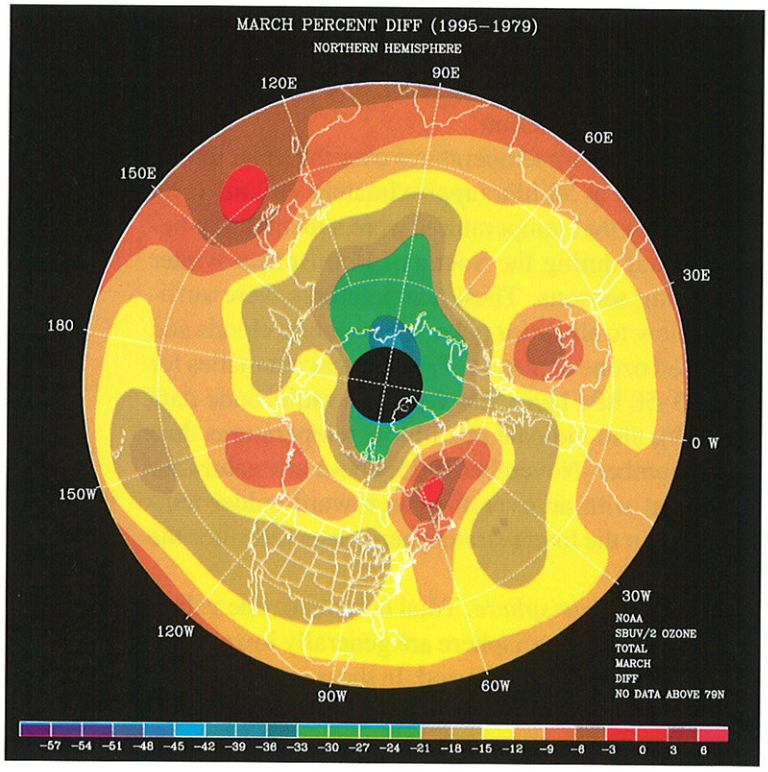


Fig. 20. Total ozone percent difference between March 1995 and the March 1979–86 base period means. Regions with no data are shown in black. (Source: CPC)

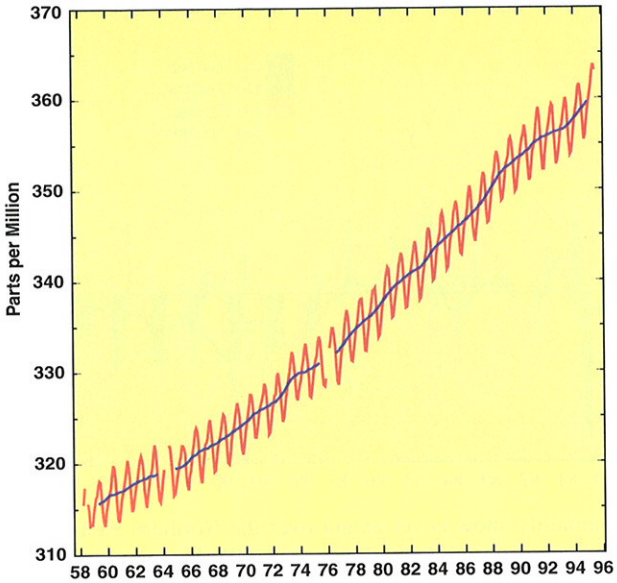


FIG. 21. Monthly mean (red line) carbon dioxide concentrations (ppm) measured at Mauna Loa, Hawaii. Blue line is the twelve-month running mean. The data through 1973 are from C. D. Keeling at Scripps Institute of Oceanography. (Data provided by the Climate Monitoring and Diagnostics Laboratory.)

bally-averaged methane mixing ratio over the period 1983–93 is approximately 0.6% per year, when referenced to the middle of the sample record (Fig. 22). The growth of methane over the past few years has slowed, probably due to a change in the anthropogenic source (Dlugokencky et al. 1994). However, the strong decrease in growth observed during 1992 and 1993 may have been associated with the eruption of Mt. Pinatubo in June 1991.

Increased methane affects the Earth's radiation balance and the chemistry of the atmosphere. While the major sources of methane have been identified, their absolute contributions to the global methane budget remain poorly quantified. Until a better understanding of the methane budget is realized, the exact causes of the observed increase will remain uncertain.

d. Northern Hemisphere Snow Cover

A predominance of below-normal snow coverage in the Northern Hemisphere during the first part of the year, and above-normal snow coverage during the latter part of the year (Fig. 23), resulted in near-normal annual mean snow cover during 1995 (25×10^6 km^2). The coincidence of near-normal snow coverage with near-record land surface temperatures (see Fig. 1) is in marked contrast to the record warm year of 1990, which had the least snow cover in the satellite record. This observation suggests that there is no simple relationship between Northern Hemisphere snow cover area and annual hemispheric mean temperature.

The first half of 1995 was marked by considerable month-to-month variability in snow cover. Most notably, considerably below-normal snow coverage was observed during February and March 1995, while considerably above-normal snow cover developed during April, mostly over North America. This heavy April snow cover brought North American values of mean spring snow cover to above normal for the first time in a decade (Fig. 24a). In contrast, below-normal snow cover dominated Eurasia during March–May (Fig. 24b), in association with significantly warmer-than-normal conditions throughout the central and northern sectors (see Section 4b). Snow cover during April was extremely low across central and northern Eurasia (see Fig. 51). These conditions extended the prolonged period of below-normal snow cover and above-normal surface temperatures that had dominated Eurasia since the late 1980s.

In contrast to the first part of the year, the last five months of 1995 showed above-normal snow cover over the Northern Hemisphere (Fig . 23) This is the first consecutive 5-month period since 1985 in which

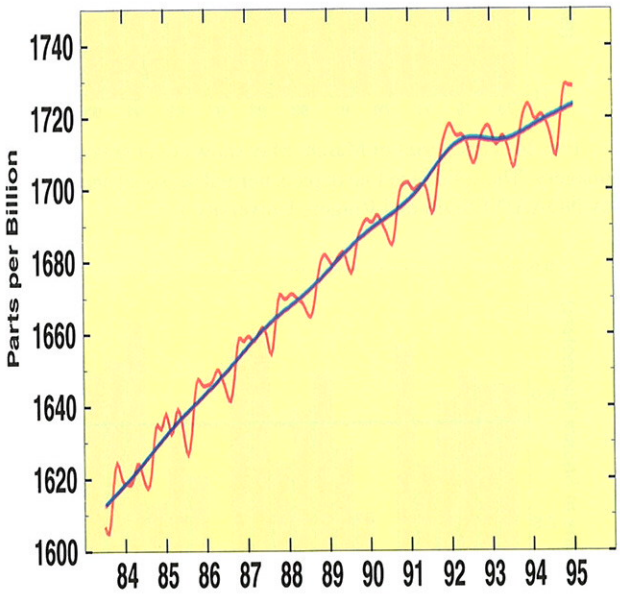


FIG. 22. Globally averaged, biweekly methane mixing ratios (ppb) by volume (red curve) determined from the NOAA/CMDL Carbon Cycle Group cooperative air sampling network. Solid blue line shows the growth with the seasonal cycle removed. (Data provided by the Climate Monitoring and Diagnostics Laboratory.)

above-normal snow cover was recorded. During September–November (SON) above-normal snow cover dominated both North America (Fig. 25a) and Eurasia (Fig. 25b). This increased snow cover was associated with abnormally cold temperatures that developed in both regions, particularly during the latter months of the year. Snow cover across North America during SON has been above normal four of the past five years (Fig. 25b).

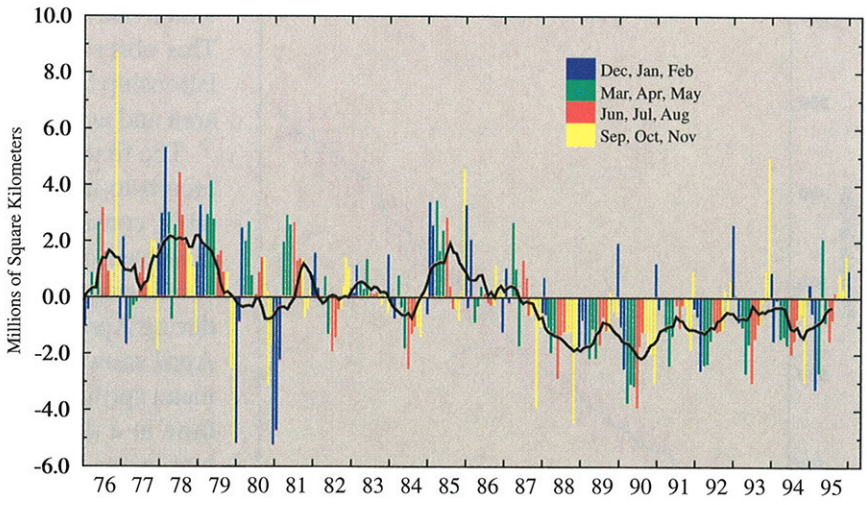


FIG. 23. Anomalies of monthly snow cover extent over the Northern Hemisphere (including Greenland) between January 1976 and December 1995. Smoothed curve is a twelve-month running mean. Anomalies are departures from the 1972–95 base period means. (Data provided by Rutgers University.)

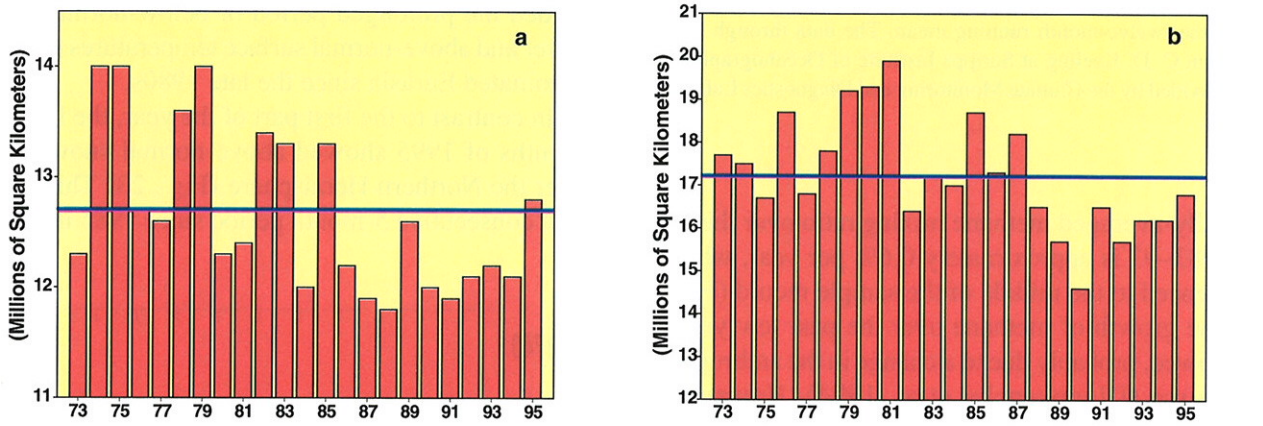


FIG. 24. Time series of March–May snow cover area (10^6 km²) for (a) North America and (b) Eurasia estimated from visual satellite imagery. The solid blue line depicts normal seasonal snow cover area. Note the change in vertical scale between plots. (Data provided by NOAA/NESDIS and Rutgers University.)

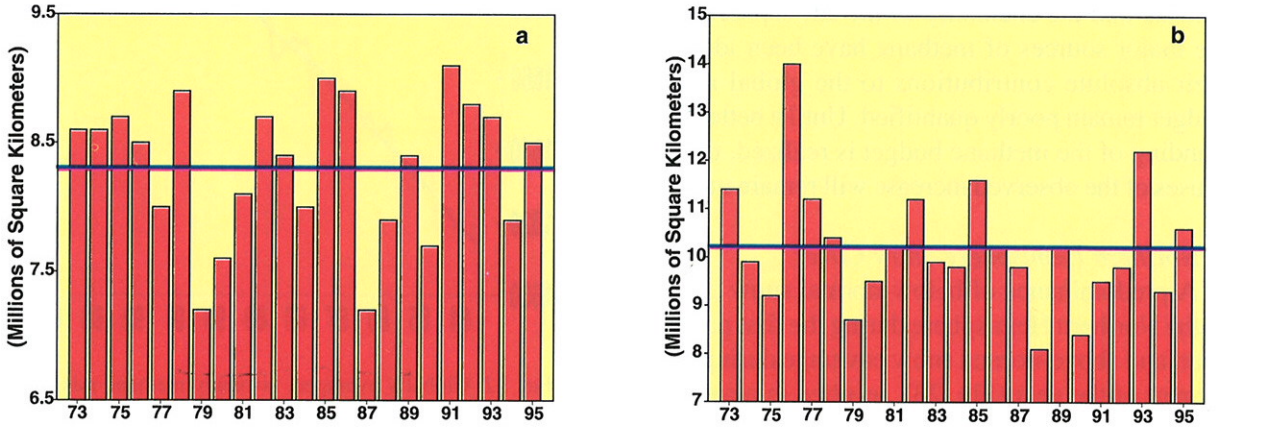


FIG. 25. Time series of September–November snow cover area (10^6 km²) for (a) North America and (b) Eurasia estimated from visual satellite imagery. The solid blue line depicts normal seasonal snow cover area. Note the change in vertical scale between plots. (Data provided by NOAA/NESDIS and Rutgers University.)

3. The evolution of recent oceanic and atmospheric anomalies in the global tropics

a. Large-scale conditions in the tropics: 1990–94

The period 1990–94 featured persistent positive sea surface temperature (SST) anomalies in the central equatorial Pacific (Fig. 26) and was the warmest 5-year period on record for the tropical Pacific as a whole. Consistent with this pattern of anomalous SST, sea level pressure (SLP) was below normal over the east-central tropical Pacific and above normal over the eastern Indian Ocean, Indonesia, and northern Australia (Fig. 27). This anomalous pressure pattern reflected a prolonged negative phase of the Southern Oscillation, as defined by the Southern Oscillation Index (SOI) (Fig. 28). Also observed during the period was a persistent pattern of weaker-than-normal low-level easterlies (westerly anomalies) throughout most of the equatorial Pacific (Fig. 29) and enhanced convection over the central equatorial Pacific (Fig. 30).

Collectively, these conditions reflected one of the most prolonged periods of warm El Niño–Southern Oscillation (ENSO) conditions of the century. By some measures, this five-year period is unprecedented (Trenberth 1995). However, according to the SOI and SST data, there is at least one other period during this century, and possibly a few others in the latter half of the nineteenth century, that featured similar, although somewhat shorter, prolonged warm (ENSO) episode conditions. The period 1911–15 appears to be most similar to the recent period, with 1911, 1912, and 1914 considered El Niño years.

Mature-phase warm-episode conditions occurred during late 1991 through mid-1992, during the first half of 1993, and from late 1994 through early 1995. During these periods, atmospheric convection was greatly enhanced over the central equatorial Pacific, the South Pacific Convergence Zone was displaced north and east of its normal position, the Intertropical Convergence Zone was shifted equatorward from its normal position in the Northern Hemisphere, and drought conditions affected northeast Australia and southeast Africa. Interestingly, near-normal conditions prevailed in the tropical Pacific during the Northern Hemisphere 1993/94 winter.

Also during 1990–94, above-normal SLP dominated the subtropical North and South Atlantic Oceans, and the high latitudes of the Southern Ocean in the east-Pacific sector, while below-normal pressure dominated the high latitudes of the Northern Hemisphere and the midlatitudes of the Southern

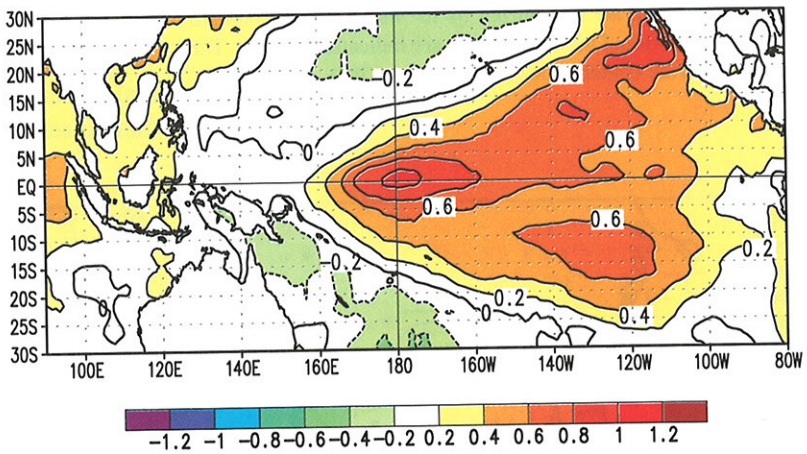


FIG. 26. Sea surface temperature (SST) anomalies for 1990–94. Contour interval is 0.2°C. Anomalies are departures from the 1950–79 base period means. (Source: CPC)

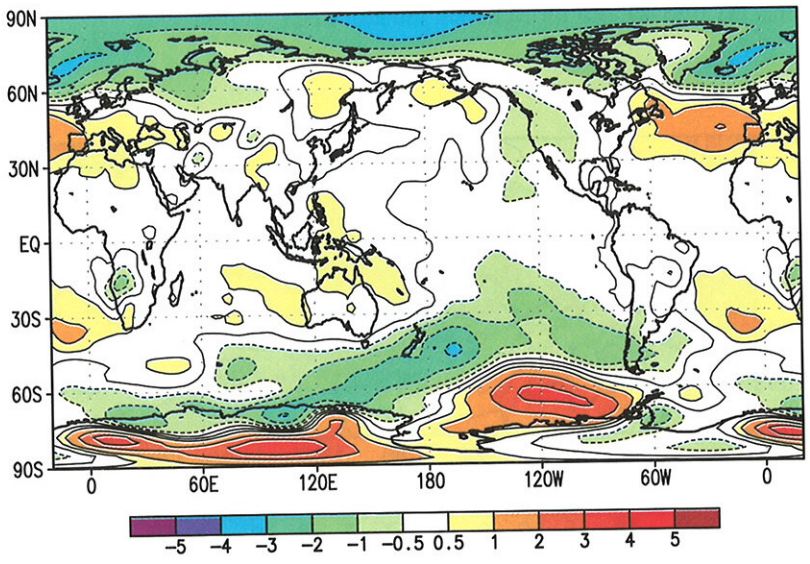


FIG. 27. Sea level pressure (SLP) anomalies for 1990–94. Contour interval is 0.5 hPa. Anomalies are departures from the 1985–89 base period means. (Source: CPC)

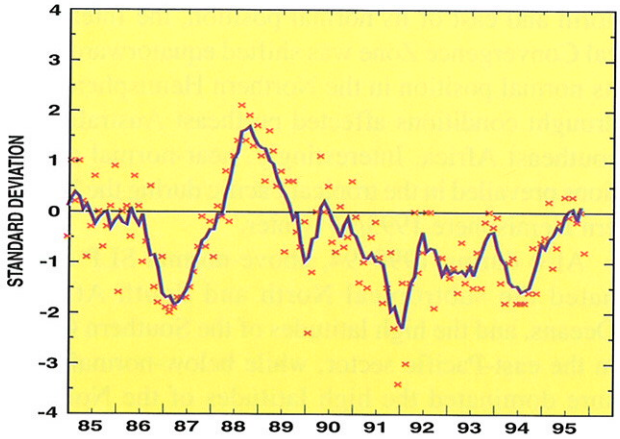


FIG. 28. Five-month running mean of the Southern Oscillation Index (SOI). Anomalies are departures from the 1951-1980 base period means and are normalized by the mean annual standard deviation. Individual monthly values are indicated by "x"s. The x-axis labels are centered on July. (Source: CPC)

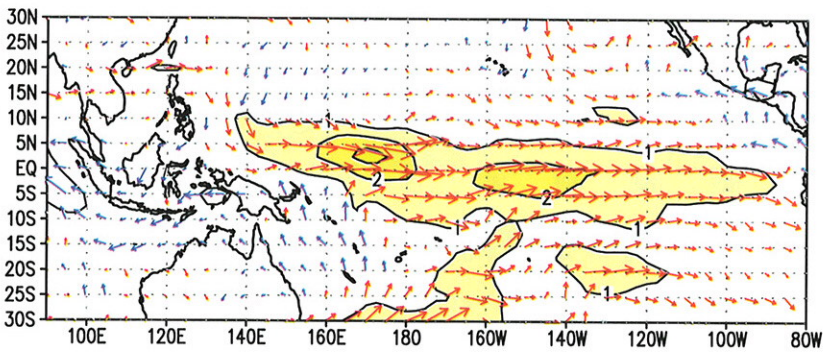


FIG. 29. Anomalous 850-hPa wind for 1990–94. Contour interval is 1 m s^{-1}. Red (blue) vectors indicate anomalous westerlies (easterlies). Anomalies are departures from the 1985–89 base period means. (Source: CPC)

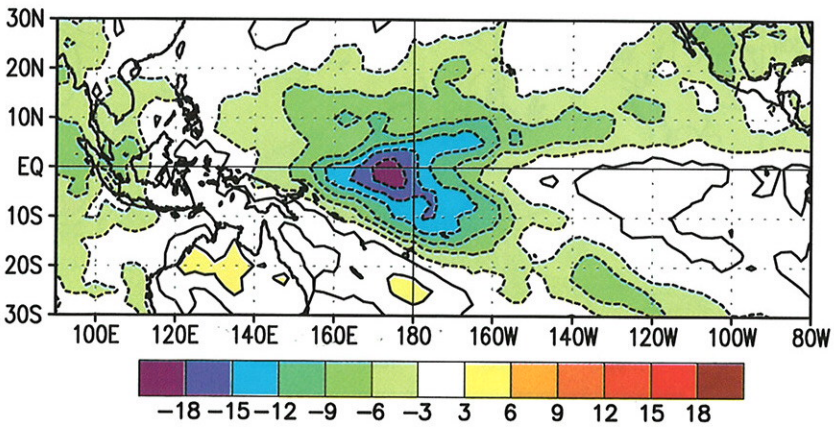


FIG. 30. Outgoing longwave radiation anomalies for 1990–94. Contour interval is 3 W m^{-2}. Anomalies are departures from the 1979–88 base period means. (Source: CPC)

Hemisphere (Fig. 27). The anomalous pressure pattern over the North Atlantic reflects a persistent positive phase of the North Atlantic Oscillation (NAO), which contributed to above-normal temperatures over Europe and western Russia during the period. The anomalous SLP pattern to the west and southwest of South America, reflects a greater-than-normal frequency of blocking episodes.

b. The 1994–95 Warm (ENSO) Episode

Mature ENSO conditions redeveloped during late 1994 for the third time in five years. This frequency of occurrence is unprecedented in the last 50 years and is comparable to that observed during the prolonged 1911–15 ENSO episode.

The 1994–95 warm episode showed signs of development as early as March–May 1994, when the equatorial low-level easterlies again became weaker than normal across the Pacific and the SOI decreased to −1.5 (Fig. 28). During May, positive SST anomalies reappeared along the equator near the date line, and the equatorial easterlies weakened further. These conditions continued to intensify during June-August 1994, as positive SST anomalies spread eastward across the central equatorial Pacific and were greater than +1.0°C along the equator between 170°E and 160°W.

During September–November, the positive SST anomalies continued to strengthen, and averaged greater than +2.0°C between the date line and 160°W. This increase was accompanied by a further weakening of the low-level equatorial easterlies over the central equatorial Pacific, particularly during late September and most of October. At times, the 850-hPa winds were nearly calm or even westerly during this period, especially over the central Pacific near the date line.

This evolution culminated in the onset of mature warm-episode conditions during December 1994–January 1995. At that time SST anomalies reached +2°C in portions of the central equatorial Pacific (Fig. 31a) and convection was

greatly enhanced in the vicinity of the anomalously warm water (Fig. 32a). Anomalous anticyclonic circulation centers developed in the upper troposphere to the north and to the south of the enhanced convection, and the midlatitude westerlies were enhanced over the North and South Pacific. This enhancement and eastward extension of the North Pacific jet stream during the period was associated with a series of intense extratropical storms that developed over the central North Pacific and then proceeded to strike the southwest coast of the United States, resulting in abnormally heavy precipitation over large portions of California and the Southwest (see Section 4a).

c. The 1995 Pacific Cold Episode

The low-level equatorial easterlies returned to near-normal intensity during January and remained near normal through May. Enhanced easterlies then developed over the western equatorial Pacific in June and subsequently persisted through the end of the year. By November, these enhanced easterlies had also spread eastward, covering the central and east-central equatorial Pacific. Thus, for the first time since the 1988–89 cold episode, stronger than normal easterlies dominated the entire equatorial Pacific.

Accompanying this evolution in the low-level wind field, the positive SST anomalies across the eastern equatorial Pacific steadily decreased after January 1995 (Fig. 31). By March–May 1995 (Fig. 31b), below-normal SSTs had developed from 120°W to the South American coast, and the maximum positive anomalies in the central Pacific had weakened considerably. Coincident with these changes, atmospheric convection returned to normal over the central equatorial Pacific, indicating the end of the 1994–95 period of mature ENSO conditions (Fig. 32b).

During JJA 1995 below-normal SSTs were observed from 160°W east-

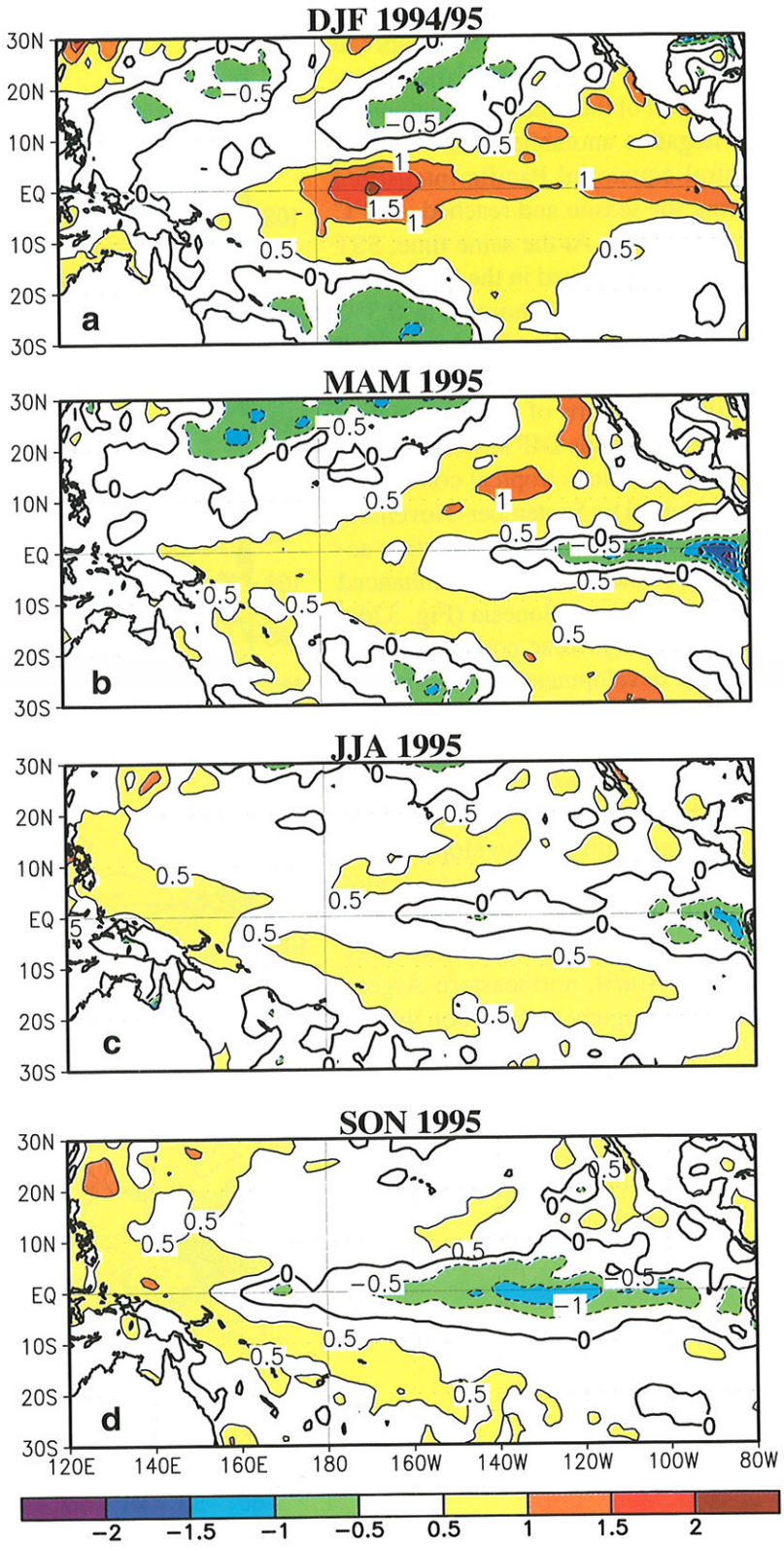


FIG. 31. Sea surface temperature (SST) anomalies for (a) DJF 1994/95, (b) MAM 1995, (c) JJA 1995, and (d) SON 1995. Contour interval is 0.5°C. Anomalies are departures from the 1950–79 adjusted OI climatology (Reynolds and Smith 1995).

ward to the South American coast (Fig. 31c). By September–November, the area of below-normal SSTs spread westward to 160°E (Fig. 31d), and expanded off of the equator. Additionally, the negative anomalies over the east-central equatorial Pacific intensified during the season and reached −1.0°C in many areas. At the same time, SST anomalies increased in the far western Pacific with SSTs more than 0.5°C above normal evident between 120°E and 150°E. Associated with this reversal in the pattern of SST anomalies from the previous DJF season, the pattern of anomalous tropical convection also reversed by September–November 1995, with suppressed convective activity near the date line and enhanced convection over Indonesia (Fig. 32d).

Collectively, these conditions indicated the development of a Pacific cold episode and reflected a dramatic change in the atmospheric and oceanic conditions from those which had dominated the Pacific sector since late 1990. Associated with the development of cold-episode conditions, observed global anomalies during 1995 included 1) drier-than-normal conditions over southern Brazil, northeastern Argentina, and Uruguay (see section 4c), 2) wetter-than-normal conditions over southeastern Africa (see section 4e), 3) enhanced hurricane activity in the tropical Atlantic (see section 4a), and 4) a stronger-than-normal Indian monsoon (see section 4b).

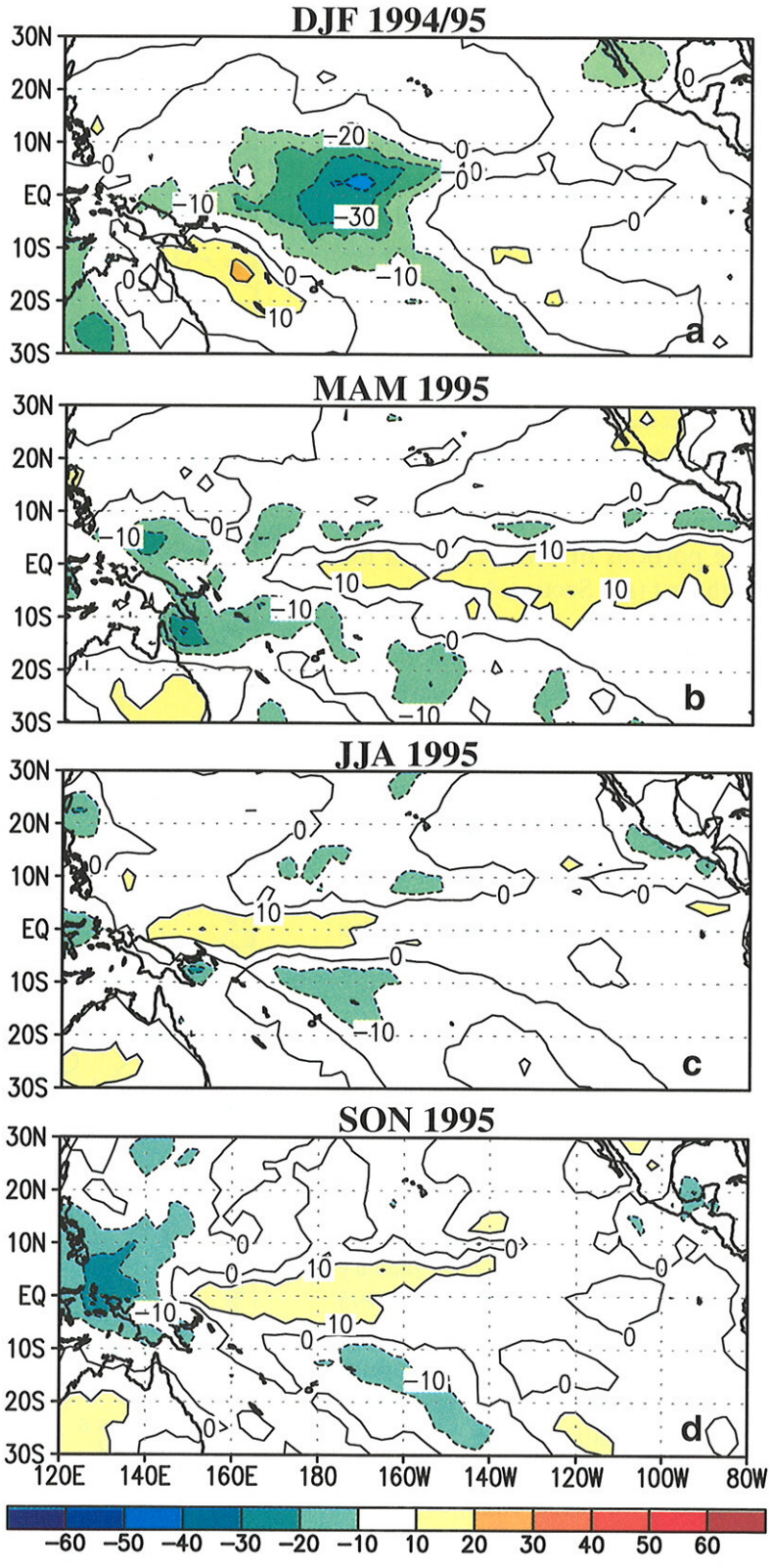


FIG. 32. Outgoing longwave radiation (OLR) anomalies for (a) DJF 1994/95, (b) MAM 1995, (c) JJA 1995, and (d) SON 1995. Contour interval is 10 W m^{-2}. Negative OLR anomalies are indicative of enhanced tropical convection. OLR anomalies are departures from the 1979–88 base period means. (Source: CPC)

4. Regional climate highlights

a. North America

1) December 1994–January 1995: Wet in western U.S., warm in East

The 1994/95 winter season brought abnormal weather conditions to large portions of North America. These conditions were particularly acute from mid-December 1994 through the end of January 1995. California and much of the western and southwestern United States received significantly above-normal precipitation during the period, while both the western United States and the eastern half of North America experienced record or near-record warmth. These conditions are attributed to a persistent and abnormal atmospheric circulation (Fig. 33), characterized in the West by below-normal upper-air heights and surface pressure and a southward shift of the jet stream, and in the East by above-normal upper-air heights and surface pressure and a northward shift of the jet stream (Figs. 33, 34).

In the West, this circulation was associated with an eastward extension of the jet core from Asia to central California. This jet stream served as a "duct" for major storm systems which were directed across the Pacific and into California, thus producing excessive precipitation and flooding throughout the state. During January, this jet core and storm track were displaced south of their normal location by approximately 18° latitude in the vicinity of the West Coast.

Farther east, the polar jet stream was shifted northward to south of James Bay, approximately 15° latitude north of normal. This flow pattern prevented the normal build up of cold air over central and western Canada and also tended to direct any cold-air masses quickly across eastern Canada and then out over the western Atlantic. These conditions, in combination with abnormally strong southwesterly flow farther south, brought extreme warmth to the eastern half of the United States and much of southern Canada during the period.

This circulation pattern reflected the most pronounced negative phase of the Tropical/Northern Hemisphere (TNH) teleconnection pattern in the historical record dating back to 1964. A negative TNH pattern is common during the mature phase of warm El Niño/Southern Oscillation (ENSO) episodes (Mo and Livezey 1986). Thus, the establishment of this pattern during the 1994/95 winter season, a period dominated by mature-phase, warm ENSO conditions (see section 3), was not unusual. Recent studies (Bell and Kousky 1996) indicate a strong linkage between the occurrence of mature ENSO conditions during the 1994/95 winter and the highly anomalous circulation features observed throughout the North Pacific and North American sectors.

In the western United States the bulk of the annual precipitation falls during the October–April wet season. During the past 10 years, below-normal precipitation has been observed over much of the region. In

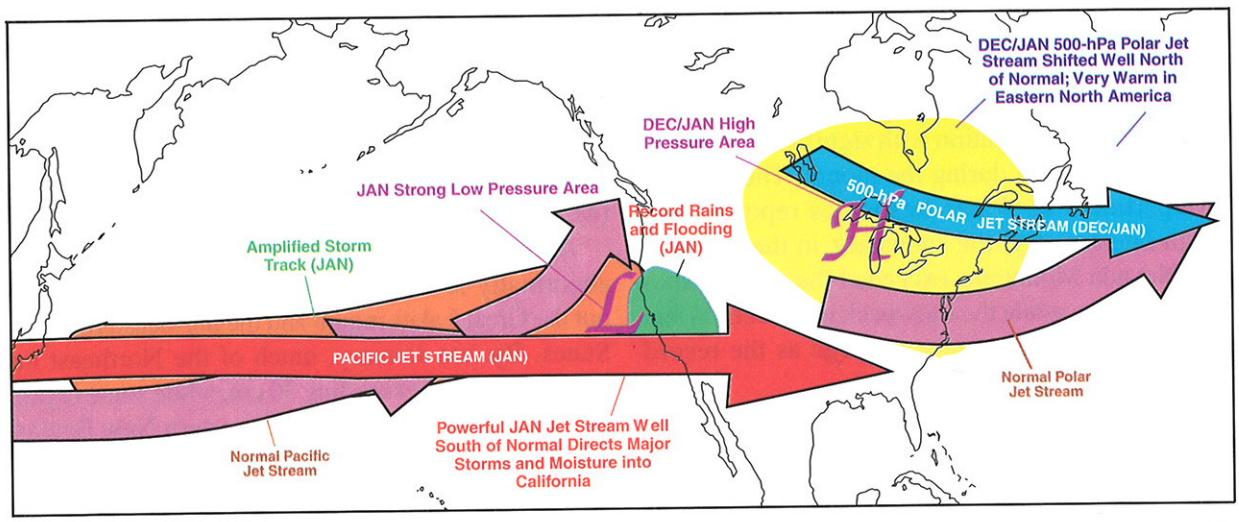


Fig. 33. Large-scale circulation features affecting the North Pacific and North America during December 1994–January 1995. The two dominant features for both months, the abnormal northward shift in the jet stream over eastern North America and the southward migration of the jet stream near the West Coast, signify a negative phase of the Tropical/Northern Hemisphere (TNH) pattern. (Source: CPC)

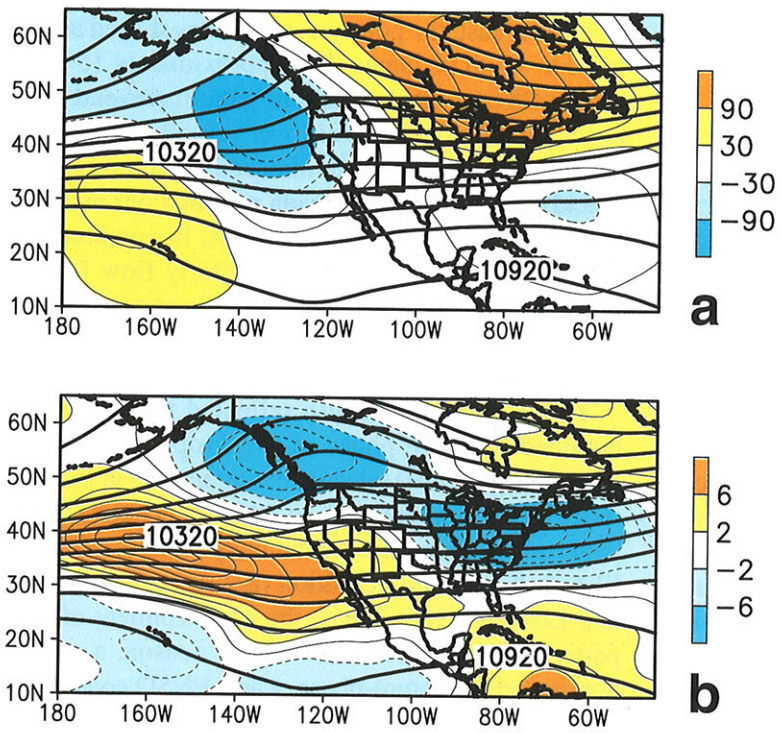


FIG. 34. December 1994–January 1995: (a) 250-hPa mean height (m) and anomaly (m, shaded) and (b) 250-hPa mean height (m) and zonal wind anomaly (m s^{-1}, shaded). Contour interval for heights (anomalies) in (a) is 120 m (30 m). Contour interval for the zonal wind anomalies in (b) is 2 m s^{-1}. Anomalies are departures from the 1979–95 base period means. (Source: CPC)

particular, the 1993/94 wet season was very dry throughout the West (Fig. 35a), so that by the beginning of the 1994/95 wet season, long-term drought was firmly entrenched throughout the region. These drought conditions lessened between October and December 1994 as near-normal precipitation covered the West, and they completely disappeared by the end of January 1995 in association with significantly above-normal precipitation during the month. The California Department of Water Resources reported that through late January, the snowpack in the northern Sierra Nevada Mountains exceeded the record January 1983 values, while the snowpack in the central and southern Sierras was almost as large as the record observed during January 1983.

According to the River Forecast Centers, the heaviest precipitation during January 1995 (950–1050 mm) fell on the southern Cascades, the northern Sierra Nevada, the windward slopes near Santa Rosa (north of San Francisco), and at Old Man Mountain near Santa Barbara (Fig. 35c). In southern California, intense periods of heavy rain and snow were observed during January, while farther north nearly continuous precipitation was observed. For example, most of northern and central California observed precipitation on all but 4–5 days during the month, and San Francisco established a new record for consecutive days with measurable precipitation during 1–16 January. Elsewhere, Mt. Shasta and Santa Rosa recorded precipitation for a record 29 days during January. In general, the excessive January precipitation, in conjunction with very heavy rainfall during March, brought October–April totals to near-normal or above-normal over most of Washington, Oregon, Idaho, Nevada, and California, with at least twice the normal seasonal total recorded in parts of southern California (Fig. 35b).

Farther east, unusually mild weather dominated eastern North America from November 1994 through January 1995 (Fig. 36). During this period, temperatures averaged 4°–5°C above normal over large portions of east-central Canada, and 2°–4°C above normal throughout the rest of east-central and southeastern Canada and the Great Lakes region. More than 250 record high temperatures were established across the northern and eastern sections of the United States during this 3-month period. According to the National Climatic Data Center, November–January statewide-average temperatures for 1994 /95 were the highest on record in New Hampshire and Vermont. Furthermore, it was one of the five warmest November–January periods in the 100 years of record in 14 other states [MD (2), NJ (2), NY (2), PA (2), RI (2), CT (3), OH (3), MA (4), MI (4), WI (4), KY (5), MN (5), VA (5), WV (5)].

Accompanying these extremely warm conditions, abnormally low snow cover was observed throughout the Great Lakes region and the northeastern United States. By late January, much of the Northeast had snowfall deficits exceeding 30 cm, while some regions of central New York and southwestern New England experienced 75–120 cm less than normal snowfall.

2) APRIL–MAY 1995: MIDWEST U.S. FLOODS

From early April through mid-June 1995, surplus precipitation covered much of the Midwest, the Plains states, and the lower Ohio Valley (Fig. 37a). The east-

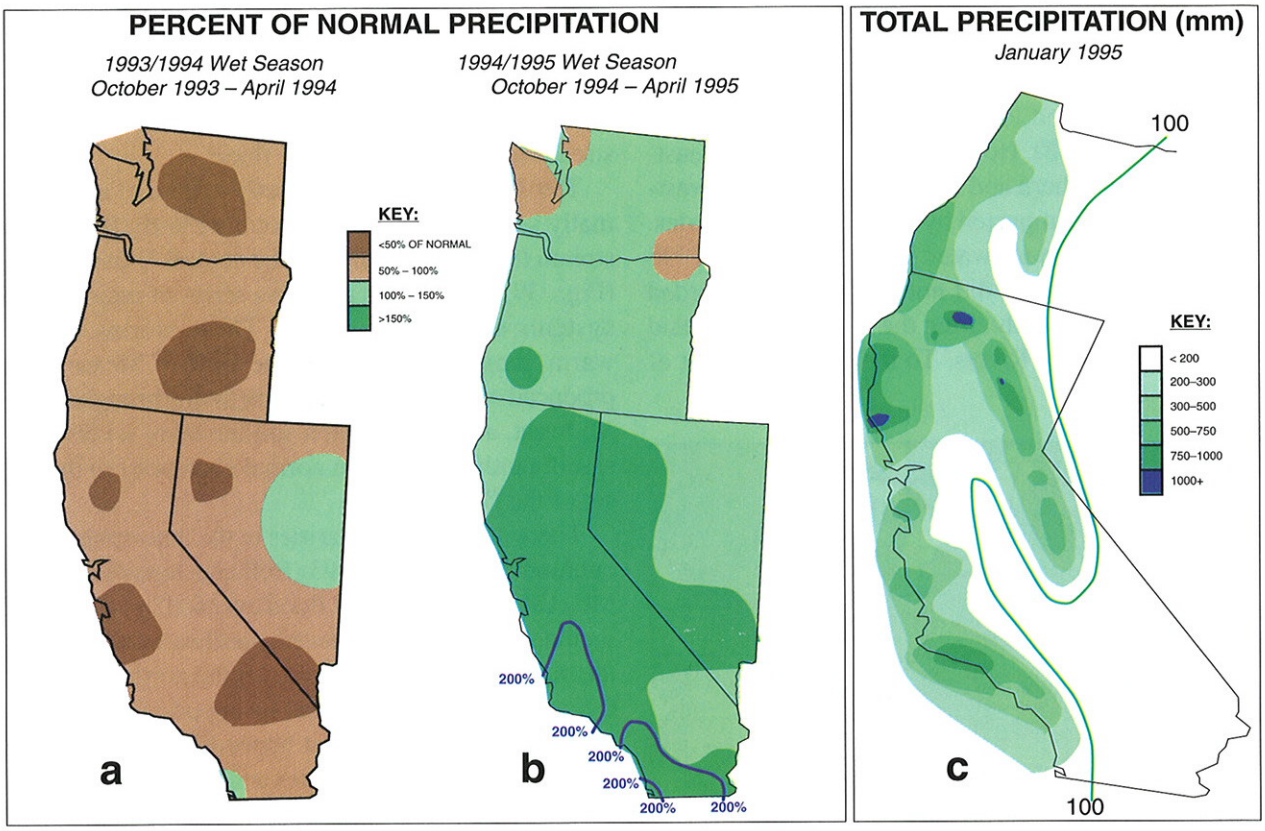


FIG. 35. Percent of normal precipitation for the (a) 1993/94 wet season, (b) the 1994/95 wet season, and (c) total precipitation (mm) during January 1995 from River Forecast Center reports. (Source: CPC)

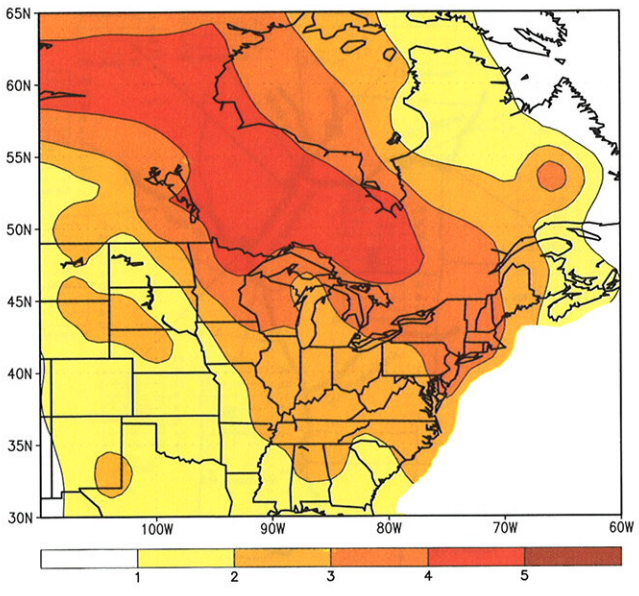


FIG. 36. Temperature anomalies during November 1994–January 1995 (°C). Anomalies are departures from the 1961–90 base period means. (Source: CPC)

ern Dakotas, the central Gulf Coast, and an area from central Kansas eastward to the western Ohio Valley received 2 to 3 times their normal precipitation for the period, with many sections receiving 450–750 mm of precipitation. The largest totals were observed in eastern Oklahoma and Kansas, southwestern and central Missouri, southern Illinois and Indiana, and central Kentucky. Despite some very large amounts, the areas receiving excessive precipitation were highly variable from one storm to the next and were stretched along an axis extending from the south-central Great Plains northeastward into the lower Ohio Valley. Most of the above areas also received surplus rains during the 1993 Midwest Flood (which peaked during July) (Fig. 37b), as did northern Missouri, Iowa, southern Minnesota, and the Dakotas. Indeed, 750–1000 mm of rain fell on some locations during the summer of 1993 as one major rainfall event after another affected the same regions.

Much of both the lower and middle Missouri and Mississippi and lower Ohio Rivers and their tributaries flooded at least briefly during April–June 1995

(Fig. 38). This area is primarily to the south and east of the regions most severely affected by river flooding in 1993, namely the middle and upper Mississippi and the middle and lower Missouri Rivers and their tributaries (Fig. 38). However, large portions of eastern Kansas, northern and central Missouri, and western Illinois were impacted by both flooding episodes.

Overall, maximum water levels during the 1995 flood approached, but did not reach, those recorded during the 1993 floods along the lower Missouri and middle Mississippi Rivers. To the north and west of this region, flooding was significantly more serious in 1993. Farther south and east, the Mississippi/Missouri confluence experienced significant flooding during 1995 and actually experienced near-normal streamflows during the 1993 flood.

The 1995 floods were directly related to an abnormally strong and persistent southwesterly flow at jet stream level (250 hPa) over the central United States (Figs. 39, 40a), which pushed a series of major storm systems across the country. These storms tapped warm, moist air from over the Gulf of Mexico and produced excessive precipitation totals throughout the Midwest, an area in which soil moisture levels were significantly higher than normal even prior to the onset of the floods.

There are many similarities in the atmospheric circulation between the 1993 (Bell and Janowiak 1995; Mo et al. 1995) and 1995 flood events (Fig. 40). These include 1) an ENSO-induced, southeastward shift of the mean jet stream position over the northern Pacific Ocean during the winter and spring prior to the onset of the events; 2) persistent upper-level troughs over both the western United States and the Canadian Maritime Provinces during the events; 3) an abnormally strong southwesterly flow at jet stream level through the middle of the country during the events, along with

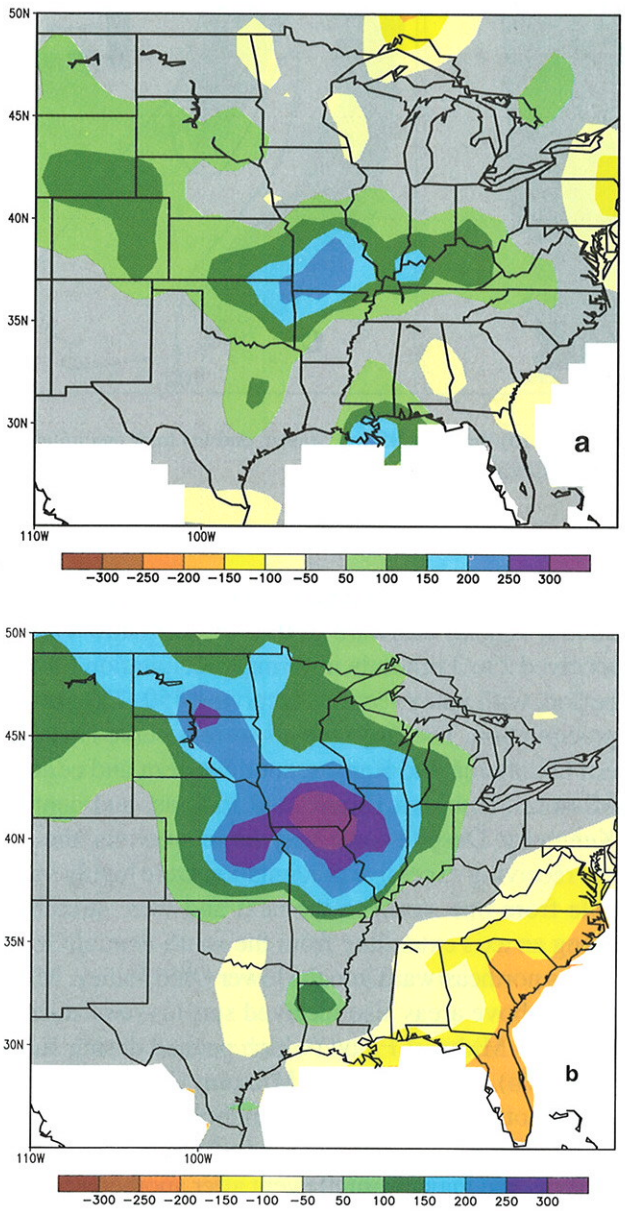


FIG. 37. Precipitation anomalies (mm) for (a) April–June 1995 and for (b) June–August 1993. Anomalies are departures from the 1961–90 base period means. (Source: CPC)

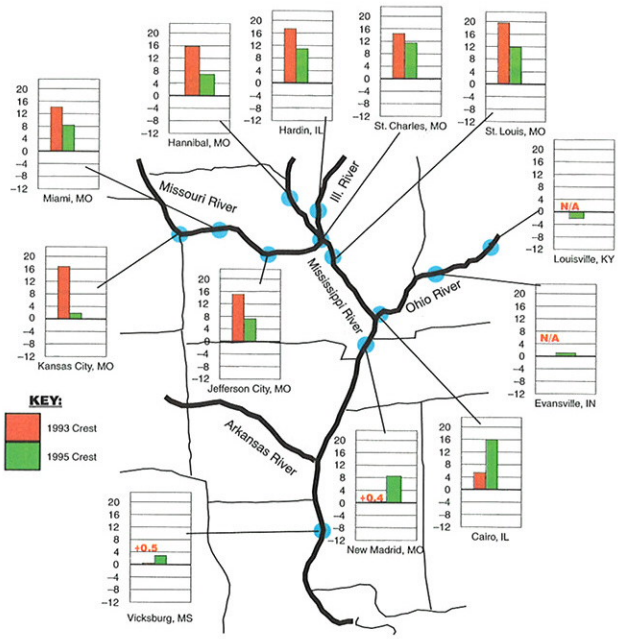


FIG. 38. Maximum river levels for 1993 (red), and 1995 (green) in feet, with respect to flood stage (at "0") for selected sites along the Missouri, Mississippi, Illinois, and Ohio Rivers. (Source: CPC)

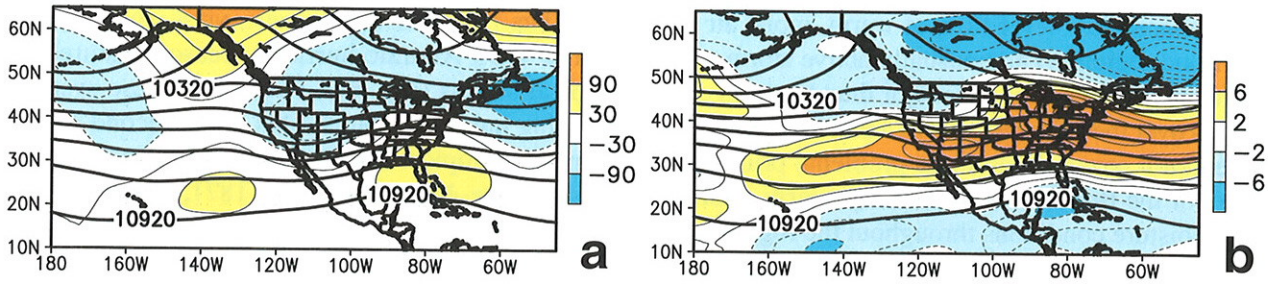


FIG. 39. April–May 1995: (a) 250-hPa mean height (m) and anomaly (m, shaded) and (b) 250-hPa mean height (m) and zonal wind anomaly (m s^{-1}, shaded). Contour interval for heights (anomalies) in (a) is 120 m (30 m). Contour interval for the zonal wind anomalies in (b) is 2 m s^{-1}. Anomalies are departures from the 1979–95 base period means. (Source: CPC)

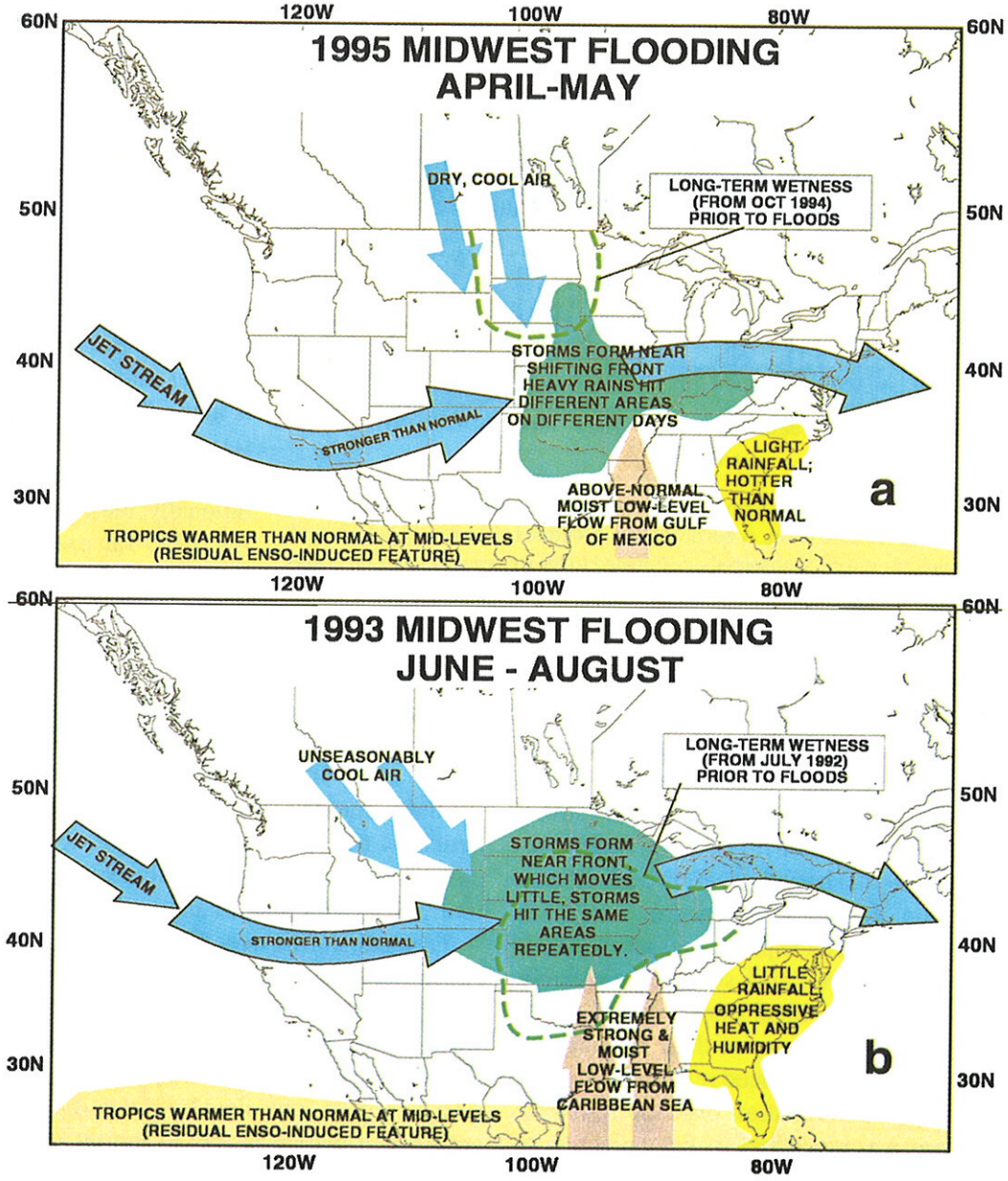


FIG. 40. A comparison of prevailing atmospheric features observed during (a) the April–May 1995 flooding episode and (b) the Midwest Flood of 1993 (bottom).

an enhanced low-level flow of warm, moist air into the flood region; 4) an unusually active storm track, which triggered a series of major thunderstorm complexes over the Midwest; and 5) a preconditioning for potentially severe hydrologic problems prior to the onset of the floods in both cases by nearly saturated soil moisture conditions throughout the region.

There are also important differences in the atmospheric circulation between the two flood events. First, the circulation anomalies during April–June 1995 tended to be weaker and somewhat less persistent than those observed during June–July 1993. Second, the moisture-laden southerly flow in the lower atmosphere (850 hPa) over the Midwest during June–July 1993 was stronger and more persistent than during April–May 1995. In July 1993, this extremely strong moisture transport, coupled with a strong, nearly stationary low-level frontal boundary, allowed for the repetitive formation of major thunderstorm complexes over the Midwest, resulting in prolonged severe flooding throughout the region. Third, substantial variability in the paths of the individual storms during April–June 1995, and in the locations of their accompanying precipitation shields, produced relatively large regional variations in precipitation over the Midwest. In contrast, there was much less spatial variability to the storm track and rain shields in June–July 1993, resulting in inundating rain events repeatedly affecting the same areas.

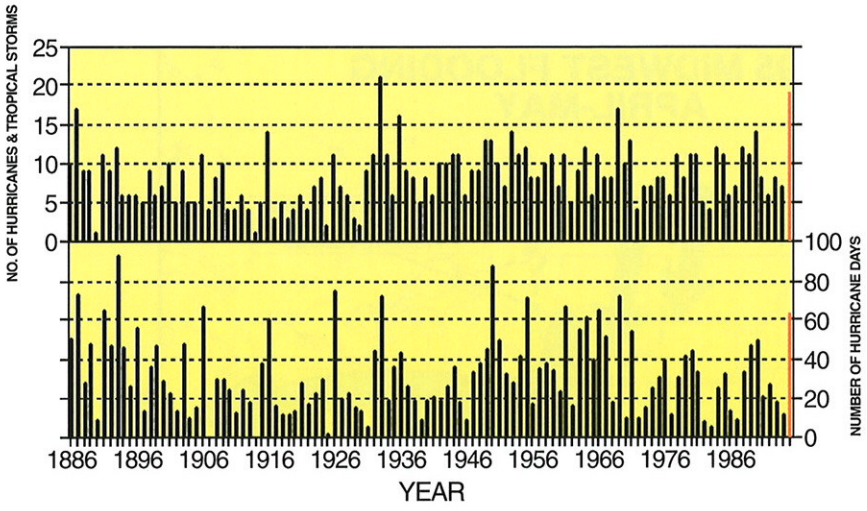


FIG. 41. Number of hurricanes and tropical storms (top) and number of hurricane days (bottom) for the North Atlantic basin. A hurricane day is defined to be four 6-hour periods during which a tropical cyclone is observed or estimated to have hurricane intensity winds. 1995 is in red. (Source: National Climatic Data Center)

3) THE 1995 ATLANTIC HURRICANE SEASON

The 1995 Atlantic hurricane season featured 19 tropical storms (Fig. 41), with 11 of these systems reaching hurricane status. This is the second largest number of tropical storms observed in any hurricane season (June–November) since 1871, and the second largest number of hurricanes observed in one season since records began in 1886. On average, 9–10 tropical storms are observed over the North Atlantic between June and November, with 5–6 of these systems typically becoming hurricanes. Interestingly, all but three tropical cyclones formed between August and October, with nine tropical storms developing during the 31-day period between 30 July and 29 August. Of these nine storms, five became hurricanes.

The active 1995 hurricane season follows four consecutive years (1991–94) of extremely low tropical storm and hurricane activity over the North Atlantic (Figs. 41). For example, the 19 tropical storms observed in 1995 is more than twice the total observed during each of the 1991-1994 seasons (6–8 storms). Additionally, the 11 hurricanes during 1995 far exceeds the 3–4 hurricanes observed each year during 1991–94. Landsea et al. (1996) note that the upsurge in hurricane activity during 1995 was most dramatic in the subtropics (equatorward of 25°N, excluding the Gulf of Mexico) where only one hurricane developed during 1991–94. As a result of this increased activity, the countries surrounding the Caribbean Sea were struck by three hurricanes (two being intense hurricanes—Luis and Roxanne) after experiencing a record five years with no hurricanes.

Tropical storms over the North Atlantic, with the exception of the Gulf of Mexico, are generally triggered by easterly waves which propagate off the African mainland and move westward across the Atlantic. However, the potential for the storm intensification is largely controlled by the vertical wind shear; strong vertical shear acts to inhibit intensification, while weak vertical shear acts to aid intensification (Gray 1968). In fact, the most prominent factor controlling the year-to-year variability in tropical storm

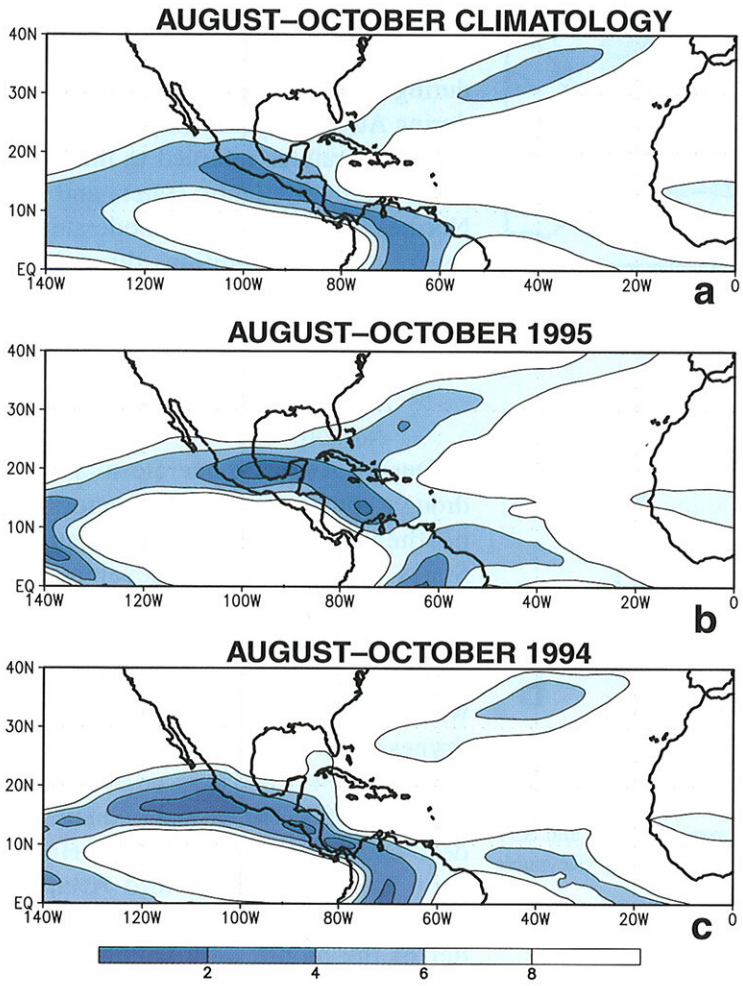


FIG. 42. Vertical wind shear (200–850 hPa) [m s^{-1}] for the (a) August–October climatology, (b) August–October 1995, and (c) August–October 1994. Climatology is based upon the 1985–95 base period. Blue shading denotes regions of weak vertical wind shear. (Source: CPC)

and hurricane activity over the North Atlantic is the strength of the vertical wind shear.

Climatologically, strong vertical shear is observed throughout the Caribbean, large portions of the subtropical North Atlantic, and the northern Gulf of Mexico (Fig. 42a). These conditions act as a major inhibitor to hurricane activity. Indeed, active hurricane years are typically associated with a pronounced weakening of the vertical shear throughout these regions, as was observed during the 1995 season (Fig. 42b). In particular, minimal vertical wind shear was observed during the 1995 hurricane season throughout the entire region from western Africa to the Gulf of Mexico and the Caribbean Sea (Fig. 42b).

Landsea et al. (1996) noted that other atmospheric and oceanic parameters were also extremely favorable for enhanced tropical storm and hurricane activity during the 1995 season. In particular, below-normal sea level pressure (Fig. 43a) and above-normal sea surface temperatures (Fig. 43b) were observed throughout the western and central subtropical North Atlantic during August–October. These overall conditions, combined with a series of intense easterly waves originating over north-central Africa, provided the primary ingredients for a highly active hurricane season throughout the subtropical North Atlantic basin.

There are apparently strong long-range predictive signals for Atlantic basin seasonal tropical cyclone activity up to 11 months in advance (Gray et al., 1992; Gray et al. 1994a). These signals are associated with three prominent phenomena 1) the El Niño–Southern Oscillation (ENSO) cycle; 2) the stratospheric Quasi–Biennial Oscillation (QBO); and 3) West African rainfall. Gray and colleagues indicated in November 1994 (Gray et al. 1994b) that the above three factors would be in a phase favorable for above-normal Atlantic tropical storm activity during 1995.

The most important identifiable phenomenon associated with year-to-year climate variability is ENSO. During the warm phase of this oscillation, above-normal sea surface temperatures are observed throughout the central and east-central equatorial Pacific. Associated with this increase in ocean temperatures, the normal pattern of tropical cloudiness and precipitation is disrupted, which in turn affects the atmospheric wind and pressure patterns throughout the Northern Hemisphere. In summer, these conditions generally contribute to enhanced vertical wind shear over the North Atlantic, thereby inhibiting hurricane activity.

The mid-1991 through early 1995 period was dominated by warm (ENSO) episode conditions. Important manifestations of these conditions included extremely persistent patterns of strong vertical wind shear and above-normal SLP over much of the subtropical North Atlantic. These conditions apparently contributed to the marked decrease of tropical storm and hurricane activity over the North Atlantic previously noted during the 1991–94 hurricane seasons.

Atmospheric and oceanic conditions throughout the

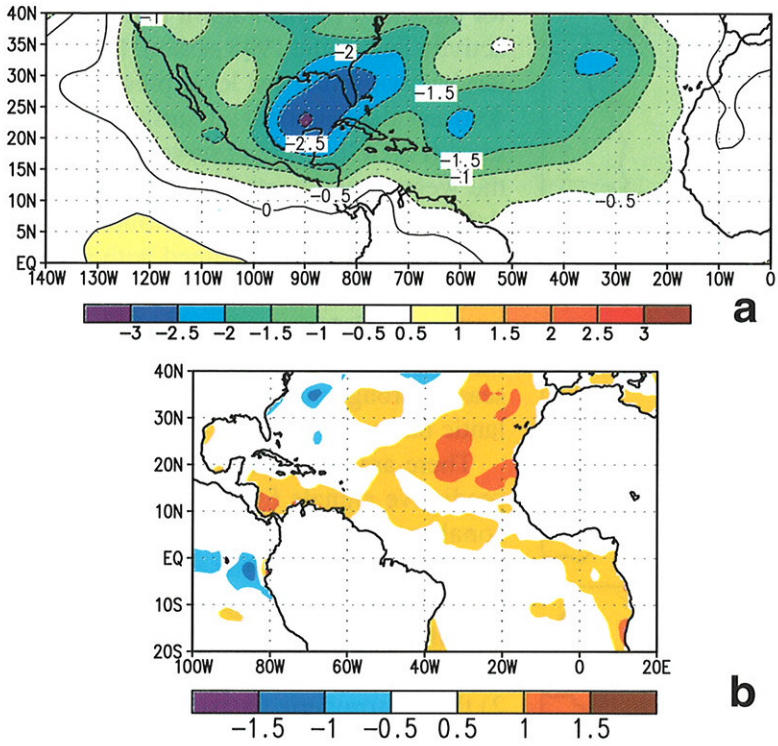


FIG. 43. (a) Sea level pressure (SLP) anomalies (hPa) for August–October 1995 and (b) sea surface temperature (SST) anomalies (°C) for August–October 1995. SLP anomalies are departures from the 1979–95 base period means and SST anomalies are departures from the 1950–79 adjusted OI climatology (Reynolds and Smith 1995). (Source: CPC)

tropical Pacific began a rapid return to normal in March 1995. This evolution marked an end to prolonged warm-episode conditions and also signaled the demise of the anomalous patterns of vertical wind shear and sea level pressure that had previously hindered Atlantic tropical storm development.

4) MID-JULY 1995: MIDWEST U.S. HEAT WAVE

In mid-July dangerously hot and humid conditions spread across most of the central and eastern United States, resulting in nearly 1000 deaths, 500 of which occurred in the Chicago, Illinois, area. During the period daily high temperatures exceeded 40°C as far north as South Dakota and Wisconsin, and dew-point temperatures reached 29°C over large portions of the Midwest. These conditions combined to produce apparent temperatures of 38°–45°C (100°–113°F) (Fig. 44). Additionally, all-time high temperatures were recorded during the event at La Crosse, Wisconsin (42°C, 13 July); Danbury, Connecticut (41°C, 15 July); Chicago/Midway, Illinois (41°C, 13 July); Chicago/O'Hare, Illinois (40°C, 13 July); and Flint, Michigan (38°C, 14 July), before a series of weak cold fronts brought relief during the third week in July. However, during August, significantly above-normal temperatures returned to the Midwest, the mid-Atlantic states, and the Northeast, contributing to moderate-to-severe drought conditions throughout the latter two regions, as described below.

5) AUGUST 1995: NORTHEAST U.S. DROUGHT

During August moderate-to-severe drought conditions developed across the northeastern quarter of the United States. These conditions developed in response to a combination of severe precipitation deficits (Fig. 45) and excessive heat (Fig. 46) during the month, which acted to exacerbate long-term dryness that had persisted since mid-March (Fig. 47), and in some areas since October 1994. The drought conditions developed after the remnants of Hurricane Erin crossed the mid-Atlantic states on August 6. During the remainder of the month only isolated light showers were observed in most of the Northeast and mid-Atlantic states, with no measurable rain reported in several areas from north-central Virginia northeastward to Massachusetts (Fig. 47).

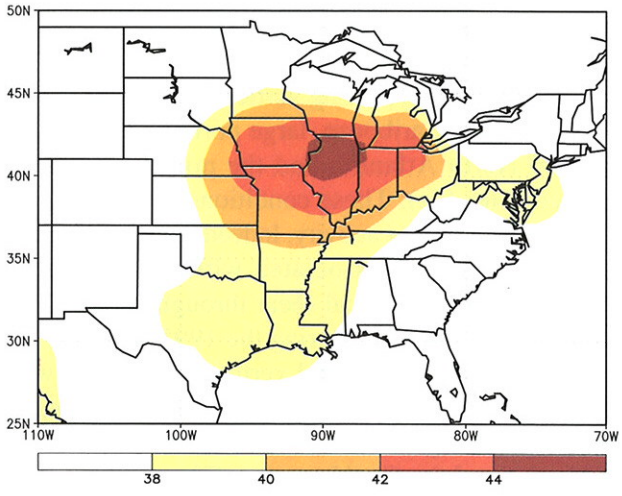


FIG. 44. Maximum apparent temperature (°C) during 13–14 July 1995. (Source: CPC)

The drought can be attributed to a large-scale displacement of the upper-level circulation features from their climatological position. Normally, a moderately strong upper-level ridge dominates the central United States during August, with troughs positioned along both the Atlantic and Pacific Coasts. During August 1995 the mean ridge axis was shifted east of normal, and was centered over eastern North America. This flow pattern forced significant midlatitude weather disturbances, along with their attendant cold frontal boundaries and frontal circulations, northward toward central and eastern Canada. The result was abnormally warm and dry conditions throughout the Northeast. These conditions enhanced an overall pattern of subnormal precipitation observed during the previous six to eleven months over much of the Northeast and mid-Atlantic states.

Normally, 400–600 mm of rainfall is measured in the Northeast and eastern mid-Atlantic between mid-March and late-August. However, most of this region recorded less than 75% of normal precipitation during this period in 1995, with localized sections of New York, southern New England, and the eastern mid-Atlantic observing less than half their normal precipitation. For example, only 250–380 mm of precipitation were measured at most locations in the Northeast, with even lesser totals (125–425 mm) recorded in eastern and southeastern New York, northeastern Pennsylvania, and southern Vermont.

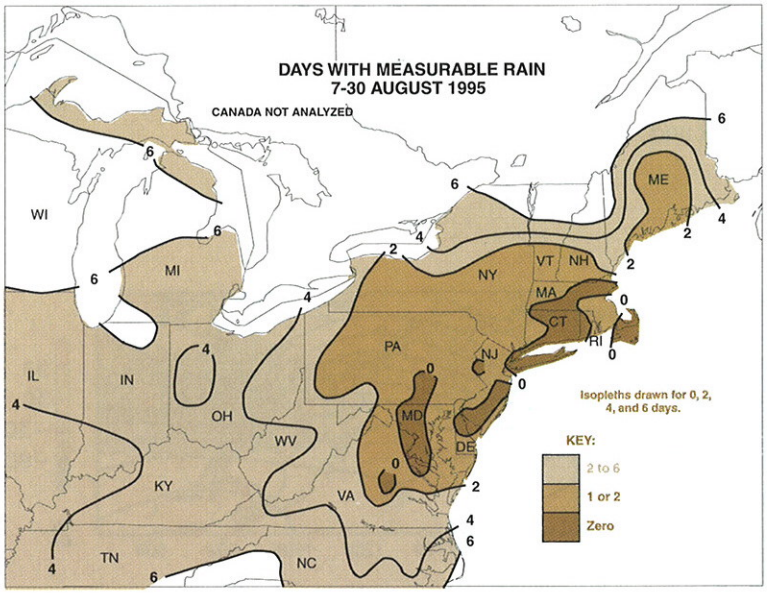


FIG. 45. Days with measurable precipitation during 7–30 August 1995. (Source: CPC)

6) NOVEMBER–DECEMBER 1995: WET IN NORTHWEST U.S., COLD IN EAST

Heavy precipitation (Fig. 48), which fell primarily as rain at all but the highest elevations, dominated the Pacific Northwest states and western Canada during November and December 1995.

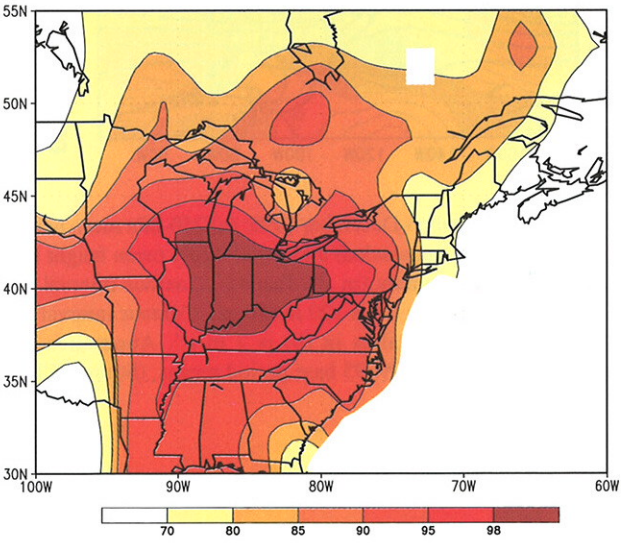


FIG. 46. Surface temperature for August 1995, expressed as percentiles of the normal (Gaussian) distribution fit to the 1961–90 base period data. (Source: CPC)

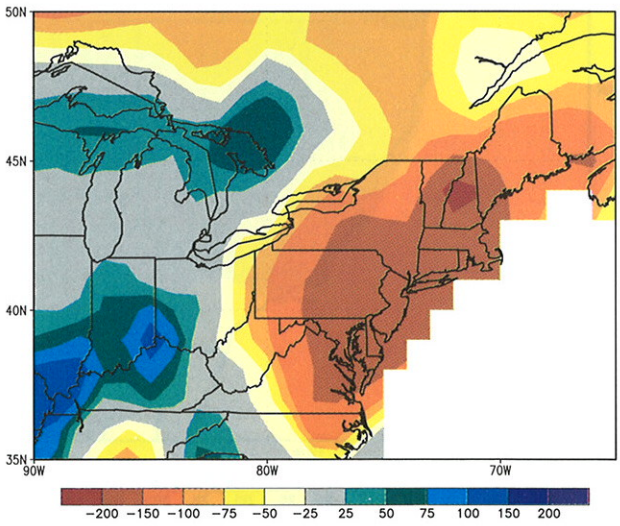


FIG. 47. Precipitation anomalies (mm) for March–August 1995. Anomalies are departures from the 1961–90 base period means. (Source: CPC)

Rainfall amounts of 200–500 mm fell on parts of western Washington and northwestern Oregon during the period, with one-day totals reaching 125–155 mm. This resulted in severe river flooding, particularly west of the Cascade Mountains.

This heavy rainfall was associated with a persistent pattern of below-normal heights at upper levels (Fig. 49a) over the central North Pacific, and above-normal heights over the western United States. This anomaly pattern was accompanied by enhanced southwesterly flow (Fig. 49b) extending from the central North Pacific to the Pacific Northwest, resulting in an abnormally strong flood of marine air into the Northwest during the period. This flow pattern also directed a series of strong, fast-moving, moisture-laden storms into the region, which directly the heavy rainfall and flooding conditions.

Farther east, well below-normal surface temperatures dominated the eastern United States during November–December 1995. This persistent cold was associated with an amplification of the climatological mean "Hudson Bay trough" (Fig. 49a), along with enhanced northwesterly flow into the region.

The circulation during November- December 1995 reflected an anomalous, planetary-scale flow pattern that extended from the central North Pacific to eastern Europe and accompanied cold episode conditions in the tropical Pacific. This circulation was in marked contrast to that observed in the Pacific/ North American sector during the previous December- January (DJ94/95) period (see Section 4a), a period when mature ENSO conditions dominated the tropical Pacific (compare Fig. 49 with Fig. 34).

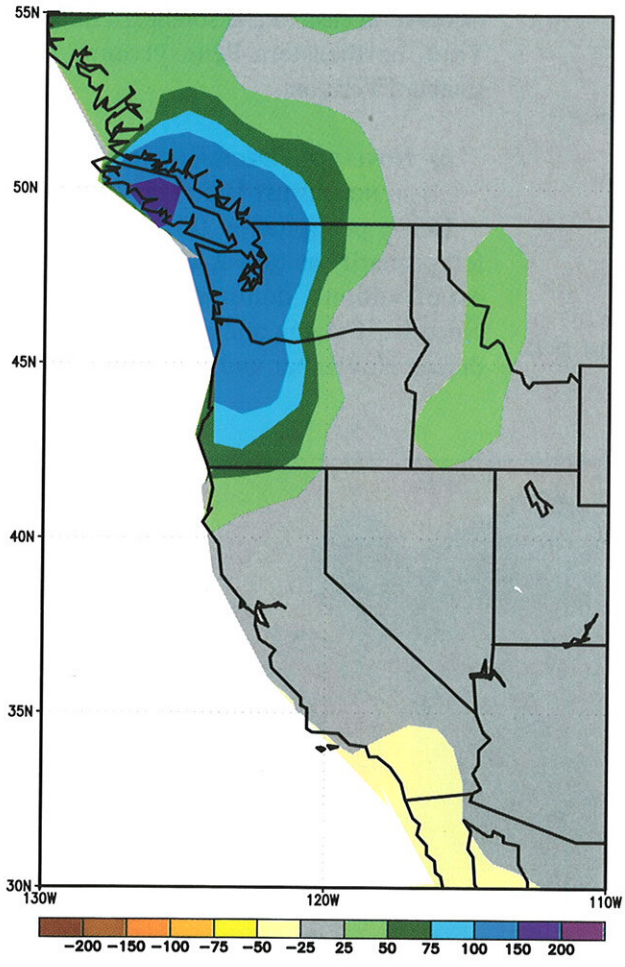


FIG. 48. Precipitation anomalies (mm) for November–December 1995. Anomalies are departures from the 1961–90 base period means. (Source: CPC)

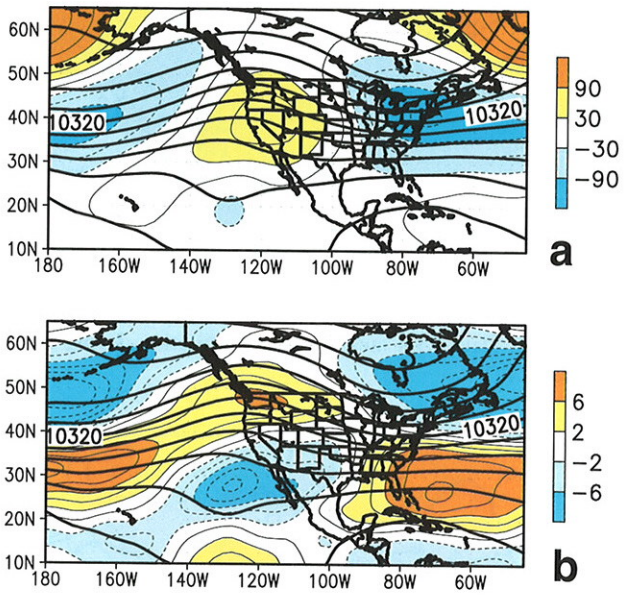


FIG. 49. November–December 1995: (a) 250-hPa mean height (m) and anomaly (m, shaded) and (b) 250-hPa mean height (m) and zonal wind anomaly (m s^{-1}, shaded). Contour interval for heights (anomalies) in (a) is 120 m (30 m). Contour interval for the zonal wind anomalies in (b) is 2 m s^{-1}. Anomalies are departures from the 1979–95 base period means. (Source: CPC)

b. Eurasia

1) JANUARY–MAY 1995: ASIAN WARMTH

January–May 1995 was one of the warmest first five months on record for large portions of western and central Russia and western Siberia. During this period surface temperatures averaged 3°–8°C above normal throughout these regions (Fig. 50). This abnormal warmth was associated with substantially below-normal snow cover extent over large portions of central and north-central Russia and western Siberia, particularly during the spring period (Fig. 24b). For example, much of this region normally experiences 20–25 days of snow cover during April. However, according to snow observations derived from the special sensor microwave imager (SSM/I) (Grody and Basist 1995), these areas recorded less than 5 days of snow cover (Fig. 51) during April 1995, as mean temperatures averaged 8°–10°C above normal.

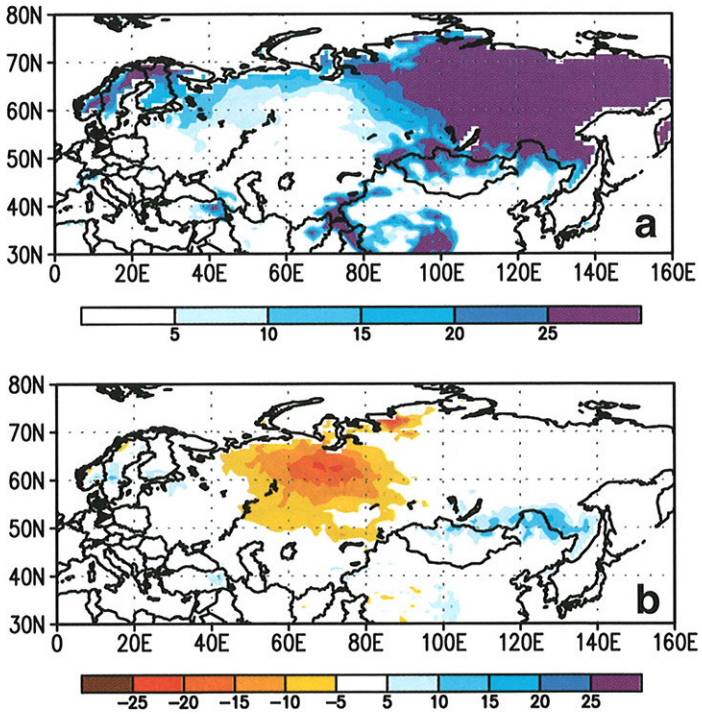


FIG. 51. (a) Snow cover extent and (b) anomaly during April 1995, as estimated by SSM/I. Units are in days. The analysis is based on once-daily observations. Anomalies are departures from the 1987–94 base period means. (Source: CPC)

These conditions were linked to an extremely anomalous atmospheric circulation pattern (Fig. 52) that persisted from mid-January through the end of May. Prominent features of this pattern included below-normal heights over the northern and northeastern North Atlantic (Fig. 52a), and above-normal heights throughout western and northwestern Russia. This overall pattern reflected a pronounced negative phase of the East Atlantic/ Western Russia (EATL/WRUS) teleconnection pattern (Bell and Halpert 1995), also referred to as the Eurasia-2 pattern by Barnston and Livezey (1987). This pattern is one of two prominent modes that affects Eurasia during most of the year. This pattern exhibits considerable month-to-month variability and rarely persists in a strong positive or negative phase (normalized magnitude greater than 1.0) for more than two consecutive months. During January–May 1995 the EATL/WRUS normalized pattern index was below −1.0 for five consecutive months for the first time in the record dating to 1964.

During January–May 1995, this anomalous circulation was associated with a marked intensification of the mean westerly flow over the eastern North Atlantic and Europe (Fig. 52b), and with mean southwesterly flow over much of eastern Europe, western Russia, and western Siberia. These conditions supported a sustained flow of relatively warm air throughout western Asia and Europe during the period, resulting in abnormally warm conditions in these areas. This pattern was also associated with significantly above-normal rainfall over large portions of western and central Europe during January and February, resulting in large-scale and severe flooding.

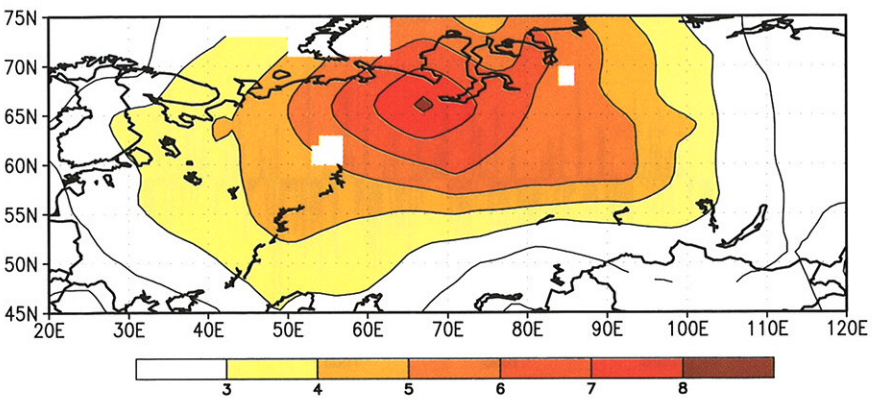


FIG. 50. Temperature anomalies (°C) during January–May 1995. Anomalies are departures from the 1961–90 base period means. (Source: CPC)

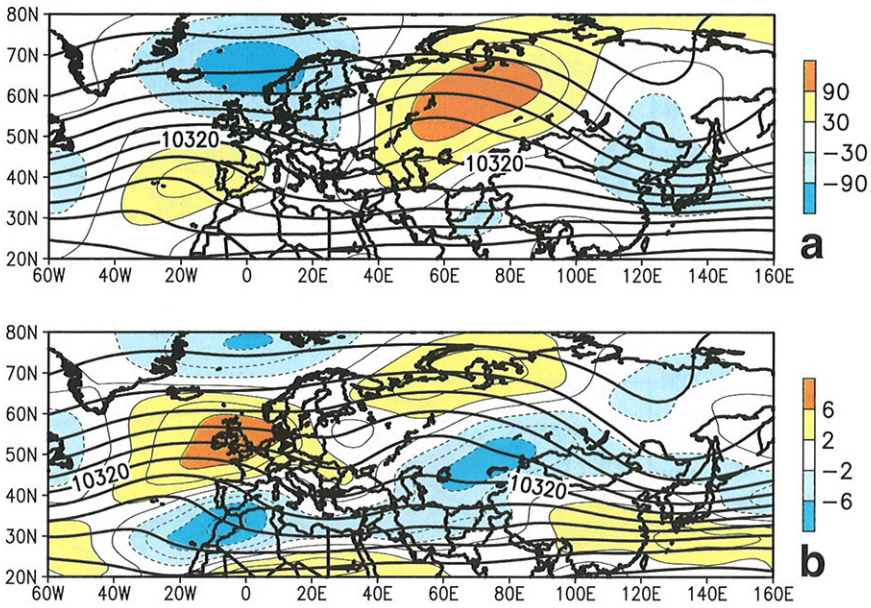


FIG. 52. January–May 1995: (a) 250-hPa mean height (m) and anomaly (m, shaded) and (b) 250-hPa mean height (m) and zonal wind anomaly (m s^{-1}, shaded). Contour interval for heights (anomalies) in (a) is 120 m (30 m). Contour interval for the zonal wind anomalies in (b) is 2 m s^{-1}. Anomalies are departures from the 1979–95 base period means. (Source: CPC)

In strong contrast to the early part of the year, the November–December 1995 period featured a persistent pattern of above-normal heights over the northern North Atlantic and below-normal heights throughout north-central Russia and western Siberia. This pattern was associated with mean northwesterly flow throughout Scandinavia and western Eurasia, resulting in below-normal surface temperatures and enhanced snow coverage during the period.

For 1995 as a whole, most of Russia reported annual mean temperatures among the warmest 10% of the 1961–90 distribution, with annual temperatures averaging 2°–4°C above normal at many locations. With respect to the countries which formerly comprised the Soviet Union, 1995 was the warmest year since records began in 1891, with an average temperature of 2.1°C above normal (Fig. 5). This value far surpasses the previous record warm year of 1990, in which mean annual temperatures averaged 1.4°C above normal.

2) JUNE–AUGUST 1995: EUROPEAN/WESTERN ASIAN HOT SPELL

Abnormally hot and dry conditions dominated many areas of Europe and western Russia during June–August (JJA) 1995, a reprise of the extremely warm conditions observed during the previous summer in many locations. Conditions were particularly acute across the British Isles, where JJA rainfall totals averaged less than 100 mm in most areas. Unofficial statistics indicate that Great Britain may have endured its driest summer in more than 3 centuries. Additionally, central England experienced its warmest August on record dating back to 1659 and its warmest July–August period since 1750 (Fig. 53).

A monthly analysis of surface temperature anomalies during June–August (Fig. 54) indicates that the abnormally warm conditions during June (Fig. 54a) were found primarily over western Russia, a continuation of abnormally warm conditions that dominated western Eurasia during January–May 1995 (discussed above). During July (Fig. 54b) the region of abnormally warm conditions moved westward and became centered over northern and northeastern Europe, and by August the region of anomalous warmth was centered over the British Isles (Fig. 54c). The abnormal conditions over

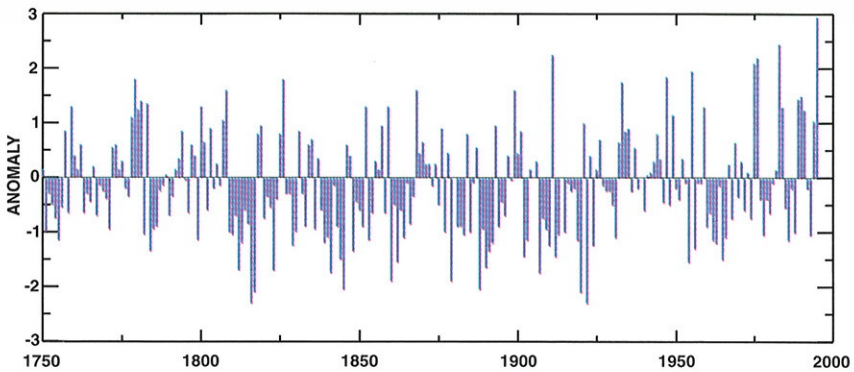


FIG. 53. July–August temperature anomalies (°C) for central England. Anomalies are departures from the 1961–90 base period means. (Source: Hadley Centre for Climate Prediction and Research, UK)

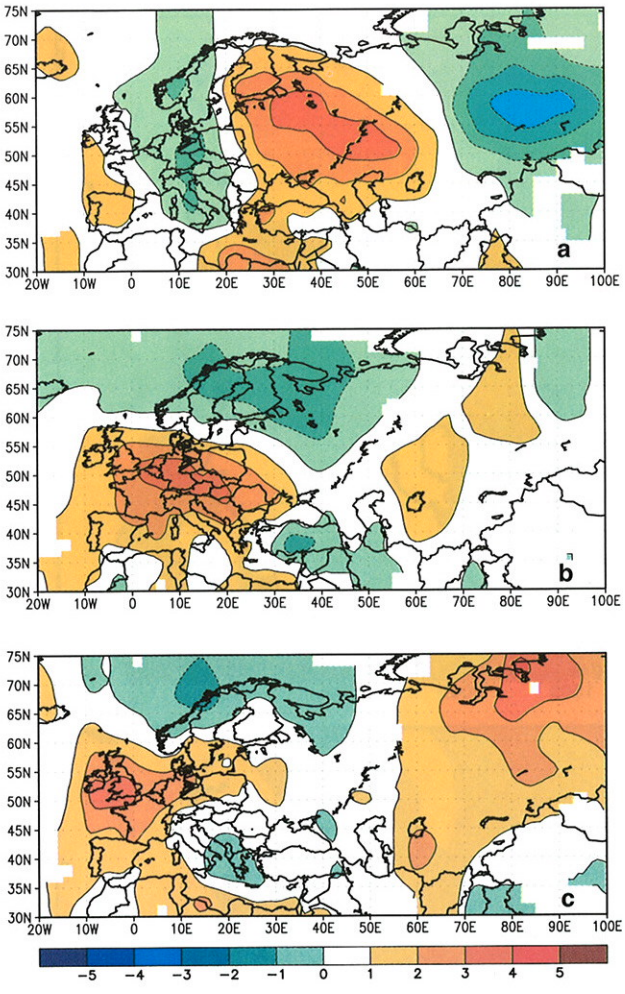


FIG. 54. Temperature anomalies (°C) for (a) June 1995, (b) July 1995, and (c) August 1995. Anomalies are departures from the 1961–90 base period means. (Source: CPC)

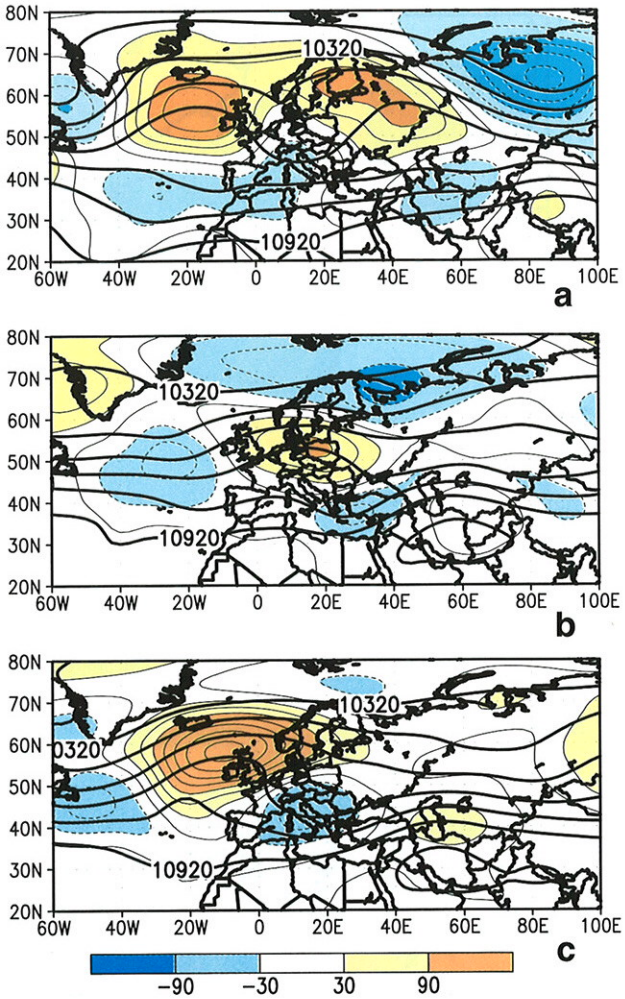


FIG. 55. Mean and anomalous 250-hPa heights (m) for (a) June 1995, (b) July 1995, and (c) August 1995. Contour interval for heights (anomalies) is 120 m (30 m). Anomalies are departures from the 1979–95 base period means. (Source: CPC)

Eurasia during JJA were related to an anomalous circulation regime (Fig. 55), characterized by a retrogressing pattern of above normal heights that moved from western Russia in June to the eastern North Atlantic by August. This pattern was associated with an overall anomalous northward shift of the main storm track during the period, as well as with a substantially reduced flow of marine air into large portions of central and northern Europe.

3) JUNE–SEPTEMBER 1995: SOUTHEAST ASIAN/INDIAN SUMMER MONSOON

Overall, the 1995 Indian monsoon season (June–September) featured near-normal rainfall over large portions of India, and substantially above-normal rainfall throughout Bangladesh, Burma, far eastern India, and large portions of Thailand. The heaviest precipitation (1500–2000 mm) was observed in the east (Fig. 56a), where totals averaged more than 300 mm above normal during the season (Fig. 56b). Above normal rainfall was also observed in the north, where totals averaged 750–1000 mm during the season (100–300 mm above normal), and in the southeast, where totals averaged 500–750 mm (100–200 mm above normal). Elsewhere, more than 1000 mm of rain fell throughout Bangladesh and Burma during the 1995 monsoon season, with totals in north-central Burma exceeding 200–250 mm above normal and totals in northeastern Bangladesh exceeding 300 mm above normal. In southern Thailand, rainfall totals averaged 2000–2500 mm (more than 300 mm above normal) during the season.

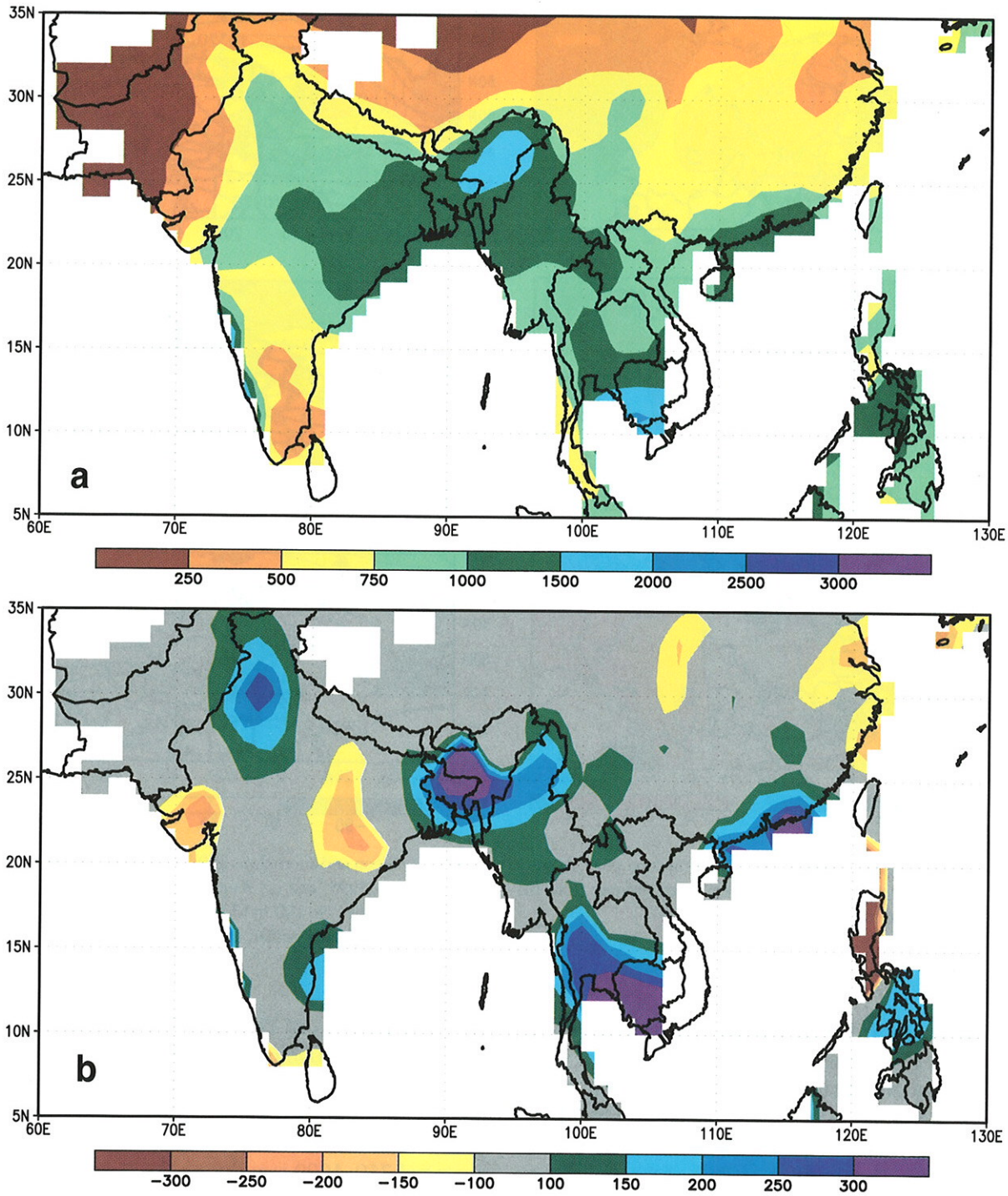


FIG. 56. (a) Total precipitation and (b) anomalies in for June–September 1995. Units are in mm. Anomalies are departures from the 1961–90 base period means. (Source: CPC)

The 1995 monsoon season was preceded during the first three weeks of June by exceptionally hot weather throughout India. During this period, temperatures averaged in excess of 38°C (100°F) throughout much of central and northern India (Fig. 57) and averaged more than 43°C (108°F) in portions of the north and northeast. This marks the second consecutive year in which a brutal heat wave prior to the summer monsoon took hundreds of lives across the Indian subcontinent. During 1995 the onset of the monsoonal rains

was delayed, beginning in late June. These rains remained generally below normal in intensity over much of India until mid-July. A sharp increase in rainfall was then observed across the Indian subcontinent in mid-July, and these heavy rains persisted through August and much of September. These rains resulted in flooding along many rivers and in numerous towns, particularly in Pakistan, Bangladesh, and southern Thailand.

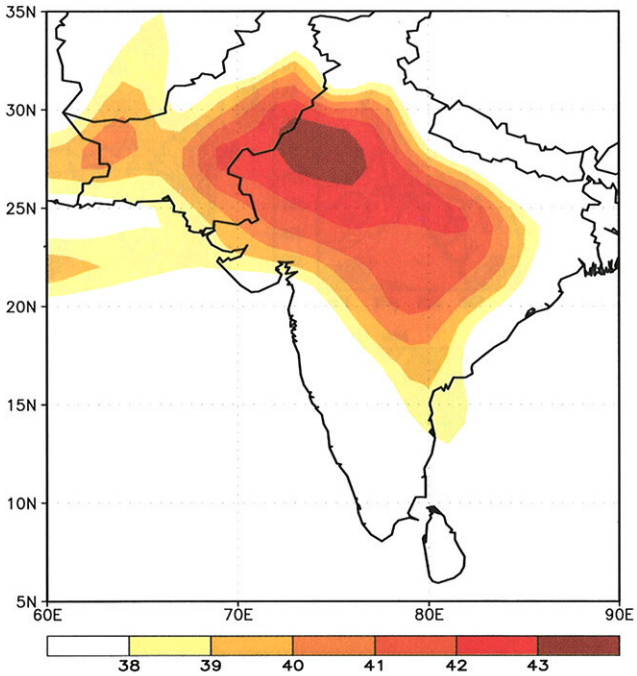


FIG. 57. Average daily maximum temperature (°C) for 1–21 June 1995. (Source: CPC)

c. South America

Rainfall during the Southern spring and early summer is of critical importance to agriculture in northeastern Argentina, Uruguay, and southern Brazil . In central Brazil (between 10° and 25°S) there is a pronounced dry season from April through August, and a pronounced rainy season from September through March. Rainfall increases over this region during September, as convection begins to shift southward from Central America to the Amazon Basin. In extreme southern Brazil (including most coastal sections north to near 20°S), Uruguay, and northeastern Argentina rainfall occurs more uniformly throughout the year. However, in these regions frost occurs regularly during May-August, thus limiting agricultural activities during this period. For the entire area from central Brazil south to northeastern Argentina planting begins during September and October.

Drier than normal conditions were observed over central Brazil (centered near 18°S, 50°W) during the entire period from September through December 1995 (Fig. 58). Over most of southern Brazil, near-normal to above-normal rainfall occurred during September and October, except for extreme southern Brazil where drier than normal conditions developed during October. Extremely dry conditions dominated nearly the entire region of central and southern Brazil during November, with many areas experiencing a continuation of the extremely dry conditions through December.

The patterns of outgoing longwave radiation (OLR) anomalies during this period (Fig. 59) indicate weaker-than-normal convection (positive OLR anomalies imply less-than-normal rainfall) over a large portion of South America, although the positive anomalies over Argentina also reflect a combination of above normal temperatures (Fig. 60a) and

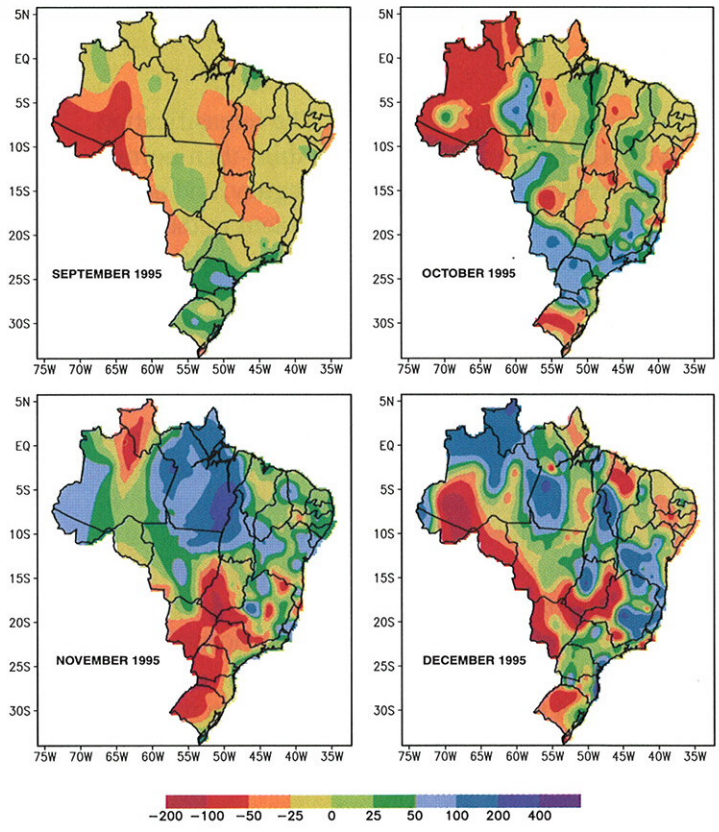


FIG. 58. Monthly precipitation anomalies (mm) during September–December 1995 for Brazil. Anomalies are departures from the 1961–90 base period means. [Source: Centro dePrevisao de Tempo e Estudos Climaticos (CPTEC)]

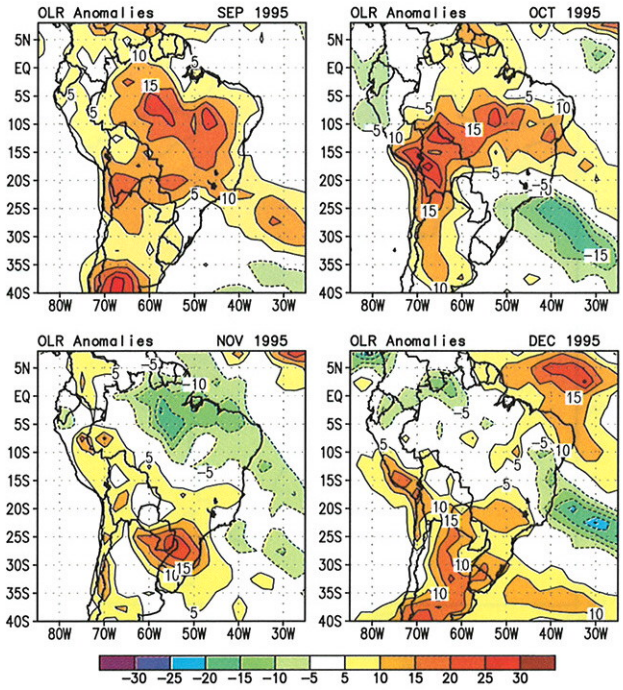


FIG. 59. Monthly outgoing longwave radiation (OLR) anomalies (W m^{-2}) for September–December 1995. Anomalies are departures from the 1979–95 base period means. (Source: CPC)

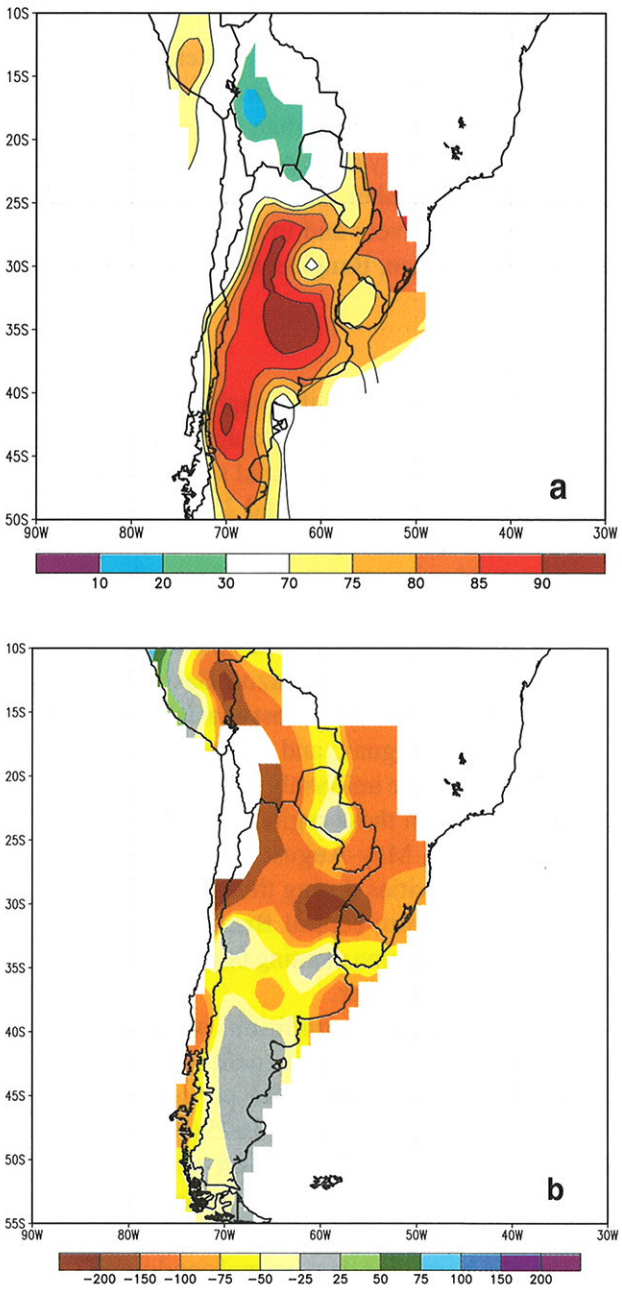


FIG. 60. (a) Temperature percentiles and (b) precipitation anomalies (mm) for September–December 1995. Anomalies are departures from the 1961–90 base period means. (Source: CPC)

below normal rainfall (Fig. 60b). The intensification between October and November of drier-than-normal conditions over southern Brazil, Uruguay, and northeastern Argentina is also clearly evident in the OLR anomaly patterns.

d. Australia

The rainy season over northern and northeastern Australia typically begins in October and ends in April. Much of the area receives more than 75% of the mean annual precipitation (with portions of extreme northern Australia recording more than 90%) during this seven-month period. For the 1994/95 wet season as a whole, precipitation totals averaged 200–500 mm above normal throughout north-central Australia (Fig. 61), and 200–400 mm below normal in the northeastern part of the country.

At Darwin the rainfall total of 2384 mm recorded during the 1994/95 wet season was the largest on record at this station dating to 1901 (Fig. 62). This total was 840 mm above the seasonal mean value of 1544 mm. Interestingly, 940 mm of precipitation, representing one-third of the total 1994/95 seasonal precipitation was recorded during January 1995. This value is the second largest monthly rainfall total recorded at Darwin in this century and is comparable to the record monthly rainfall total of 1014 mm observed in March 1977.

In the Northeast, the below-normal precipitation during the 1994/95 wet season (Fig. 61) contributed to severe precipitation deficiencies for the 13-month period ending in April 1995 (Fig. 63). Precipitation has been below normal in this region since the 1991/

92 rainy season (Fig. 64), in association with the long-term ENSO conditions during the first half of the 1990s. However, a return to slightly above-normal precipitation during October and November of 1995 helped to ease this dryness. The change in the precipitation pattern over the Northeast accompanied the transition from warm-episode to cold-episode conditions in the tropical Pacific during the second half of the year (see section 3).

In the extratropics severe precipitation deficits also covered much of eastern and southern Australia for the 13-month period ending in April 1995 (Fig. 63). In the east-central region, these dry conditions began to ease during October–November 1995, with a return to slightly above-normal precipitation throughout the region. Wet conditions were particularly prominent in November, when large areas received abundant rainfall, with significant flooding in southern Queensland. Despite this late-year rainfall, precipitation totals for the period April 1991 to December 1995 were among the lowest on record over a large part of this region. In the southeast, significant precipitation deficits had abated by the end of July (Fig. 65), in response to above-normal precipitation during the May–July period (Fig. 66).

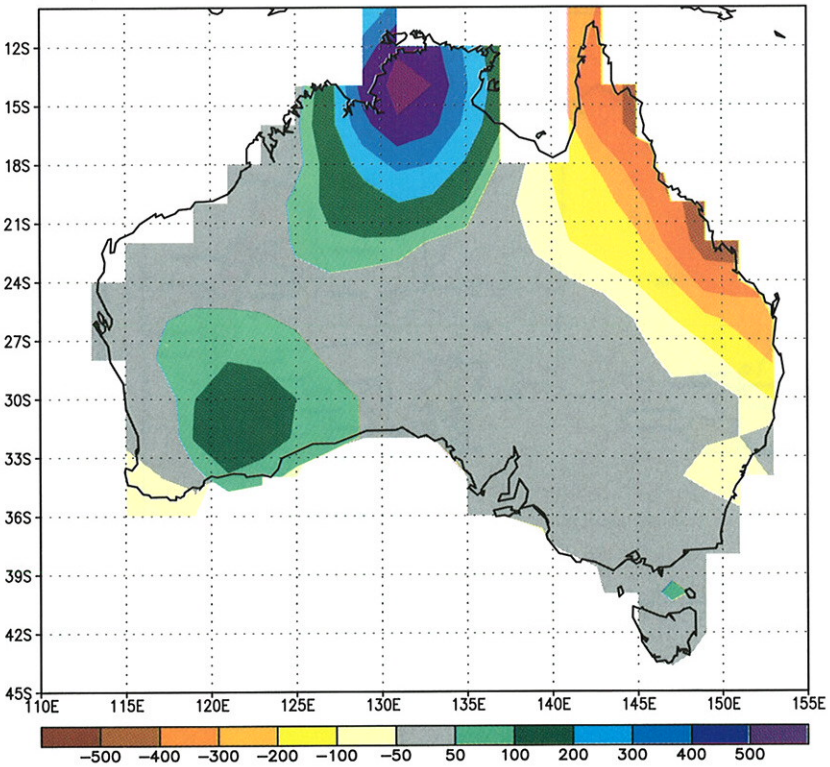


FIG. 61. Precipitation anomalies (mm) during October 1994–April 1995. Anomalies are departures from the 1961–90 base period means. (Source: CPC)

In Western Australia, Tropical Cyclone "Bobby" struck northwestern Australia near Onslow during February 1995, producing torrential rain (425 mm in 48 hours) and destructive winds. "Bobby" drifted southeast, generating widespread heavy rain and flooding across the interior of Western Australia—over 300 mm in areas that normally receive 225–275 mm throughout the entire year. This rainfall contributed substantially to the positive precipitation anomalies evident in the southwest during the October 1994–April 1995 period (Fig. 61).

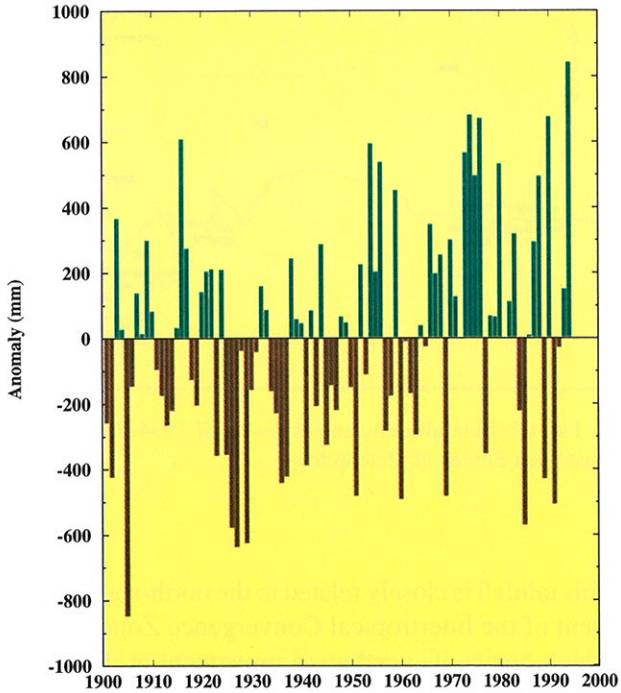


FIG. 62. Precipitation anomalies (mm) at Darwin, Australia for October–April. Anomalies are departures from the 1901–95 base period means. (Source: CPC)

e. Africa

1) JUNE–SEPTEMBER 1995: WESTERN AFRICA RAINY SEASON

The Sahel region receives about 90% of its annual mean precipitation during the June–September period.

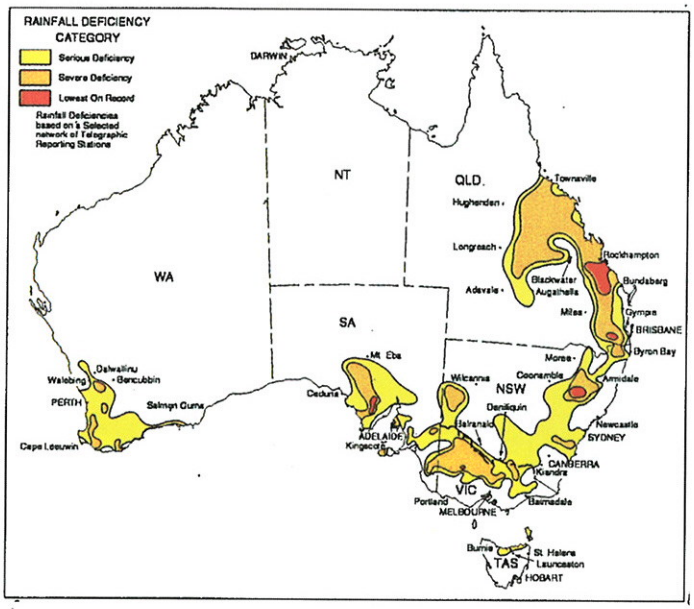


FIG. 63. Rainfall deficiencies for April 1994–April 1995. (Source: Australian Bureau of Meteorology)

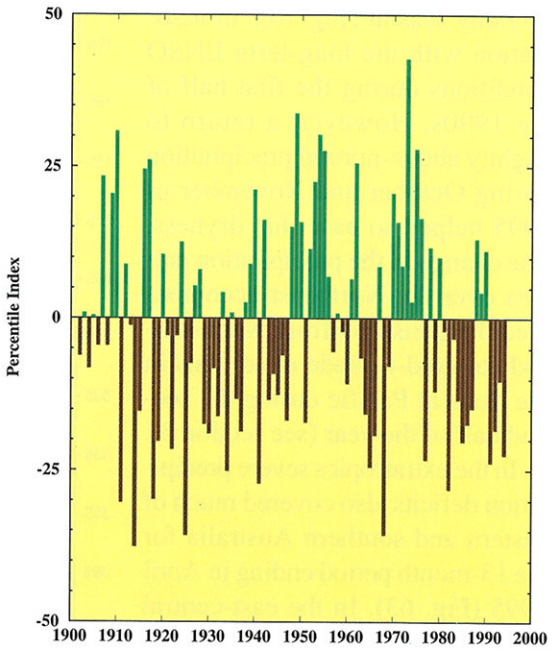


FIG. 64. Precipitation index (average gamma percentiles of station precipitation within the region) for northeastern Australia during October–April. Percentiles are computed for the 1961–90 base period. (Source: CPC)

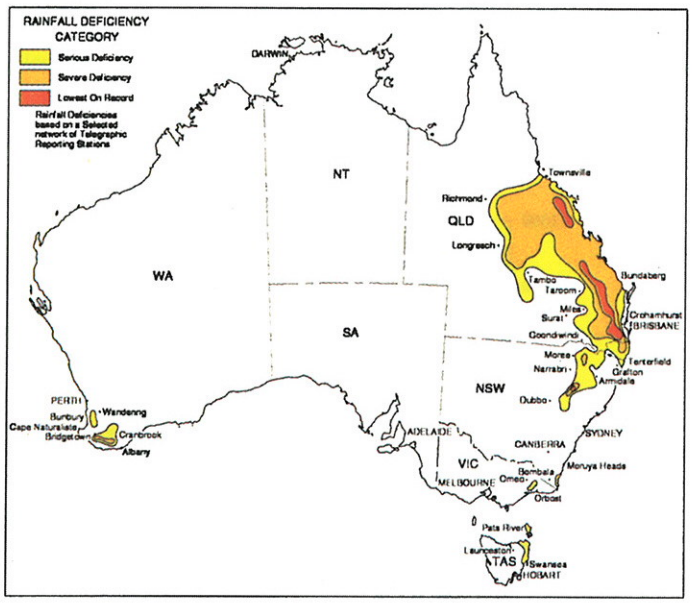


FIG. 65. Rainfall deficiencies for April 1994–July 1995. (Source: Australian Bureau of Meteorology)

This rainfall is closely related to the north-south movement of the Intertropical Convergence Zone (ITCZ), which begins its northward movement at the beginning of the Northern Hemisphere Spring and reaches its northernmost position (15°N) during August. During the 1995 rainy season much of the Sahel recorded near-normal rainfall totals (Fig. 67b), relative to the 1961–90 base period. This follows a significantly wetter-than-normal rainy season during 1994 and a near-normal year during 1993. This is the first time since the late 1970s that rainfall totals in the Sahel have been normal or above-normal for three consecutive years.

During 1995 above-normal rainfall was confined primarily to southwestern sections, where eastern Sierra Leone, northern Liberia, northern Cote d'Ivoire, and southern Guinea recorded more than 1000 mm of precipitation (Fig 67a) during the season (150–250 mm above normal). The most significant dryness stretched from southern Mauritania southeastward to Mali and Burkina Faso. Southern Senegal also experienced rainfall deficits with totals averaging between 600–700 mm during the season (Fig. 67a).

During June rainfall was generally near normal to above normal across the Sahel. However, rainfall deficits developed over Mauritania and Mali. Most countries in the Gulf of Guinea region also observed rainfall below 70% of normal during the month, except the coastal areas of Cote d'Ivoire, Benin, and Ghana, where stations reported above-normal rainfall.

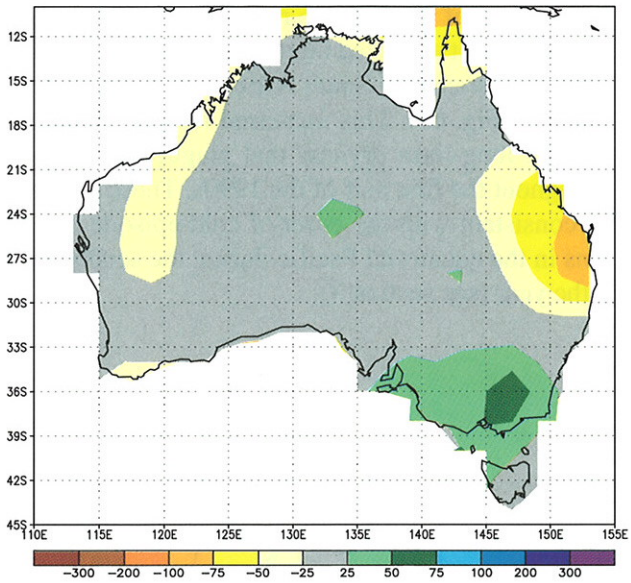


FIG. 66. Precipitation anomalies (mm) during May–July 1995. Anomalies are departures from the 1961–90 base period means. (Source: CPC)

In July rainfall tended to be near normal or slightly below normal across the Sahel region. However, dry conditions prevailed in Mali and eastern Niger where rainfall was generally only 50% to 80% of normal. During August and September, rainfall was again near average across most of the Sahel. However, rainfall was particularly abundant (over 150% of normal) in a few locations, including southeastern Burkina Faso and parts of Benin and Senegal. Rainfall also improved significantly in southwestern Mali, Niger, and northern Burkina Faso during the period, where normal to above-normal rainfall (95%–170%) totals were recorded.

2) OCTOBER–APRIL 995: SOUTHERN AFRICA RAINY SEASON

In southern Africa, the rainy season typically lasts from October to April, and reaches maximum strength between November and March. The region as a whole receives more than 75% (some parts more than 90%) of its mean annual precipitation during this seven-month period. Significant precipitation is rare throughout the region after mid-May. The year-to-year variability in rainfall over southern Africa shows a strong relationship to the ENSO cycle, with below-normal (above-normal) rainfall generally observed during Pacific warm (cold) episodes (Ropelewski and Halpert 1987, 1989).

Overall, rainfall totals during the 1994/95 rainy season were significantly below normal over large portions of southern Africa and Madagascar (Fig. 68). Rainfall deficits exceeding 150 mm (Fig. 68b) were observed throughout Namibia, southeastern Angola, much of Botswana, Zimbabwe, Mozambique, the southern two-thirds of Madagascar, and the northeastern section of South Africa. In many of these regions, the observed rainfall totals were generally 50–75% of normal, while in central Namibia the totals were only 25–50% of normal.

The rainy season in southern Africa was characterized by a slow onset, with rainfall deficits during November and December 1994 averaging 50 –200 mm across the subcontinent. These dry conditions improved slightly during January 1995, particularly over portions of Zimbabwe, northeastern South Africa, and parts of Botswana, where heavy rainfall (100–200 mm, over 150% of normal) was observed. However, during late January-February, abnormally dry condi-

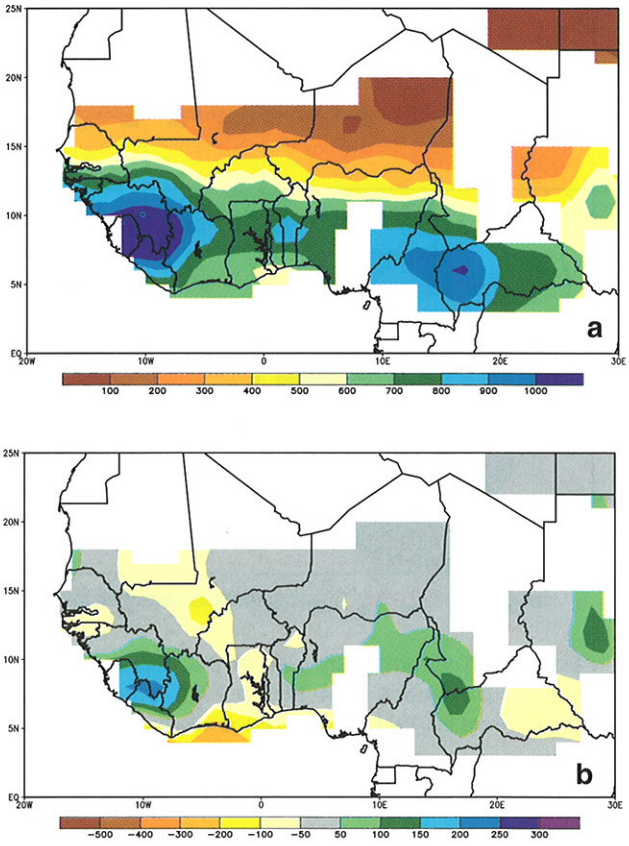


FIG. 67. (a) Total precipitation and (b) precipitation anomalies in mm for June–September 1995. Anomalies are departures from the 1961–90 base period means. (Source: CPC)

tions once again dominated southern Africa, with totals among the lowest 10% of climatological occurrences over southern Botswana, northern Zimbabwe, and central Mozambique. Dryness persisted through March over much of southern Africa, although heavy late-month rains provided much-needed moisture to many areas from Botswana and central Zimbabwe southward. However, below-normal rainfall continued through April in many regions, allowing moisture shortages to increase across much of southern Africa.

The onset of the 1995/96 rainy season in southern Africa brought a marked increase in rainfall totals for much of east-central South Africa and southwestern Namibia (Fig. 69). This increased rainfall helped to ease the long-term dryness that plagued the region throughout the first half of the 1990s. These changes are consistent with the onset of cold-episode conditions in the equatorial Pacific during the second half of the year (see section 3).

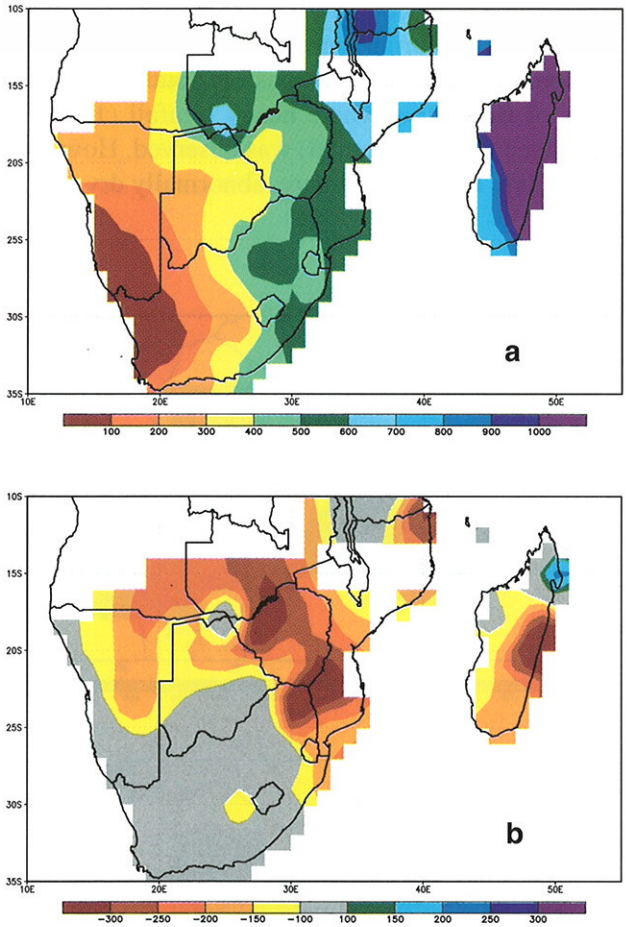


FIG. 68. (a) Total precipitation and (b) precipitation anomalies in mm for November 1994–March 1995. Anomalies are departures from the 1961–90 base period means. (Source: CPC)

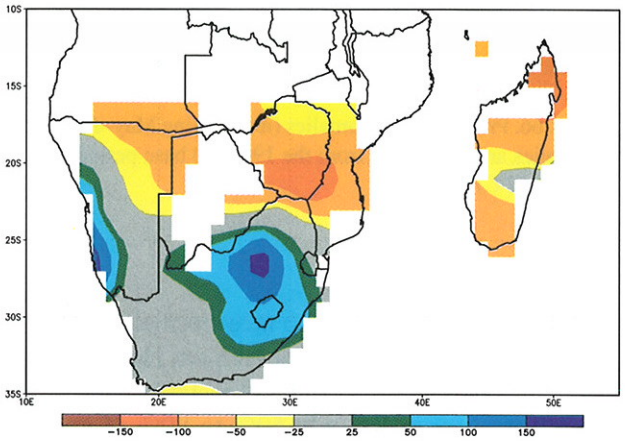


FIG. 69. Precipitation anomalies (mm) for November–December 1995. Anomalies are departures from the 1961–90 base period means. (Source: CPC)

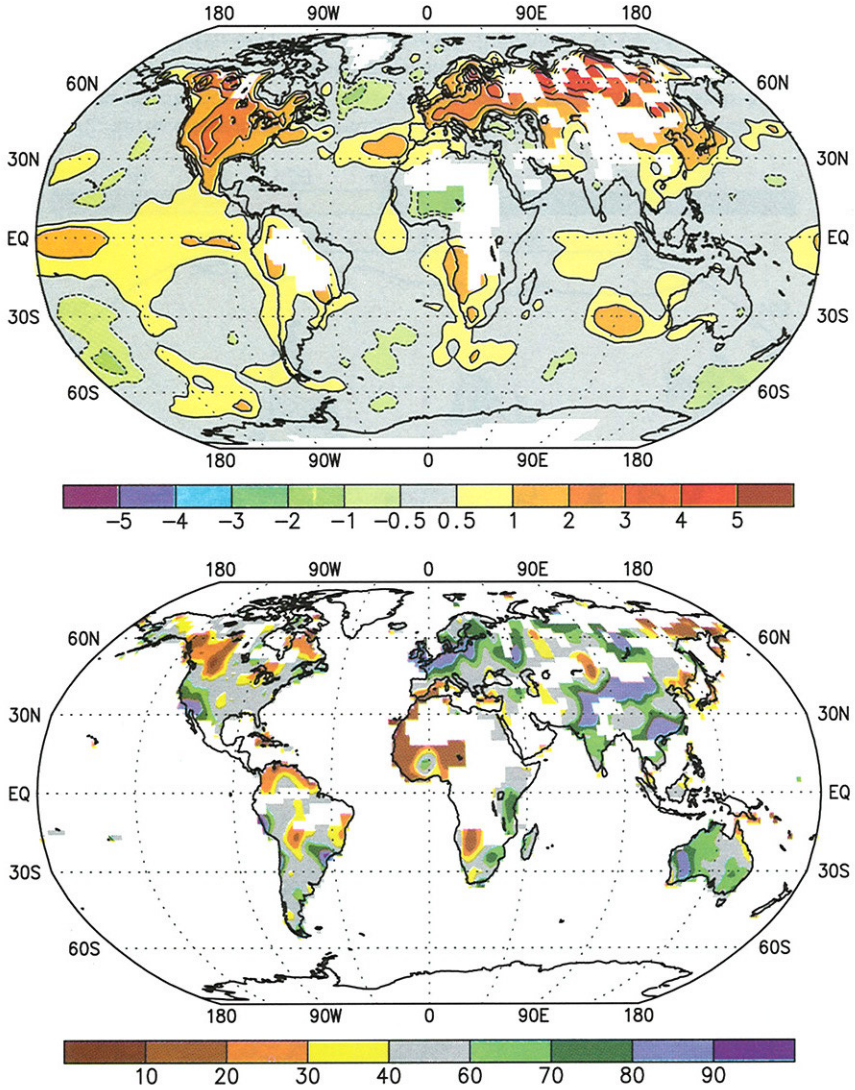


FIG. 70. Surface temperature anomalies (top, °C) and precipitation percentiles based on a gamma distribution fit to the 1961–90 base period (bottom) for December 1994–February 1995. Temperature anomalies are based on station data over land (1961–90 base period) and sea surface temperature data over water (adjusted OI climatology, Reynolds and Smith 1995). The analysis is omitted in data-sparse regions (white areas). (Source: CPC)

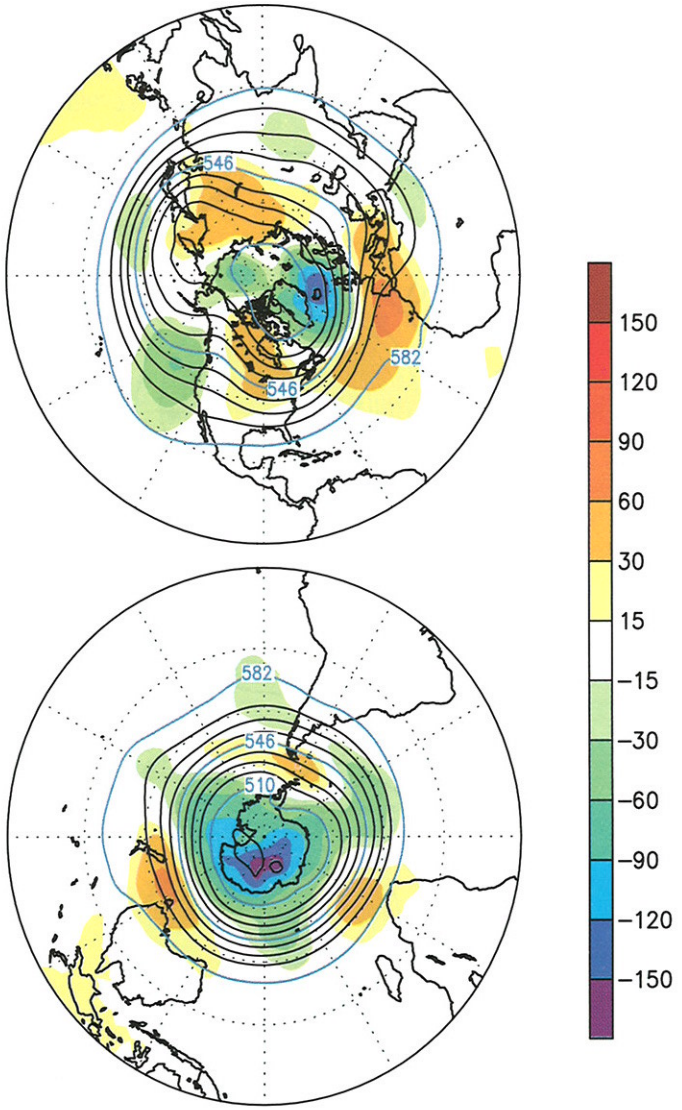


FIG. 71. Northern Hemisphere (top) and Southern Hemisphere (bottom) 500-hPa geopotential height (contours, interval is 9 dm) and anomalies (shading) for December 1994–February 1995. Anomalies are departures from the 1979–88 base period means. (Source: CPC)

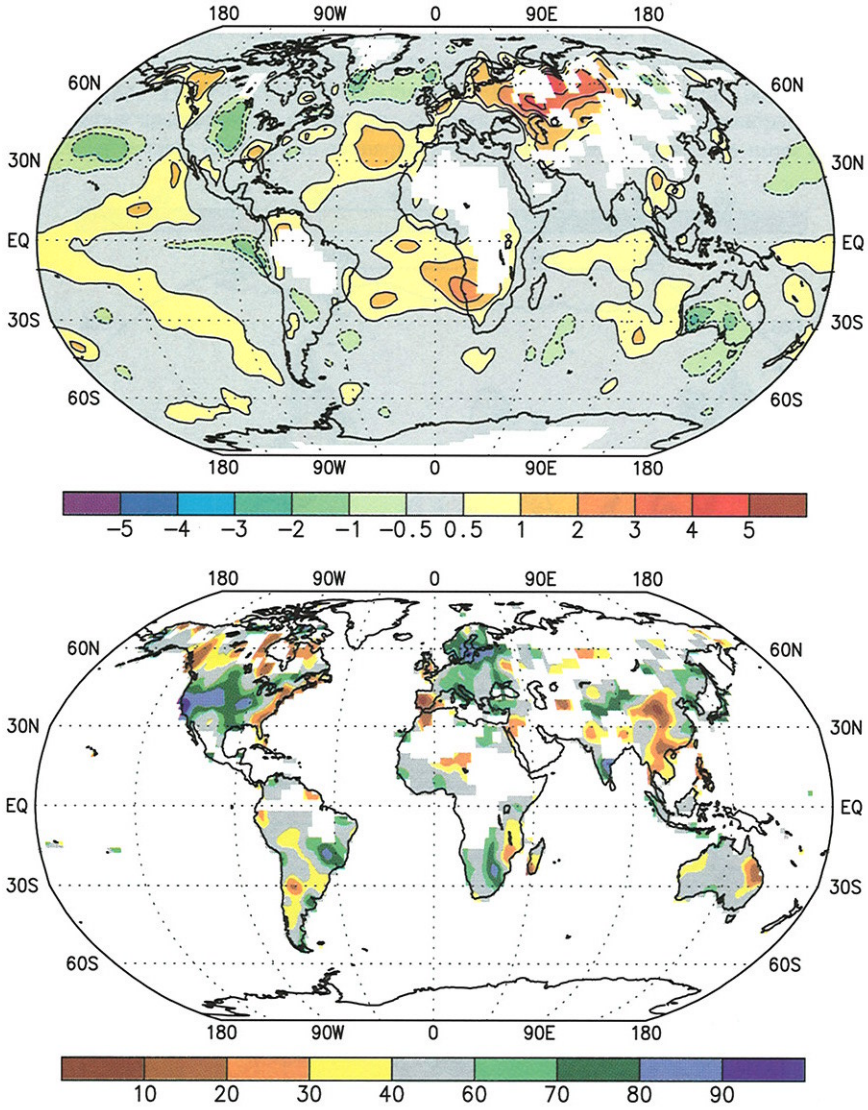


FIG. 72. Surface temperature anomalies (top, °C) and precipitation percentiles based on a gamma distribution fit to the 1961–90 base period (bottom) for March–May 1995. Temperature anomalies are based on station data over land (1961–90 base period) and sea surface temperature data over water (adjusted OI climatology, Reynolds and Smith 1995). The analysis is omitted in data-sparse regions (white areas). (Source: CPC)

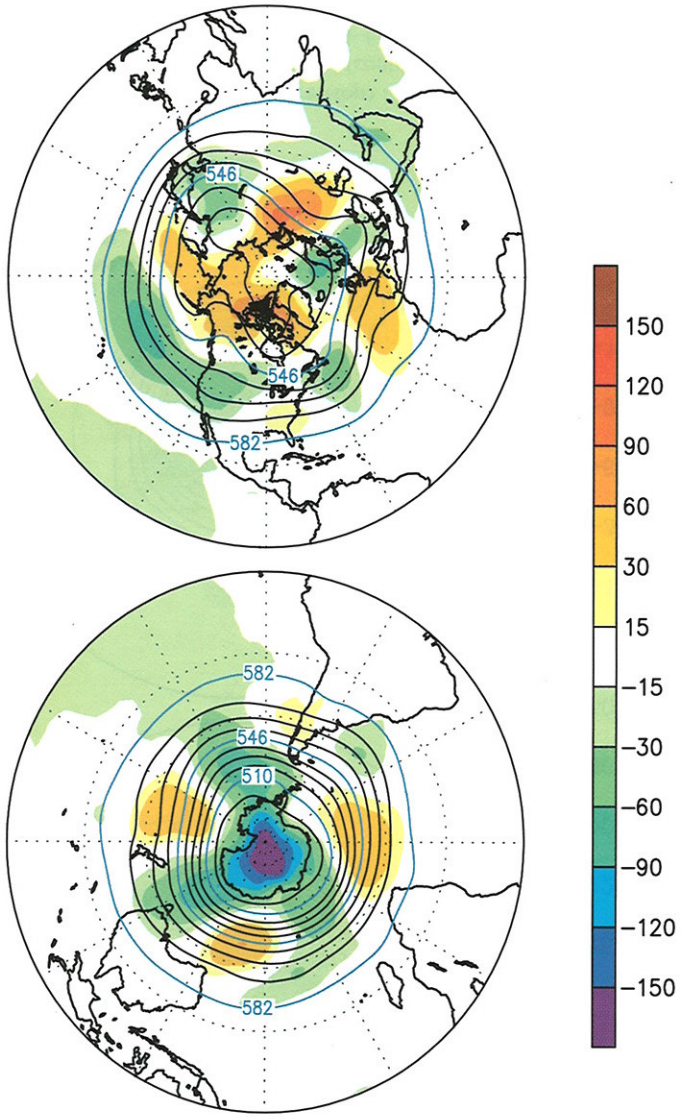


FIG. 73. Northern Hemisphere (top) and Southern Hemisphere (bottom) 500-hPa geopotential height (contours, interval is 9 dm) and anomalies (shading) for March–May 1995. Anomalies are departures from the 1979–88 base period means. (Source: CPC)

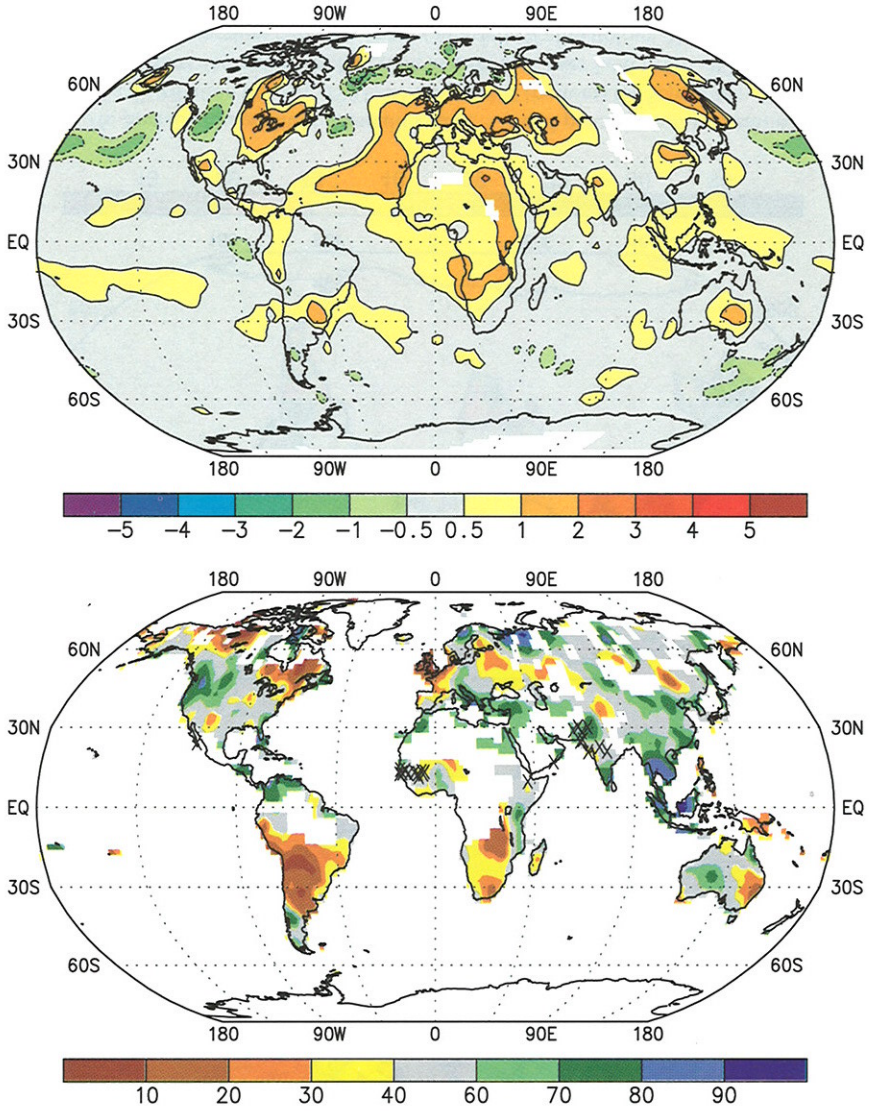


FIG. 74. Surface temperature anomalies (top, °C) and precipitation percentiles based on a gamma distribution fit to the 1961–90 base period (bottom) for June–August 1995. Temperature anomalies are based on station data over land (1961–90 base period) and sea surface temperature data over water (adjusted OI climatology, Reynolds and Smith 1995). The analysis is omitted in data-sparse regions (white areas). (Source: CPC)

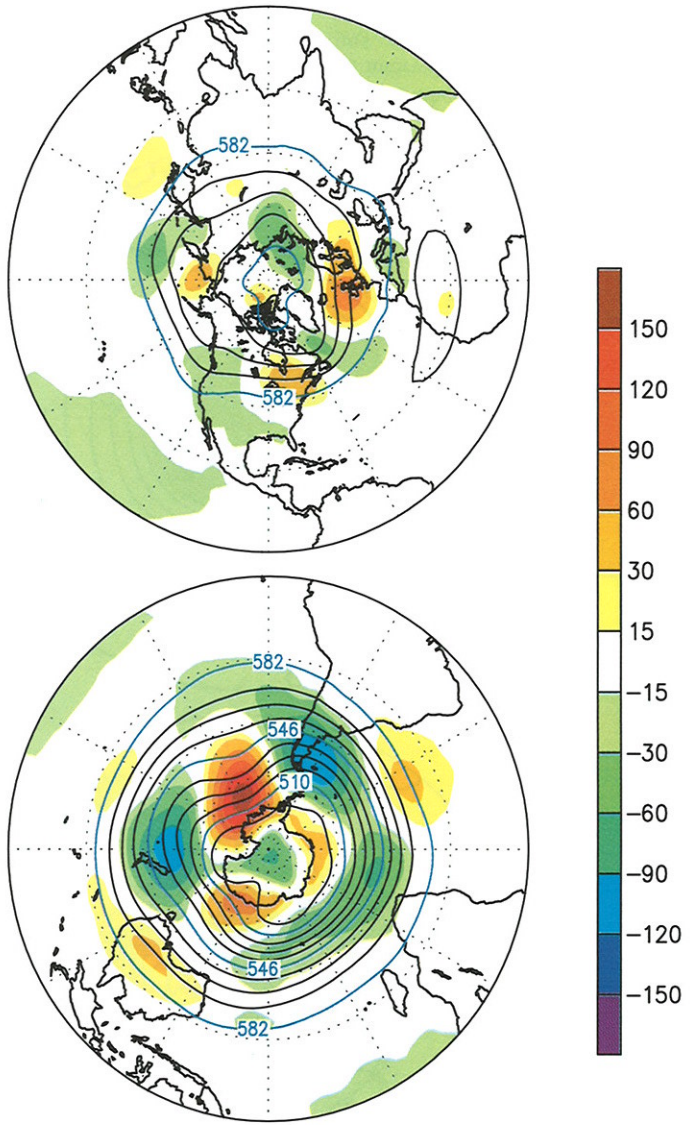


FIG. 75. Northern Hemisphere (top) and Southern Hemisphere (bottom) 500-hPa geopotential height (contours, interval is 9 dm) and anomalies (shading) for June–August 1995. Anomalies are departures from the 1979–88 base period means. (Source: CPC)

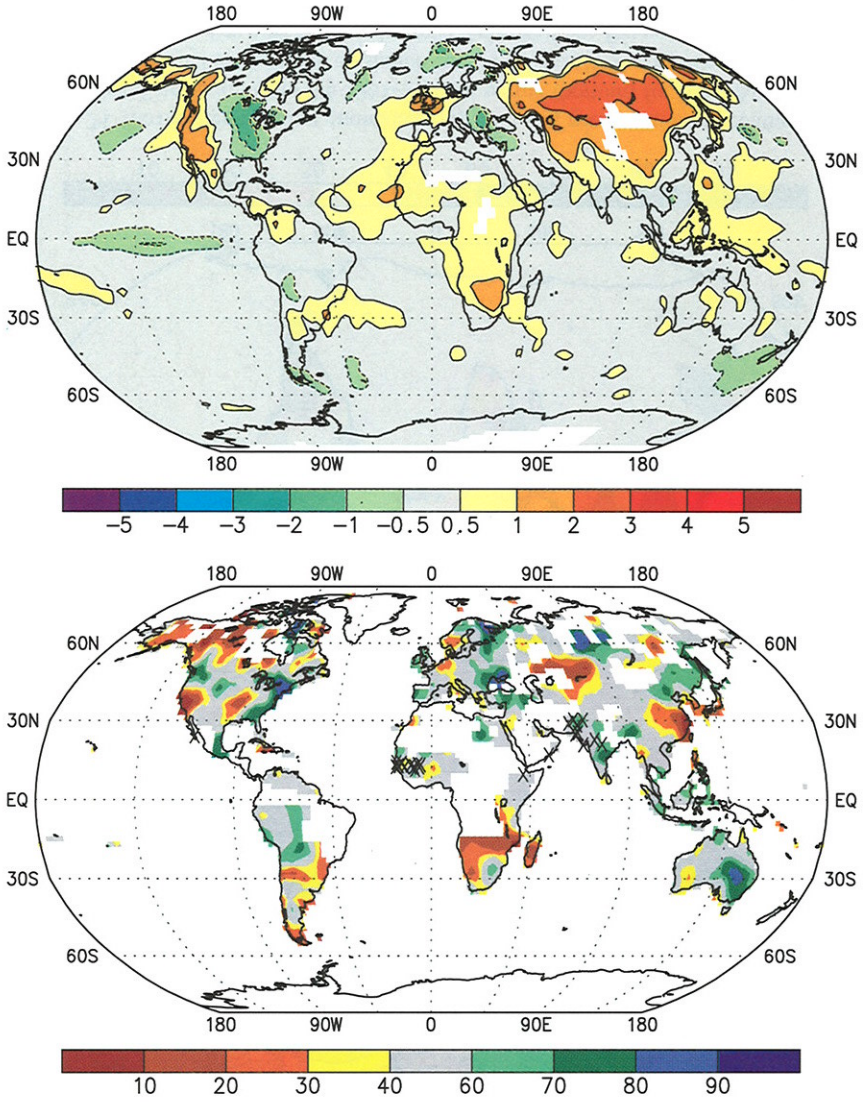


FIG. 76. Surface temperature anomalies (top, °C) and precipitation percentiles based on a gamma distribution fit to the 1961–90 base period (bottom) for September–November 1995. Temperature anomalies are based on station data over land (1961–90 base period) and sea surface temperature data over water (adjusted OI climatology, Reynolds and Smith 1995). The analysis is omitted in data-sparse regions (white areas). (Source: CPC)

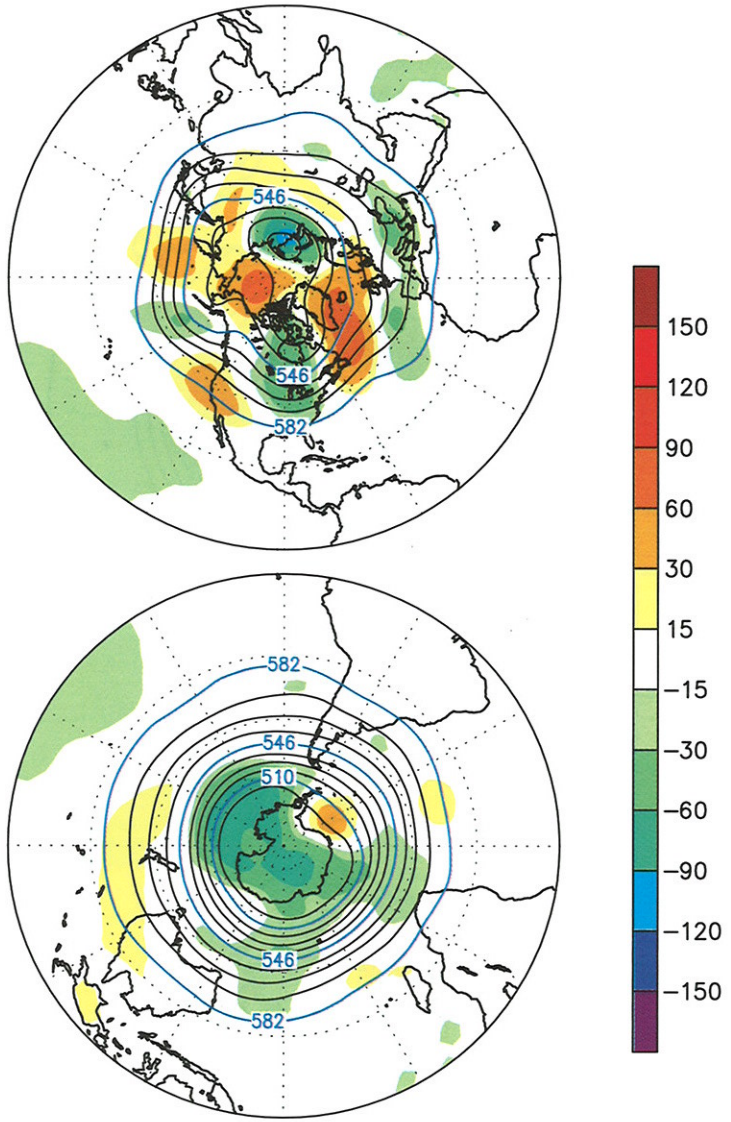


FIG. 77. Northern Hemisphere (top) and Southern Hemisphere (bottom) 500-hPa geopotential height (contours, interval is 9 dm) and anomalies (shading) for September–November 1995. Anomalies are departures from the 1979–88 base period means. (Source: CPC)

Appendix: Contributors

Air Resources Laboratory/ERL/NOAA
- J. Angell

Australian Bureau of Meteorology, National Climate Centre, Climate Analysis Section
- W. Wright

Climate Prediction Center/NCEP/NWS/NOAA
- A. Basist
- A. Clausen
- D. Garrett
- M. Gelman
- J. Harrison
- C. Long
- D. Miskus
- R. Nagatani
- R. Tinker

Climate Monitoring and Diagnostics Laboratory/ERL/NOAA
- J. Peterson
- E. Dlugokencky

Climatic Research Unit, University of East Anglia, (UK)
- P. Jones

Department of Geography, Rutgers University
- D. Robinson

Deutscher Wetterdienst, Hamburg, Germany
- G. Rosenhagen

Hadley Centre for Climate Prediction and Research, (UK)
- D. Cullum
- C. Folland
- M. O'Donnell
- D. Parker

Institute for Global Climate and Ecology, (Russia)
- G. Gruza

Instituto Nacional de Pesquisas Espaciais, CPTEC (Brazil)
- I. Cavalcanti

National Climatic Data Center/NESDIS/NOAA
- W. Brown
- M. Crowe
- R. Heim Jr.

Acknowledgments. This assessment would not have been possible without the cooperation and contributions from various scientists representing a cross-section of the NOAA climate community. We also wish to acknowledge the contributions from the scientists outside of NOAA in other federal laboratories, at universities, and at several sites around the world. All of these scientists are in the contributors list (Appendix) and we thank them for their timely and useful input. We are especially grateful to those international scientists who contributed their time and effort. We also would like to acknowledge the Brazilian Instituto Nacional de Meteorologia (INMET), which provided data that was used in the Brazilian precipitation figures. We also wish to thank R. Rosen for his early efforts and ideas on getting this document published in BAMS. In addition, we would like to thank T. Karl, N. Canfield, and an anonymous reviewer for their comments that helped to strengthen the article.

References

Barnston, A. G., and R. E. Livezey, 1987: Classification, seasonality and persistence of low-frequency atmospheric circulation patterns. *Mon. Wea. Rev.*, **115,** 1083–1126.

Bell, G. D., and M. S. Halpert, 1995: Interseasonal and interannual variability: 1986–1993. NOAA Atlas No. 12. [Available from Climate Prediction Center, 5200 Auth Rd. Rm 605, Camp Springs, MD, 20746.]

——, and J. E. Janowiak, 1995: Atmospheric circulation during the Midwest floods of 1993. *Bull. Amer. Meteor. Soc.*, **76,** 681–696.

——, and V. E. Kousky, 1996: Diagnosis of the Northern Hemisphere extratropical atmospheric response to ENSO. Submitted to *Mon. Wea. Rev.*

Dlugokencky, E. J., K. A. Masarie, P. M. Lang, P. P. Tans, L. P. Steele, and E. G. Nisbet, 1994: A dramatic decrease in the growth rate of atmospheric methane in the Northern Hemisphere during 1992. *Geophys. Res. Let.*, **21,** 45–48.

Gray, W. M., 1968: Global view of the origin of tropical disturbances and storms. *Mon. Wea. Rev.*, **96,** 669–700.

——, C. W. Landsea, P. W. Mielke, Jr., and K. J. Berry, 1992: Predicting Atlantic seasonal hurricane activity 6–11 months in advance. *Wea. Forecasting,* **7,** 440–455.

——, ——, ——, and ——, 1994a: Predicting Atlantic Basin seasonal tropical storm activity by June 1. *Wea. Forecasting,* **9,** 103–115.

——, ——, ——, and ——, 1994b: Extended range forecasting of Atlantic seasonal hurricane activity for 1995, as of 30 November 1994. Department of Atmospheric Sciences, Colorado State University, Fort Collins, CO, 9 pp.

Grody, N. C., and A. N. Basist, 1996: Global identification of snowcover using SSM/I measurements. *IEEE Transactions on Geoscience and Remote Science,* **34,** 237–249.

Kalnay, E., and Coauthors, 1996: The NCEP/NCAR 40-year Reanalysis Project. *Bull. Amer. Meteor. Soc.*, **77,** 437–471.

Keeling, C. D., R. B. Bacastow, and T. P. Whorf, 1982: Measurements of the concentration of carbon dioxide at Mauna Loa Observatory, Hawaii. *Carbon Dioxide Review: 1982.* W. C. Clark, Ed., Oxford University Press, 377–385.

Landsea, C. W., W. M. Gray, G. D. Bell, and S. B. Goldenberg, 1996: The extremely active 1995 Atlantic hurricane season: Environmental conditions and verification of forecast results. Submitted to *Mon. Wea. Rev.*

Mo, K. C., and R. E. Livezey, 1986: Tropical–extratropical geopotential height teleconnections during the Northern Hemisphere winter. *Mon. Wea. Rev.*, **114,** 2488–2515.

——, J. Nogues-Paegle, and J. Paegle, 1995: Physical mechanisms of the 1993 summer floods. *J. Atmos. Sci.*, **52,** 879–895.

NCDC, 1981: Tropical Cyclones of the North Atlantic Ocean, 1871–1980. United States Department of Commerce (DOC), National Oceanic and Atmospheric Administration (NOAA), National Weather Service (NWS), Environmental Data and Information Service, Environmental Research Laboratories, Asheville, NC, and the DOC/NOAA/NWS/National Meteorological Center, National Hurricane Center, Coral Gables, FL, 180 pp.

Reynolds, R. W., and T. M. Smith, 1995: A high-resolution global sea surface temperature climatology. *J. Climate,* **8,** 1571–1583.

Ropelewski C. F. and M. S. Halpert, 1987: Global and regional scale precipitation patterns associated with the El Niño/Southern Oscillation. *Mon. Wea. Rev.,* **115,** 1606–1626.

——, and ——, 1989: Precipitation patterns associated with the high index phase of the Southern Oscillation. *J. Climate,* **2,** 268–284.

Spencer, R. W., J. R. Christy, and N. C. Grody, 1990: Global atmospheric temperature monitoring with satellite microwave measurements: Method and results 1979–1984. *J. Climate,* **3,** 1111–1128.

Thoning, K. W., P. P. Tans, and W. D. Komhyr, 1989: Atmospheric carbon dioxide at Mauna Loa Observatory 2. Analysis of the NOAA/GMCC data, 1979–1985. *J. Geophys. Res.,* **94,** 8549–8565.

Trenberth, K. E., and T. J. Hoar, 1996: The 1990–1995 El Niño–Southern Oscillation event: Longest on record. *Geophys. Res. Lett.,* **23,** 57–60.

